TARGETED DELIVERY OF SIRNA TO THE TUMOR

Shyh-Dar Li

A dissertation submitted to the faculty of the University of North Carolina at Chapel Hill in partial fulfillment of the requirements for the degree of Doctor of Philosophy in the School of Pharmacy.

Chapel Hill
2008

Approved by,

Pilar Blancafort, Ph.D., Assistant Professor, Department of Pharmacology

Moo J. Cho, Ph.D., Associate Professor, School of Pharmacy

Leaf Huang, Ph.D., Professor, School of Pharmacy

Russell Mumper, Ph.D., Professor, School of Pharmacy

Xiao Xiao, Ph.D., Professor, School of Pharmacy

ABSTRACT

SHYH-DAR LI: Targeted Delivery of siRNA to the Tumor
(Under the direction of Leaf Huang, Ph.D.)

We have developed a surface-modified LPD (liposome-polycation-DNA) nanoparticle formulation by mixing cationic liposomes, a polycationic peptide and nucleic acids (mixture of DNA and siRNA) at a fixed ratio, followed by post-inserting a PEGylated lipid. This self-assembled nanoparticle formulation was around 100 nm in diameter with 90% encapsulation efficiency for siRNA. The nucleic acid was complexed with the peptide into a compact core, which was coated with two lipid bilayers. The inner lipid bilayer was stabilized by the charge-charge interaction between the cationic lipids and the compact core. Upon addition of a PEGylated lipid, the outer lipid bilayer was stripped off and the lipid anchor was inserted into the outer leaflet of the inner bilayer, resulting in approximately 10.6 mol% modification of PEG (polyethylene glycol) on the surface of the nanoparticles. The high degree of PEGylation completely shielded the charge of the nanoparticles with the zeta potential close to neutral (-5.6 ± 4.5 mV) and abolished the reticuloendothelial uptake in the isolated liver.

When i.v. injected into tumor bearing mice (s.c. human lung cancer xenograft model in the nude mice), the nanoparticles delivered 70-80% injected siRNA/g into the tumor, while the normal organs only showed a moderate uptake (10-20% injected siRNA/g). After the conjugation of a targeting ligand, anisamide, at the distal end of the PEG, the intracellular delivery of siRNA into the sigma receptor expressing tumor was significantly enhanced. This led to efficient EGFR silencing, significant apoptosis induction and tumor growth

inhibition at the dose of 1.2 mg siRNA/kg for three consecutive injections. The experimental murine lung metastasis model was established by i.v. injecting the mouse melanoma cells, which were stably transduced with a luciferase gene by retrovirus, into the mice. An improved metastatic tumor delivery of siRNA was discovered by using the nanoparticles. When combinatorial siRNA sequences were delivered, the oncogenes (MDM2, c-myc and VEGF) in the lung metastasis were silenced simultaneously, leading to 70-80% tumor load reduction and 30% prolongation in animal lifespan. The nanoparticle formulation showed minimal to no otoxicity in both animal models. The results promise the potential use of this formulation clinically.

ACKNOWLEDGEMENTS

I would like thank my academic advisor, Dr. Leaf Huang, for his guidance and support on my research. I also thank my committee members, Drs. Xiao, Mumper, Cho and Blancafort, for their suggestions on my dissertation project. The kind assistance from the Huang lab during my graduate research and study is acknowledged. I also appreciate the supports from my friends, family and my beloved wife.

Sumio Chono, Yun-Ching Chen, Joyeeta Sen and Christine Conwell are acknowledged for their help on this project. The data shown in **figures 4.1**, **4.2**, **5.5** and **5.7** were generated by S.C. Y.-C. C. obtained the results described in **figures 3.10** and **3.11**. J.S. synthesized the DSPE-PEG-anisamide. C.C. and S.C. obtained the TEM picture shown in **figure 2.3**.

TABLE OF CONTENTS

LIST OF TABLES

LIST OF FIGURES

1.0 INTRODUCTION

siRNA has been called “one of the most exciting discoveries in biology in the last couple of years” [1]. With a specific sequence, siRNA (21-23 nucleotides) can selectively inhibit gene expression by base-pairing to complementary mRNA transcribed from the target gene. This complex drives the formation of the RNA induced silencing complex (RISC) which digests the target mRNA and uses the anti-sense strand of the siRNA as a template to seek and destroy all copies of the target mRNA [1]. RNAi has quickly become one of the most powerful and indispensable tools in molecular biology. By targeting to the mRNA that encodes for a disease-associated protein, siRNA is also currently being applied as a therapeutic agent in antiviral therapy, neurological diseases, and cancer therapy [1]. However, siRNA is vulnerable to nuclease degradation and cannot pass through membrane barriers due to its hydrophilic nucleic acid backbone. Delivery of siRNA has thus become one of the major research focuses in the RNAi field since 2004 and the progress of which before 2007 has been reviewed by Kim and Rossi [2,3]. Delivery strategies can be generally categorized into two approaches, including chemical modification and nanoparticle formulation. Over the past year, significant advance in siRNA delivery has been made. The key discoveries and technologies are highlighted and compared in this chapter. The perspectives and future directions are also discussed.

1.1 DELIVERY BARRIERS FOR SIRNA

There are at least five major barriers that prevent efficient delivery of siRNA into target cells [4], including (a) siRNA degradation by the nuclease in the blood and extracellular fluids, (b) non-specific elimination by the reticuloendothelial system (RES) in the liver and spleen, (c) extravasation of siRNA into the target tissue, (d) cell membrane penetration and (e) escape of the siRNA from the endosome and/or the carrier into the cytoplasm. To achieve a significant gene silencing effect, a variety of different strategies have been developed to overcome the barriers.

1.2 SIGNIFICANT PROGRESS OVER THE PAST YEAR

1.2.1 Chemical modification approach

Chemical modification of siRNA involves the modification on the nucleic acid backbone to increase the nuclease resistance and/or the conjugation of a lipophilic moiety at the end of sequence to improve the membrane penetration [2,4]. Backbone chemistry includes 2'-fluoro, 2'-O-methyl and phosphothioate. Cholesterol is the most commonly used moiety for increasing the cellular bioavailability.

1.2.1.1 Mechanisms and optimization of in vivo delivery of lipophilic siRNA

Cholesterol-conjugated siRNA has been shown to silence gene in vivo, especially in the liver and the intestine. Wolfrum et al. synthesized a variety of lipid-conjugated siRNA to study

the mechanism of tissue targeting [5]. They found that selective tissue uptake of the siRNA conjugates was due to the binding with serum lipoproteins. Conjugates that had high affinity for serum albumin over lipoproteins showed little liver uptake, leading to an insignificant RNAi effect. On the other hand, lipophilic siRNA that showed high association with lipoproteins had improved liver uptake and gene silencing activity. They demonstrated that high-density lipoprotein (HDL) enhanced the uptake of conjugated siRNA in the liver, gut, kidney and steroidogenic tissues via the scavenger receptor BI (SR-BI). Some lipophilic siRNA also bound with low-density lipoprotein (LDL) and were delivered to the liver through the LDL receptor. Additionally, the transmembrane protein Sid1 was required for the cellular uptake of the conjugated siRNA complexed with lipoproteins. It is noted that cholesterol conjugated siRNA against apolipoprotein B (apoB) decreased the serum level of LDL, which happened to be its major carrier. It is expected that the gene silencing effect of the subsequent administrations should be compromised. It may be argued that the serum level of LDL can serve as a regulator for the degree of gene silencing in order to maintain a desirable pharmacological effect. Nevertheless, when the siRNA is designed for other targets, the activity will be highly dependent on the LDL level in the individual, leading to a possible high degree of variability.

Recently, DiFiglia and colleagues utilized the facts that the cholesterol conjugated siRNA is carried by the LDL and LDL receptors have been detected in the brain to deliver siRNA into the mouse brain [6]. The cholesterol conjugated siRNA targeting human huntingtin (Htt) mRNA was introduced intrastriatally into the striata of mice that received adeno associate virus (AAV) containing expanded or wild-type Htt cDNA earlier. Both wild-type and mutant human Htt were down-regulated in the mouse striatum by a single

injection of the cholesterol-siRNA. The treatment significantly prolonged the survival of striatal neurons, reduced neuropil aggregates, decreased inclusion size, and improved the movement of the treated mice.

1.2.1.2 Dynamic PolyConjugates for targeted delivery of siRNA

Rozema et al. attached the backbone modified siRNA with the so-called dynamic PolyConjugates composed of a backbone polymer (amphipathic poly(vinyl ether)), a pH sensitive linker (CDM, carboxy dimethylmaleic anhydride), polyethylene glycol (PEG) and a targeting ligand (NAG, N-acetylgalactosamine) [7]. The amine group in the backbone polymer was masked with PEG and the ligand via the pH sensitive linker. PEGylated approach was utilized to improve the pharmacokinetics of the conjugate and the NAG ligand was employed to enhance the hepatocyte delivery by targeting the asialoglycoprotein receptor. Once the conjugates were internalized by the receptor-mediated endocytosis and trapped inside the acidic endosome, the acid labile linker was cleaved and the amine group in the polymer was unmasked, which destabilized the endosomal membrane and mediated endosome rupture. Using this delivery technology, they successfully demonstrated effective knockdown of two endogenous genes in the mouse liver: apoB and peroxisome proliferator-activated receptor alpha (ppara). Downregulation of apoB led to a significant reduction in serum cholesterol with little toxicity.

1.2.2 Nanoparticle approach

Different from the chemical modification method, the nanoparticle formulation strategy usually involves with encapsulating native siRNA into the particles, which prevents the

direct contact of nucleases with the siRNA. In addition, with the size around 100 nm, the renal clearance for the nanoparticles is minimal, resulting in prolonged blood circulation time and selective tissue accumulation [e.g. highly vasculatured tumor via the enhance permeability and retention (EPR) effect]. Nanoparticles can be generally categorized into two groups: lipid based and polymer based. Usually, four major components are incorporated in the formulation to overcome delivery barriers, including (a) a cationic carrier to condense siRNA into nanoparticles, (b) PEG to introduce steric hindrance for the nanoparticles to improve the circulation time and pharmacokinetics, (c) a targeting ligand to enhance the intracellular delivery and (d) an endosomolytic component, such as poly-imidazole or poly-histidine, to increase the bioavailability of the internalized siRNA. The advance of the nanoparticle formulation in these four aspects is discussed in the following sections and summarized in **table 1.1**.

Table 1.1 Summary of siRNA delivery technologies using nanoparticle approach

Advances	Strategies	
	Functional components	Examples
Improved nanoparticle complexation	1. Incorporation of a high MW nucleic acid 2. Introduce sticky overhangs to the siRNA	1. Calf thymus DNA [8] 2. A_{5-8}/T_{5-8} overhangs [9]
Improved pharmacokinetics	Surface coating with a hydrophilic polymer	PEGylation [8,10-12]
Enhanced intracellular delivery	Surface conjugation of a targeting ligand	Anisamide [8], transferrin [10], transferrin antibody [12]
Increased endosomal release	Incorporation of an endosomolytic component	1. poly-imidazole [10] 2. poly-histidine [12]

1.2.2.1 Complexation of siRNA with cationic carriers

The most commonly used method for forming nanoparticles with siRNA is through a self-assembling process mediated by charge-charge interaction, in which the cationic vector binds

with the anionic nucleic acid. The particle complexation is usually performed in a diluted concentration to avoid aggregation. Several groups found that cationic carriers, especially for polymers, formed looser complexes with siRNA than with plasmid DNA, resulted in unstable particle formation and reduced delivery efficiency [8,9]. This is probably due to the fact that the molecular weight of the siRNA is too low for an efficient polymer interaction. Li et al. mixed a carrier DNA, calf thymus DNA (average size 50 kbp), with the siRNA in their system to enhance the particle compaction [8]. The siRNA mixing with the calf thymus DNA was tightly complexed with protamine into a solid core, which was further coated with cationic lipid bilayers [so-called LPD (liposome-polycation-DNA) nanoparticles]. This improved formulation showed 10-30% decreased size and 20-80% increased delivery efficiency comparing with the formulation without the carrier DNA. Although the calf thymus DNA with limited immuno-stimulating CpG motifs did not enhance the immunotoxicity of the formulation; the foreign DNA containing nanoparticles may not be suitable for human use. Bolcato-Bellemin and colleagues added short complementary $A_{5\text{-}8}/T_{5\text{-}8}$ overhangs to make the siRNA bind to each other and form a large "gene-like" structure [9]. They found that the siRNA with the sticky overhangs had increased complex stability with polyethyleneimine (PEI), improved RNase protection and enhanced gene silencing up to 10-fold. After released in the cytoplasm, the sticky siRNA did not induce interferon response, suggesting the approach may be a good alternative.

1.2.2.2 Modification of nanoparticles with PEG

PEGylation technology has been widely used to improve the stability, blood circulation time and pharmacokinetics of biopharmaceutical agents, such as nucleic acids and proteins. Surface coating of PEG on the liposomes has been shown to prevent particle aggregation and

reduce the opsonization with the serum proteins, leading to decreased RES uptake and prolonged circulation time. Thus, surface PEGylation has been commonly employed in the nanoparticle field. Since PEG may interfere with the charge-charge interaction during the particle formation due to its steric hindrance, the PEGylation process is often performed after the particles are formed, especially for the lipid-based nanoparticles [8,12]. Linear cationic polymer, on the other hand, is usually PEGylated before complexed with siRNA [11], and therefore, has less problem of forming aggregates. For PEGylated cationic polymer, the positively charged functional groups are still available for siRNA if the ratio of PEG/charged groups is designed properly. Whereas the surface charge of the lipid based vesicles is greatly shielded by PEG and no longer accessible for siRNA.

Although significant efforts have been placed on finding other type of materials to replace PEG, little success has been reported.

1.2.2.3 Conjugation of a targeting ligand

For membrane impermeable drugs, such as siRNA, extracellular release is not a good design for the delivery. Once the nanoparticles extravasate in the local tissue (e.g., solid tumor), an intracellular uptake mechanism is needed to increase the bioavailability of siRNA. Conjugating a targeting ligand on the surface of the nanoparticle is the most commonly used strategy. A variety of targeting ligands have been used, including small molecule ligand [8], peptide [13], protein [10] and antibody [12]. After the ligand binds with the receptor overexpressed on the target cell surface, the receptor-mediated endocytosis is triggered for the internalization of the siRNA containing nanoparticles. However, some problems have been reported regarding the use of the targeting strategy. First, the antibody conjugated liposomes (immunoliposomes) had reduced circulation time after repeated injections,

suggesting that an immune response against the immunoliposomes was produced [14]. Second, the high-affinity binding of the ligand and receptor often results in tight association of the targeted nanoparticles with the target cells near the vasculature, leading to reduced tissue penetration [15]. Therefore, the new criteria for selecting targeting ligands have been changed: (a) an endogenous ligand that does not induce immune response, (b) a ligand that binds with the surface receptors overexpressed in the target cell and triggers rapid endocytosis, (c) a ligand that binds with the receptor with a relatively low affinity allowing improved tissue penetration [15].

It is noted that the modification of a targeting ligand on nanoparticles does not increase the target tissue accumulation but improve the intracellular delivery. Li et al. demonstrated that the pharmacokinetic parameters (clearance, area under the curve and mean residence time) remained the same for non-targeted and targeted nanoparticles, while the targeted nanoparticles showed improved intracellular delivery and RNAi effect [8]. Bartlett also published similar results showing that the targeted nanoparticles had similar pharmacokinetics as the non-targeted nanoparticles, but had enhanced gene silencing effect [10].

1.2.2.4 Incorporation of an endosomolytic component

Once internalized into the target cell, the nanoparticles are trapped inside the endosome/lysosome and finally degraded in the acidic and enzyme-rich environment. The siRNA needs to be released to the cytoplasm in order to have its pharmacological activity. To further improve the RNAi activity, an endosomolytic component is incorporated in the nanoparticle formulation. Usually, the endosomolytic agent contains multiple neutral amine groups with a pKa around 6.5, such as crowded tertiary amines [16,17], histidine [10] and

imidazole [12]. At physiological pH, the amine groups stay neutral; while in the endosome (pH 5-6), the amine groups are protonated. This results in reduced free proton concentration and increased pH in the endosome. Due to the continuous influx of proton and its counter anion, chloride, into the endosome to maintain the low pH, the osmotic pressure in the endosome rises rapidly. Eventually, the endosome ruptures and nanoparticle/siRNA is released. The process is called the proton sponge effect [16] and has been experimentally verified [17]. The release of siRNA from the nanoparticle is probably the result of protein competition for polymer binding, although it has not been experimentally verified. The strategy has been shown to significantly increase the RNAi effect of the formulation [12]. For a cationic lipid based delivery system, formation of charge complex between the cationic lipid and the anionic endosomal lipid may lead to local dehydration and destabilization of the endosomal membrane [18], resulting in the release of the siRNA/lipid complex into the cytoplasm.

1.2.3 Other approaches

Kumar et al. developed a chimeric peptide consisting of a 29-amino-acid peptide derived from rabies virus glycoprotein (RVG) tethered to a 9-arginine (9R) peptide [13]. The RVG peptide was shown to specifically bind to the acetylcholine receptor expressed in neuronal cells and the 9R could complex with siRNA as a delivery moiety. They demonstrated that siRNA could be transvascularly delivered into the neuronal cells with the chimeric peptide by i.v. injection. Specific gene silencing and antiviral activity was observed with little toxicity. Medarova et al. chemically conjugated a polyarginine peptide, a siRNA and a near infrared fluorescent dye (Cy5.5) onto a dextran coated magnetic nanoparticle to image the

tumor accumulation and the RNAi effect of the formulation by magnetic resonance imaging (MRI) and optical imaging [19].

1.2.4 Management of immunotoxicity of siRNA

siRNA can be potent triggers for the immune response, particularly when associated with delivery vesicles that facilitate intracellular uptake. Judge et al. identified 5'-UGUGU-3' within siRNA as one immunostimulatory motif and showed that the sequence recognition mechanism is stringent enough that minimal base substitution can have profound effects to reduce the immune response [20]. They showed that immune stimulation by synthetic siRNA can be completely diminished by selective incorporation of 2'-O-methyl (2'OMe) uridine or guanosine nucleosides into one strand of the siRNA duplex. The modified siRNA had full gene silencing activity and was tested in mice without generating cytokine induction, toxicity or off-target effects [21]. Recently, Robbins and colleagues showed that 2'-O-methyl-modified siRNA acted as a TLR7 antagonist that abolished the inflammatory toxicity of the immunostimulatory siRNA and a small-molecule TLR7 agonist, loxoribine [22].

1.3 PERSPECTIVES FOR SIRNA DELIVERY

siRNA based gene therapy has become one of the major focuses in the gene therapy field. First, the action site of siRNA is located in the cytosol, which avoids the requirement of nuclear delivery; a significant barrier for plasmid DNA based therapy. Second, siRNA is the most efficient antisense agent among oligonucleotides with a relatively low off-target effect.

Third, like all other oligonucleotides, siRNA can be chemically synthesized in high quantity and purity to meet the standards of a pharmaceutical grade drug. The significant progress over the past year highlighted above promises the future of siRNA as a new class of promising pharmaceutical. However, there are still several challenges ahead. In this section, different strategies for siRNA delivery are compared and the future perspectives are discussed.

1.3.1 Viral vs non-viral vector; expression vector vs synthetic siRNA

Unlike non-viral approach, viral delivery employs an expression vector to be transcribed into shRNA (short hairpin RNA) after delivered into the nucleus. shRNA then translocates into the cytoplasm and is processed by the Dicer into siRNA. Once the expression vector is integrated into the chromosome of the infected cell, siRNA is continuously expressed, which promises its long-term therapeutic effect. However, viral vector suffers from poor tissue targeting and high immunogenecity [23], resulting in little success compared to non-viral vectors. The difficulty in nuclear delivery bars the success of using non-viral vector to deliver a siRNA expression vector. In addition, the short half-life of siRNA requires multiple injections of the non-viral formulation to achieve a significant therapeutic effect [8,12,13,19,24]. Although chemical modification may improve the biochemical stability of siRNA in the cytosol, more effort should be placed to solve this problem, such as the design of a sustained release carrier.

1.3.2 Chemical modification vs nanoparticle formulation approach

Wolfrum et al. showed that the lipophilic siRNA bound with different endogenous carriers for tissue targeting [5]. However, the application of the chemically conjugated siRNA is still limited for liver diseases. Different types of conjugation and their pharmacokinetics need to be studied to broaden the scope of the approach. Nanoparticle vector is mainly focused on the delivery to the highly vascularized inflammatory tissue or tumor by utilizing the EPR effect of the nanoparticle. Combination of these two approaches may expand the application and prolong the RNAi effect. Since the lipophilic siRNA binds to a natural nanoparticle carrier, i.e., lipoprotein, both approaches have the same limitation of being effective only with tissues equipped with a leaky vasculature. Delivery of siRNA to tissues with a tight vasculature, such as brain and muscle, will continue to be a challenge. In this regard, tissue-tropic viral vectors, such as AAV, may be a good alternative.

1.3.3 Self-assembled nanoparticles vs chemically conjugated nanoparticles

Self-assembled nanoparticles are formed by mixing siRNA with a vector and the siRNA is encapsulated inside the nanoparticles by non-covalent forces. Preparation of chemically conjugated nanoparticles usually involves with a series of chemistry, and the siRNA is attached to the surface of the vector by covalent bonds. The magnetic nanoparticle used by Medarova et al. [19] is a good example of the latter nanoparticle carrier. These two types of nanoparticles can be compared in two aspects, stability and drug/carrier ratio. Fist, siRNA is encapsulated inside the self-assembled nanoparticles, which prevents direct contact of the siRNA with nucleases and increases the stability. However, conjugation of siRNA on the

surface of the nanoparticles does not offer equal protection. During the chemical conjugation and purification process, loss of siRNA or its stability likely occurs. Additionally, shelf-life and scale-up production of the nanoparticles needs to be studied. On the other hand, self-assembled nanoparticles is usually prepared by mixing different components before use [8,11,12], which avoids the storage of the nanoparticles. Polymer and lipid vectors can be easily scaled up. Second, self-assembled nanoparticles provide a much higher drug/carrier ratio compared to the chemically conjugated nanoparticles. For examples, Bartlett and Davis demonstrated that each of their self-assembled nanoparticles contained ~2,000 siRNA molecules [25], while Medarova's chemical conjugation method could only attach three siRNA molecules to a single nanoparticle [19]. Here, we predict that self-assembled nanoparticles will continue to dominate for siRNA delivery.

1.3.4 Multiple siRNA sequences delivery

Using multiple siRNA sequences to attack different regions of the same target mRNA or to simultaneously silence different genes is a common practice in RNAi research. Recently, Castanotto et al. found that siRNA can potentially compete or hinder the transport and incorporation of other siRNA sequences into the RNA-induced silencing complex (RISC) when used in a combinatorial approach [26]. TAR RNA binding protein is one of the sensors for selecting and incorporating the sequences of siRNA. Therefore, combinatorial siRNA strategy can be problematic. Improved pharmacological effects may only be achieved when different targets are simultaneously silenced. Theoretically, siRNA against the gene with a long half-life should be given first followed by the siRNA targeting the gene with a shorter half-life. siRNA targeting an abundant mRNA may have to be administered multiple times

for sufficient gene silencing before the treatment of other siRNA. Therefore, intensive pharmacokinetic and pharmacodynamic studies should be performed to fine tune the dosing regimen (dose, interval, frequency, order) for the combinatorial approach in order to achieve a synergistic effect.

1.3.5 Targeting diseased cells vs the surrounding vascular endothelial cells

There has been an increased interest of targeting the surrounding vascular endothelial cells in a diseased tissue (so-called anti-angiogenesis approach), especially for tumor and inflammatory diseases. There are several advantages for the anti-angiogenesis approach. First, endothelial cells directly facing the blood are more accessible for treatment compared to the diseased cells. Taking tumor as an example, the intratumoral pressure is significantly higher compared to the peripheral, often resulting in low tissue penetration of the siRNA formulation. Second, multiple mutated signal transduction pathways are often found in the tumor cells, which makes it difficult to treat the disease by using a limited number of siRNA sequences. On the other hand, vascular biology is usually more constant and therefore, more readily for intervention. Third, specific antibody can be produced to transvascularly deliver nanoparticles into the target tissue. Oh and colleagues showed that the aminopeptidase P antibody targeted nanoparticles to the caveolae of mouse lung endothelium [27]. The caveolae then operated as a pump, transporting the antibody conjugated nanoparticles from the blood across the endothelium into the lung tissue. Approximately 80% injected dose/g tissue was achieved within 30 min with minimal uptake in other tissues. Although most of the published methods used diseased cell targeting approach, it is anticipated that an increased number of research utilizing vascular targeting method will be reported.

1.3.6 Other critical issues

Other than the topics discussed above, there are at least five critical issues that need to be considered for developing a siRNA formulation.

1.3.6.1 siRNA release from the nanoparticles

Significant effort has been placed on improving the complexation of siRNA into nanoparticles, while the mechanism of siRNA release in the cytoplasm needs further study. Only the released siRNA is bioavailable. If the siRNA can be programmed for sustained release, the RNAi effect can be greatly prolonged.

1.3.6.2 Pharmacokinetics/biodistribution

Pharmacokinetic study allowing describing and predicting the behavior, efficacy and toxicity of siRNA formulation will eventually become a prerequisite. Several methods have been used for the study of pharmacokinetics of siRNA, including fluorescence labeling [8], radioisotope labeling [10], RNase protection assay [12] and LC-MS method. From the pharmaceutical point of view, only the LC-MS method is robust enough to perform the validated analysis. Unfortunately, LC-MS method is still limited by its low sensitivity. Therefore, a sensitive LC-MS method for siRNA is urgently needed.

1.3.6.3 Stability

Stability is a key issue for pharmaceutical products. Stability test has to be performed in the early stage of formulation development, which will eventually affect its clinical use. Stability can be monitored by measuring the particle size, zeta potential, encapsulation

efficiency and gene silencing activity. For an unstable formulation, lyophilization is a commonly used method for long term preservation [28].

1.3.6.4 Toxicity

Preliminary toxicity of the formulation can be evaluated by blood chemistry, liver enzyme analysis, body-weight monitor and proinflammatory cytokine analysis in rodents. However, dose escalating study should be done in non-human primates to study the complement depletion and antibody production against the nanoparticle formulation [11].

1.3.6.5 Dose

The required dose reflects the delivery efficiency of a formulation. Low required dose usually results in low side effects from the delivery vector and improved therapeutic window. **Table 1.2** indicates that the self-assembled nanoparticles showed the highest delivery efficiency according to the required dose, followed by the chemically conjugated nanoparticles and chemically modified siRNA.

Table 1.2 Comparison of the siRNA formulations

Category	Formulation	Required dose (mg/kg)	Times of repeated injections	Native siRNA (N) or modified siRNA (M)	Target tissue	Re-ference
Self-assembled nanoparticles	Anisamide-LPD	1.2	3	N	Tumor	[8]
	Transferrin-cyclodextran polycation	2.5	2-3	N	Tumor	[24]
	Immuno-lipoplex	3	3	M	Tumor	[12]
Peptide based vector	RVG peptide-9R	2.5	3	N	Brain	[13]
Chemically conjugated nanoparticles	Magnetic nanoparticles	~6	4	N	Tumor	[19]
Chemically modified nanoparticles	Dynamic Poly-conjugates	~2.5	1	M	Liver	[7]
	Cholesterol-siRNA	50	1	M	Liver	[5]

2.0 DEVELOPMENT AND CHARACTERIZATION OF THE LPD (LIPOSOME-POLYCATION-DNA) NANOPARTICLE FORMULATION FOR SIRNA

LPD (liposome-polycation-DNA) nanoparticles prepared by mixing cationic liposomes, a polycationic peptide, and nucleic acids showed a virus like structure at a certain composition. Nucleic acids were condensed by the peptide and formed a compact core, which was coated by two lipid bilayers. The inner bilayer was hypothetically supported by charge-charge interaction of the cationic lipids and the negatively charged complex core. In this study, we showed that LPD had improved stability compared to the cationic liposomes after the post-insertion of 10 mol% DSPE-PEG (distearoyl phosphatidyl ethanolamine-polyethylene glycol 2000). The light scattering data showed that the small size particle population significantly increased after PEGylation in the cationic liposomes compared to the LPD nanoparticles. LPD prepared by a multivalent cationic lipid, DSGLA (distearoyl guanidine lysine amide), had enhanced stability compared to that consisting of DOTAP (dioleoyl triammonium propane), a monovalent cationic lipid. The data suggest that stability of the LPD could be further improved by an enhanced charge-charge interaction. Distinct nanoparticle structure of the LPD after PEGylation was still found in the negative-stained electronic microscopy, while the cationic liposomes were transformed into tubular micelles under the same condition. Size exclusion chromatography data showed that approximately 60% of the total cationic lipids (62.8 ± 4.6%), which was located in the outer bilayer of the LPD according to the calculation, was stripped off during the PEGylation; and about 20% of the input DSPE-

PEG (20.6 ± 3.4%) was incorporated onto the inner bilayer of LPD with about 10.6 mol% of DSPE-PEG presented on the particle surface. This led to a complete charge shielding (zeta potential = -5.6 ± 4.5 mV) and abolishment of liver sinusoidal uptake in the isolated liver perfusion model. Our results demonstrated the importance of the supported bilayer in improving the stability of a nanoparticle formulation.

2.1 INTRODUCTION

Prolongation of the circulation half-life by surface incorporation of PEG in liposomes was demonstrated by our group in 1990 [29]. Surface modification by PEG was shown to reduce non-specific uptake of liposomes by the reticuloendothelial system (RES) in the liver and the spleen and thus improved its pharmacokinetic property. PEGylation approach has been used in a variety of nanoparticle systems to enhance the drug delivery.

LPD (liposome-polycation-DNA) nanoparticle was developed earlier in our lab [30] and has been used for the delivery of peptide [31] and nucleic acid, including plasmid DNA [30], oligonucleotide and siRNA [8,32-34]. LPD was prepared by mixing cationic liposomes, a polycationic peptide and nucleic acids at a fixed ratio. The self-assembled nanoparticles are around 100 nm in diameter. The detail structure of the LPD was demonstrated by the cryo-TEM (transmission electron microscopy) (**figure 1A**) [35], showing that the nucleic acid was complexed by protamine to form a compact core, which was coated with two cationic lipid bilayers (**figure 1B**). According to the calculation on the cryo-TEM picture (**figure 1A**), the ratio of the surface area of the inner bilayer and outer

bilayer was 1:1.8, indicating that approximately 36.4% of the total lipids was located in the inner bilayer and 63.6% was in the outer bilayer. The formation mechanism of the LPD has been proposed (**figure 1C**) [35]. First, the cationic peptide interacted with the nucleic acid and formed a negatively charged complex, which then interacted with the cationic liposomes via a charge-charge interaction. Second, upon the strong charge-charge interaction, the liposomes collapsed onto the peptide-nucleic acid complex core. Third, two separate lipid bilayer membranes appear on the surface of the LPD nanoparticle as the result of bilayer fusion and re-organization. In this model, the inner bilayer is directly in contact with the core and is supported and stabilized by the charge-charge interaction of the cationic lipids and the negatively charged complex core. We hypothesized that a supported bilayer tolerates a high level of DSPE-PEG, which is a surfactant, better than a regular bilayer. This unique feature of LPD may provide us an opportunity to modify the formulation with a high amount of DSPE-PEG to achieve an enhanced surface shielding and thus improve the pharmacokinetic property of the nanoparticle formulation.

In this study, we evaluated the tolerance of liposomes and LPD to DSPE-PEG micelle by using light scattering and TEM. We also titrated the input amount of DSPE-PEG micelle for the post-insertion and monitor the stability of the nanoparticles. Size exclusion chromatography was performed to purify and characterize the PEGylated LPD. Finally, the surface shielding effect of the PEGylated LPD was assessed by measuring the zeta potential and the non-specific uptake by the liver sinusoidal cells in the isolated liver perfusion model.

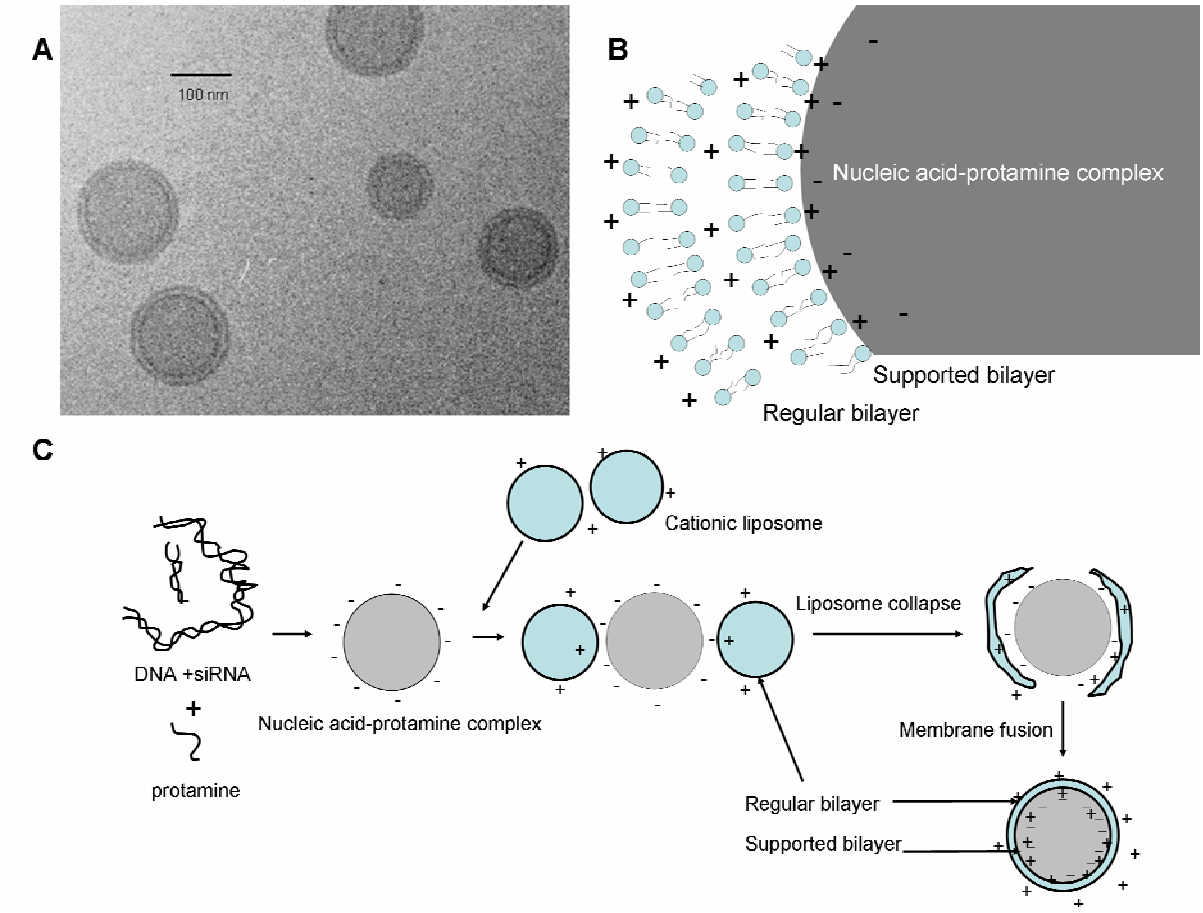

Figure 2.1 Illustration of the formation of LPD.
Cryo-TEM photograph (A), the illustration of the double lipid bilayer structure (B) and proposed mechanism for the formation of the LPD nanoparticles (C). Figure 1A was reproduced from Tan et al. with the authors' permission [35].

2.2 MATERIALS AND METHODS

2.2.1 Materials

DOTAP (dioleoyl triammonium propane) (**figure 2.2A**), NBD-DOTAP (nitrobenzosadiazol-DOTAP), NBD-PE (NBD-phosphatidyl ethanolamine), cholesterol, DSPE-PEG_{2000} (distearoyl phosphatidyl ethanolamine-polyethylene glycol 2000), and DSPE-PEG_{2000}-carboxyfluorescein (DSPE-PEG-CF) were purchased from Avanti Polar Lipids, Inc.

(Alabaster, AL). Protamine sulfate (fraction X from salmon sperm), calf thymus DNA (for hybridization, phenol-chloroform extracted and ethanol precipitated), and Sepharose CL 2B were from Sigma-Aldrich (St. Louis, MO). DSGLA (distearoyl guanidine lysine amide) was synthesized in our lab and the structure is shown in **figure 2.2A**.

Anti-luciferase siRNA (GL3) (target sequence 5'- CTT ACG CTG AGT ACT TCG A -3') was purchased from Dharmacon (Lafayette, CO) in deprotected, desalted, annealed form. Fluorescein (FAM) labeled siRNA (3' end of the sense strand) was used to evaluate the incorporation efficiency of the LPD for siRNA. Cy3 labeled siRNA was used for the isolated liver perfusion study.

2.2.2 Experimental animals

Female C57BL/6 mice of age 6-8 week (16-18 g) were purchased from Charles River Laboratories (Wilmington, MA). All work performed with animals was in accordance with and approved by the IACUC committee at the University of North Carolina at Chapel Hill (UNC).

2.2.3 Preparation of siRNA containing LPD nanoparticles

Two different methods were developed for the preparation of unmodified LPD nanoparticles. The two methods used the same ratio of cationic liposomes, protamine and nucleic acid, and the characteristics (particle size, zeta potential and encapsulation efficiency) of the nanoparticles prepared by the two methods were similar to each other.

Method 1: Small unilamellar liposomes consisting of DOTAP and cholesterol (1:1 molar ratio) were prepared by thin film hydration followed by membrane extrusion through a 50 nm polycarbonate membrane by 10-15 times. The total lipid concentration of the liposome was fixed at 10 mM and the liposome size was 90-100 nm. LPD was composed of DOTAP/cholesterol liposome, protamine, and the mixture of siRNA and calf thymus DNA (1:1 weight ratio). To prepare LPD, 15 μl of protamine (2 mg/ml), of 138 μl nuclease free water, and 24 μl of a mixture of siRNA and calf thymus DNA (2 mg/ml) were quickly mixed in a 1.5 ml tube. The complex was allowed to stand at room temperature for 10 min before the addition of 123 μl of DOTAP/cholesterol liposome (total lipid concentration = 10 mM). LPD nanoparticles were kept at room temperature for another 10 min before further application.

Method 2: LPD was obtained by quickly mixing suspension A (8.3 mM liposomes (DOTAP: cholesterol = 1: 1, molar ratio) and 0.2 mg/ml protamine in 150 μl nuclease free water) with solution B (0.16 mg/ml siRNA and 0.16 mg/ml calf thymus DNA in 150 μl nuclease free water) followed by incubation at room temperature for 10 min.

PEGylated LPD was prepared by incubating the LPD suspension (300 μl) with 37.8 μl micelle solution of DSPE-PEG (10 mg/ml) at 50°C for 10 min. PEGylated LPD was allowed to stand at room temperature for 10 min.

The charge ratio of the formulation was about 1:5 (-:+). The particle size was measured using the submicron particle sizer (NICOMP particle sizing systems, Autodilute^{PAT} Model 370, Santa Babra, CA) in the NICOMP mode. The zeta potential of various LPD formulations diluted in 1 mM KCl was determined by using a Zeta Plus zeta potential analyzer (Brookhaven Instruments Corporation, Holtsville, NY). PEGylated LPD was

freshly prepared and used within 20 min for the following experiments. For size exclusion chromatography, either 10 mol% NBD-DOTAP labeled liposomes, 10 mol% DSPE-PEG-CF labeled DSPE-PEG or FAM-siRNA was used for the preparation of the PEGylated LPD.

2.2.4 Negative stain electron microscopy

Transmission electron microscope (TEM) images were acquired using a Phillips CM12 (FEI, Hillsboro, OR). Briefly, freshly prepared formulations (5 μl) samples were dropped onto 300 mesh carbon-coated copper grids (Ted Pella, Inc., Redding, CA) and allowed a short incubation (5 min) at room temperature. Grids were then stained with 1% uranyl acetate (40 μl) and wicked dry. All images were acquired at an accelerating voltage of 100 kV. Gatan Digital Micrograph software was used to analyze the images.

2.2.5 Size exclusion chromatography

Ten μl of the samples was loaded onto a PBS pre-equilibrated Sepharose CL 2B column (1 × 10 cm). Elute fractions (200-300 μl) were collected, diluted 1:1 in ethanol, and analyzed for fluorescence intensity by a plate reader (λ_{ex}: 485 nm, λ_{em}: 535 nm) (PLATE CHAMELEON Multilabel Detection Platform, Bioscan Inc., Washington, DC).

2.2.6 Cellular Uptake Study

NCI-H1299 cells ($1X10^5$ cells/well) were seeded in 12-well plates (Corning Inc., Corning, NY) 20 h before experiments. Cells were treated with different formulations at a

concentration of 100 nM siRNA in serum containing medium at 37 ^{o}C for 4 h. Cells were washed twice with PBS, followed by incubation with lysis buffer (0.3% triton X-100 in PBS) at room temperature for 1 h. Fluorescence intensity of cell lysate was determined by a Perkin Elmer LS 50B Luminescence spectromer (Norwalk, CT) (λex: 494 nm, λem: 519 nm). For free ligand competition study, cells were co-incubated with 50 μM haloperidol with formulations. Alternatively, cells were fixed with methanol at room temperature for 1 min, mounted onto a glass slide, and imaged by a Nikon fluorescence phase contrast optical microscope.

2.2.7 Isolated liver perfusion study

C57BL/6 mice were sacrificed and the interior vena cava was incised to allow the blood flush out when 3 ml of warm PBS was infused into the mouse liver through the portal vein. cy3-siRNA containing LPD formulations (300 μl) were incubated with 50 μl mouse serum at 37°C for 10 min, and then diluted with PBS (final volume = 1 ml). The complex was infused into the isolated liver via the portal vein. Finally, the liver was perfused with 3 ml warm PBS, excised, fixed in 3.6% paraformaldehyde in PBS for overnight, and frozen sectioned (5 μm in thickness). Sections were washed with PBS, permeabilized with 0.1% triton X-100 in PBS, stained with Alexa Fluor® 488 Phalloidin (Invitrogen, Eugene, OR), mounted with the DAPI containing medium (Vectashield®, Vector Laboratories Inc., Burlingame, CA) and imaged using a Leica SP2 confocal microscopy.

2.2.8 Statistical analysis

Data are presented as the mean ± SD. The statistical significance was determined by using the analysis of variance (ANOVA, one way) or the two-sided student t-test. P values of <0.05 were considered to be significant.

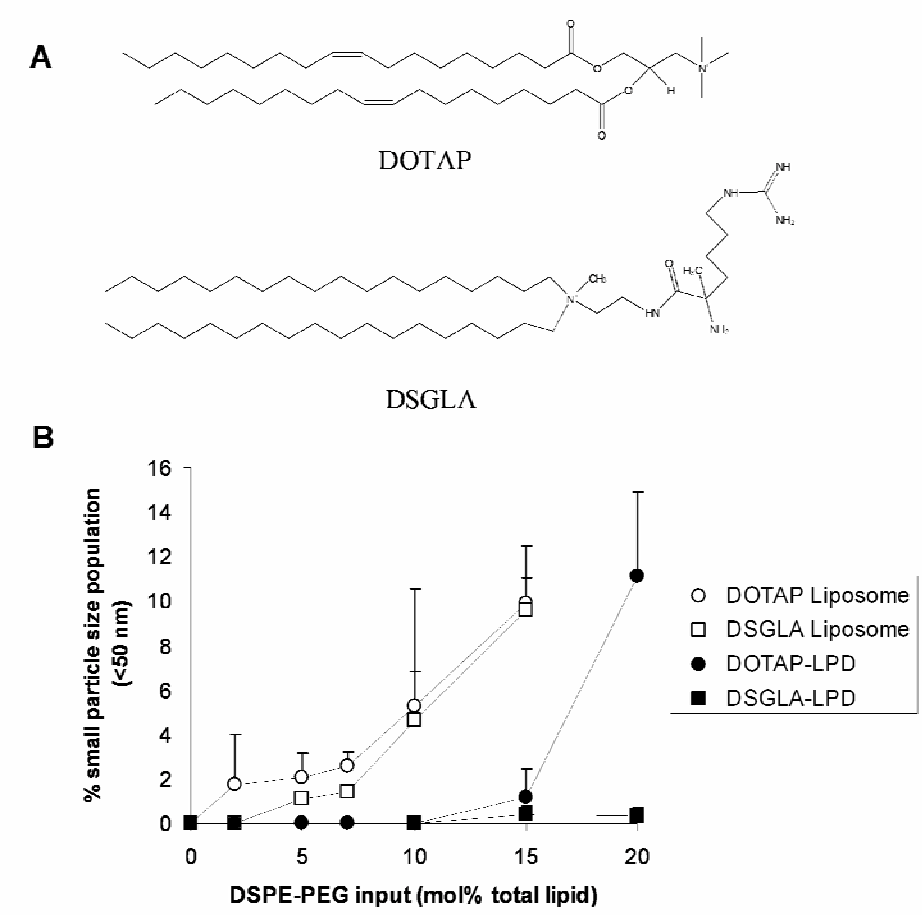

Figure 2.2 Stability of the nanoparticle formulations upon different degree of PEGylation.
(A) Chemical structures of DOTAP and DSGLA. (B) Size distribution of different PEGylated formulations. Data = mean ± SD, n = 4-6

2.3 RESULTS AND DISCUSSION

DSPE-PEG has been used widely in the lipid based nanoparticle formulations, such as liposomes, to increase the blood circulation time [36]. It is also known that incorporation of too much DSPE-PEG will disrupt the integrity of the lipid membrane due to its detergent like properties [37]. This causes the increase of membrane permeability and drug release. Since the unmodified LPD contains two lipid bilayer membranes, incubation with DSPE-PEG may strip off the membranes from the nanoparticles and form micelles of smaller particle size. Here, we examined the stability of nanoparticle formulations after the addition of different amounts of DSPE-PEG by measuring their particle size distribution. By using dynamic light scattering, only one narrow size distribution around 100 nm was revealed for all four formulations, i.e., liposomes and LPD composed of either DOTAP or DSGLA, before the addition of DSPE-PEG (**figure 2.2B**). However, after the addition of DSPE-PEG, a population of smaller particles appeared in a dose dependent manner for both DOTAP and DSGLA liposomes. It is noted that pure DSPE-PEG micelle was undetectable at the concentrations used in this experiment. Thus, the smaller size particles must came off from the nanoparticles upon the introduction of DSPE-PEG. The light scattering method can quickly determine the stability of the nanoparticles. The LPD formulations showed significantly higher stability compared to the liposomes. When 10 mol% of DSPE-PEG was added, the LPD formulations remained relatively stable, while the liposome formulations showed a significant increase in the smaller size population (~5%). The light scattering data (**figure 2.2B**) is consistent with the observation by TEM (**figure 2.3**), in which no distinct particles were found in the DOTAP liposomes after PEGylation; only tubular mixed micelles were present. On the other hand, nanoparticles around 100 nm in diameter were still found in

the PEGylated LPD formulation containing DOTAP (**figure 2.3**). It is also noticed that DSGLA (contains 3 positive charges)-LPD showed an improved stability compared to DOTAP (contains 1 positive charge)-LPD (**figure 2.2B**), suggesting that LPD was stabilized by charge-charge interaction. Dynamic light scattering is a convenient method to assess the relative stability of the particles. For example, smaller size particles were found in the TEM photographs of the PEGylated LPD (**figure 2.3**, arrow heads), while light scattering data showed no presence of smaller particles (**figure 2.2B**). It is known that particles of larger sizes showed significant higher light scattering compared to smaller size particles at the same concentration. Nevertheless, the dynamic light scattering data provided a quantitative comparison of the relative stability of different nanoparticle formulations.

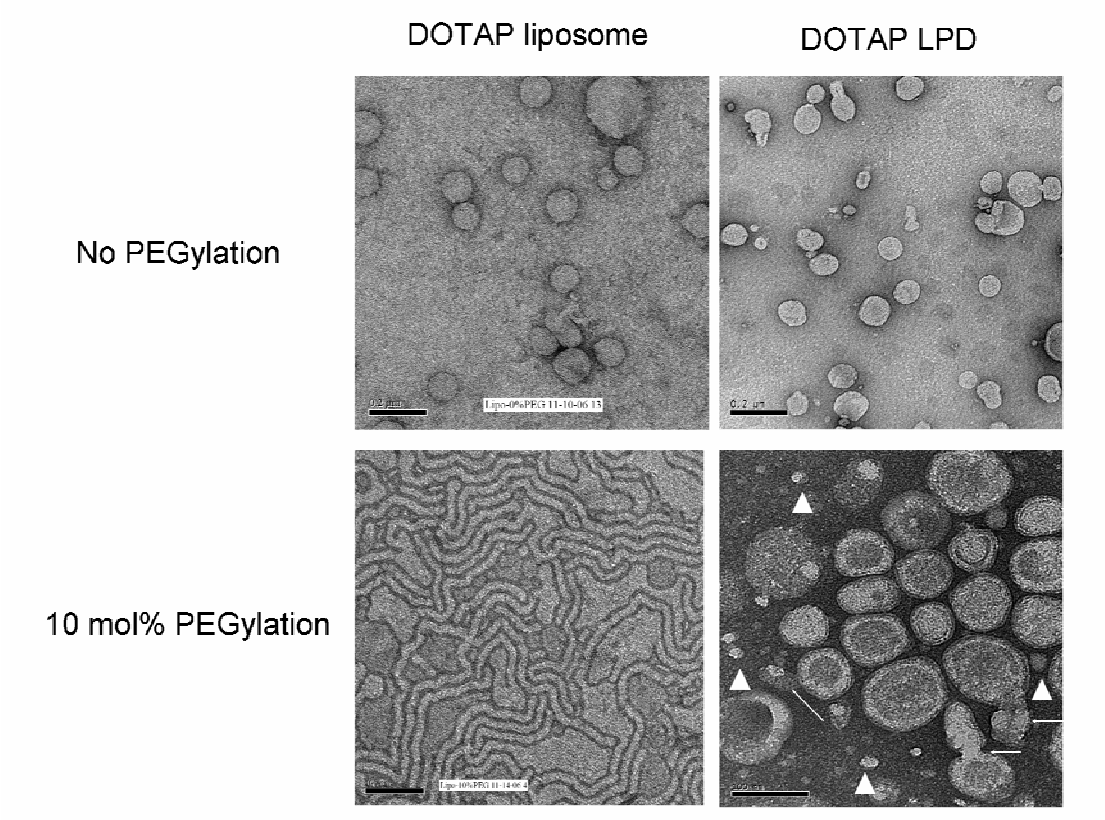

Figure 2.3 TEM photographs of liposomes/PEGylated liposomes and LPD/PEGylated LPD.
Upper panel scale bar = 200 nm, lower panel scale bar = 100 nm. Arrows indicate the "sprouts" of the particles and arrow heads indicate the small particles.

As can be seen in **figure 2.3**, after 10 mol% PEGylation, DOTAP liposomes had transformed into tubular micellar structures, indicating the instability of the formulation. In the PEGylated LPD, however, "sprouts" were found in some of the particles (**figure 2.3**, arrows), suggesting that the lipids in the surface of the LPD were being stripped off and became smaller particles (**figure 2.4**, arrow heads).

To further characterize the LPD nanoparticles, we used 10 mol% NBD-DOTAP labeled liposomes, 10 mol% DSPE-PEG-CF labeled DSPE-PEG or FAM-siRNA to prepare the PEGylated LPD. Sepharose CL 2B column was used to separate particles of different sizes. In this study, a neutral liposome formulation (DOPC/Cholesterol/NBD-PE = 49/49/2, molar ratio, mean particle size around 100 nm) was used to calibrate the column. Cationic liposomes and unmodified LPD containing excess positive surface charges formed aggregates in the elution medium (PBS) and thus, could not be studied by the chromatography. As shown in **figure 2.4A**, pure DSPE-PEG could be clearly separated from the 100 nm-nanoparticles by the size exclusion column. At least two particle populations were observed in the NBD-DOTAP labeled PEGylated LPD (**figure 2.4B**). The first major peak coincided with that of the 100 nm-nanoparticles, and the second peak lied between the peaks of micelles and 100 nm-nanoparticles. Nevertheless, the PEGylated liposomes (NBD-DOTAP labeled) showed less significant first peak but a smear of particle size distribution, suggesting the lipid membrane was disrupted in this formulation. The observation is consistent with the dynamic light scattering (**figure 2.2B**) and TEM data (**figure 2.3**). Moreover, the AUC of the first peak of the PEGylated LPD (NBD-DOTAP labeled) was about 37.2% (37.2 ± 4.6%, n = 3). The data suggest that approximately 37.2% of the total lipids were associated with the nanoparticles, while the rest of the lipids were stripped off by

the DSPE-PEG micelles and formed smaller particles (< 100 nm). As mentioned earlier, approximately 36.4% (36.4 ± 3.2%, n = 5) of the total lipids was located in the inner lipid bilayer of the LPD, suggesting that only the inner lipid bilayer stayed with the nanoparticles. The inner cationic lipid bilayer was in direct contact with the negatively charged surface of the nucleic acid/protamine core and therefore, was more tolerated to PEGylation compared to the outer bilayer. However, further increase of the input DSPE-PEG to 20 mol% caused damage of the supported bilayer. Only 24.2% of the total cationic lipids remained associated with the nanoparticles (data not shown), indicating that 35% of the lipids in the supported bilayer was removed. Although the inner bilayer of the LPD was stabilized by charge-charge interaction, it could only tolerate a finite amount of DSPE-PEG. **Figure 2.4C** shows that around 20.6% (20.6 ± 3.4%, n = 3) of the DSPE-PEG (DSPE-PEG-CF labeled) was incorporated with the nanoparticles (first peak) after heating, while about 80% of the DSPE-PEG formed smaller particles with the cationic lipids stripped off from the nanoparticles. **Figure 2.4D** indicates that the nanoparticles eluted with the first peak containing 90% of siRNA, 37.2% of the total lipids and 20.2% of the input DSPE-PEG was the major contributor for siRNA delivery for the PEGylated LPD formulation.

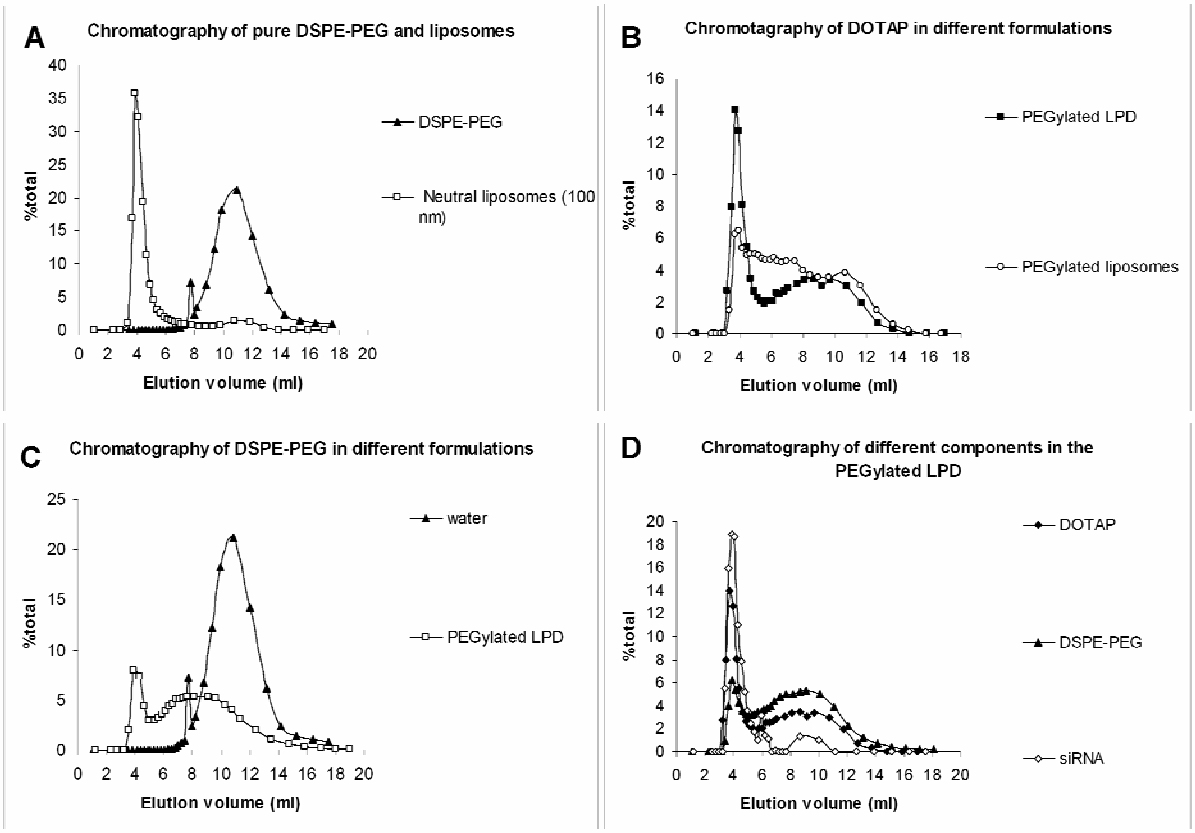

Figure 2.4 Size exclusion chromatography of different samples.
(A) chromatography of pure DSPE-PEG and liposomes; (B) chromatography of DOTAP in different formulations; (C) chromatography of DSPE-PEG in different formulations; (D) chromatography of different components in the PEGylated LPD. DOTAP liposomes was labeled with NBD-DOTAP, DSPE-PEG micelle was labeled with DSPE-PEG-CF and siRNA was labeled with FAM-siRNA. Data are representative chromatography from 2-3 batches of formulations.

Ten microliter of the PEGylated LPD contained 0.71 μg siRNA (loading amount for column), 36.71 nmole lipids and 3.99 nmole DSPE-PEG. The nanoparticles eluted in the first peak contained 0.64 μg siRNA, 13.66 nmole lipids and 0.81 nmole DSPE-PEG. Assuming that DSPE-PEG was inserted only into the outer leaflet of the supported bilayer and the lipid content in the outer and inner leaflet of the bilayer were the same, we calculated that 10.6 mol% of the outer leaflet was modified with DSPE-PEG. This led to a complete charge shielding, in which the zeta potential of the purified PEGylated LPD was -5.6 ± 4.5 mV (**figure 2.5C**).

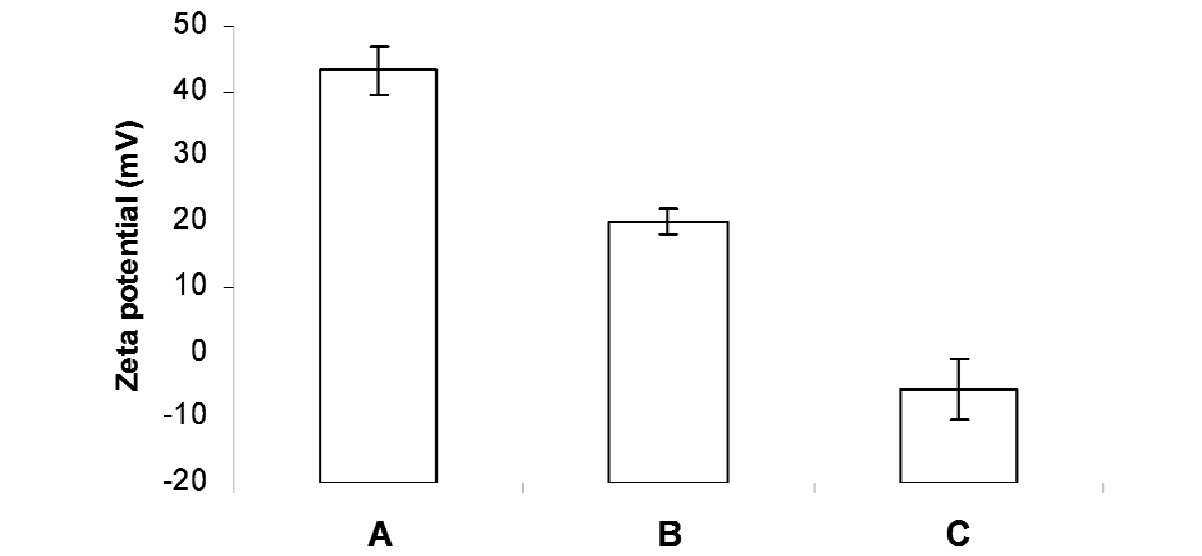

Figure 2.5 Zeta potential of different formulations.
(A) LPD; (B) LPD + 10 mol% DSPE-PEG; (C) LPD + 10 mol% DSPE-PEG after purified by the size exclusion column (first peak). Data = mean ± SD, n = 3

To demonstrate that the DSPE-PEG was incorporated onto the LPD, we conjugated the anisamide ligand (AA) onto the distal end of the PEG and compared the delivery efficiency of the LPD-PEG and LPD-PEG-AA into the sigma receptor expressing cells, NCI-H1299. The chemical structures of the DSPE-PEG and DSPE-PEG-AA are shown in **figure 2.6**. LPD-PEG-AA showed enhanced siRNA delivery into the receptor positive cells (4-fold increase) and the improved delivery was partially inhibited by excess amount of the free ligand (**figure 2.7**) [32,33]. The delivery efficiency of the LPD-PEG-AA was not enhanced in the receptor negative cells, CHO (data not shown). The data suggested that DSPE-PEG and DSPE-PEG-AA were incorporated onto the surface of the LPD. Once the AA ligand was attached to the LPD, the PEGylated LPD showed improved selectivity for sigma receptor positive cells.

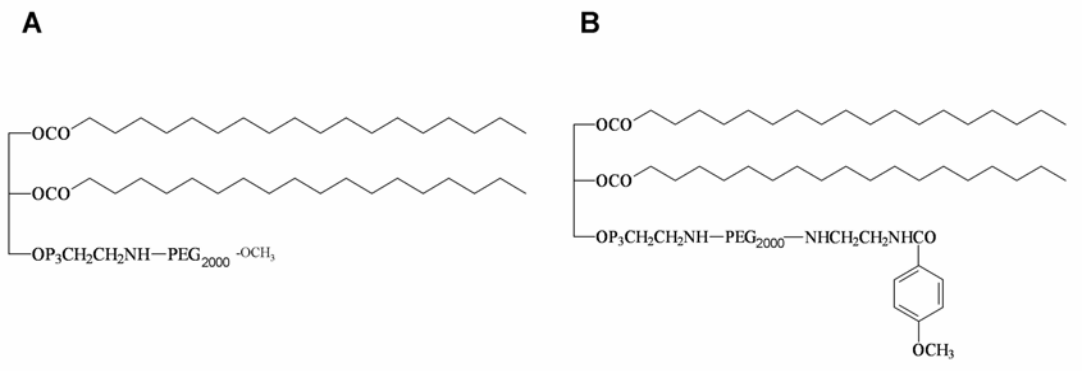

Figure 2.6 Chemical structures of DSPE-PEG (A) and DSPE-PEG-anisamide (B).

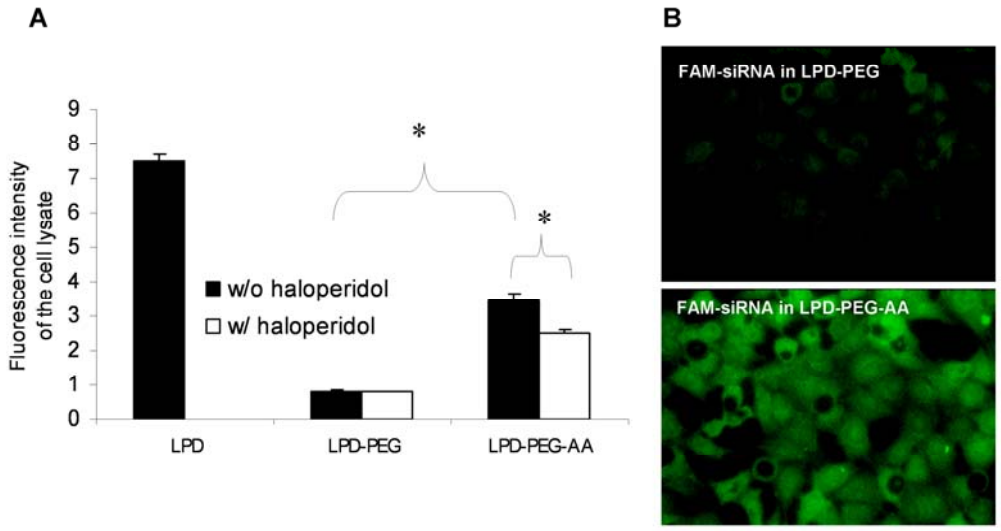

Figure 2.7 Fluorescence intensities of cells (A) and fluorescence photographs of cells (B) treated with FAM-siRNA containing formulations.
H1299 cells were incubated with different formulations at 37°C for 4 h in the presence (white bars) or absence (black bars) of 50 μM haloperidol. Cells were washed and lysis. Cells lysates were analyzed for fluorescence intensities by a fluorescence spectrometer (λex: 494 nm, λem: 519 nm). Alternatively, cells were imaged with a fluorescence microscope. * indicates the significant difference between two groups ($p<0.05$).

As shown in **figure 2.5**, the zeta potential of the LPD, PEGylated LPD and purified PEGylated LPD were 43.2, 20.04, and -5.6 mV, respectively. Approximately 90% siRNA was encapsulated in the purified PEGylated LPD, which was a neutral delivery vehicle. A neutral carrier is desirable for in vivo drug delivery because of its improved pharmacokinetics and reduced non-specific interaction with cells or serum protein.

To further investigate if the PEGylated LPD showed reduced RES uptake in the liver, we performed a liver perfusion assay. As shown in **figure 2.8**, 10 mol% PEGylated LPD showed little sinusoidal uptake in the liver, while 0 or 5 mol% PEGylated LPD had significant RES uptake. The data suggest that sufficiently PEGylated LPD showing reduced RES uptake in the liver may exhibit improved pharmacokinetics for delivering siRNA when i.v. administered.

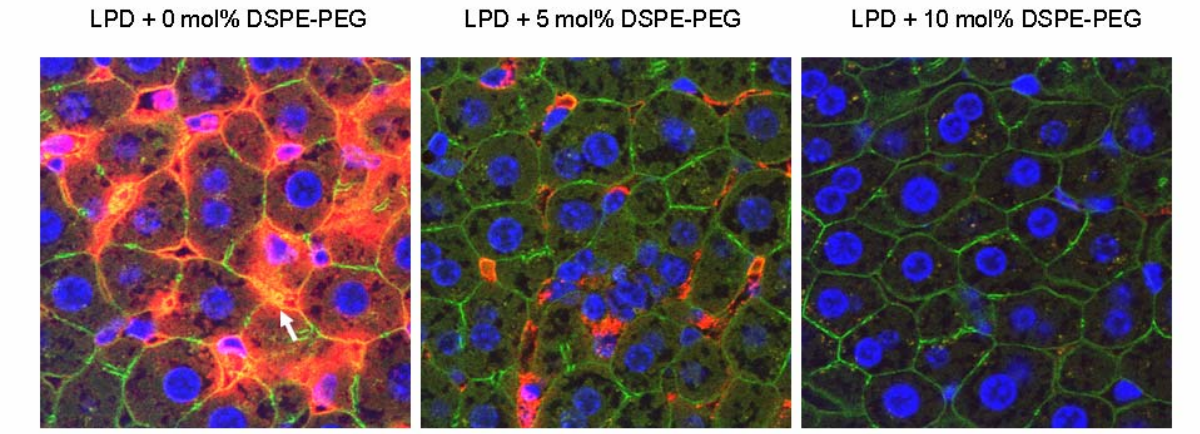

Figure 2.8 Liver sinusoidal uptake of cy3-siRNA (red) in different LPD formulations.
F-actin outlining the cellular morphology was stained with Alexa Fluor® 488 Phalloidin (green) and nuclei were stained with DAPI (blue). Magnification = 1,600 x. Data are representative pictures from 3 mice in each group.

Here, we proposed a model to describe the formation of the PEGylated LPD nanoparticles (**figure 2.9**). After the addition of DSPE-PEG micelles at 50^{o}C, the micelles acted like detergents and stripped off the outer lipid bilayer of the LPD. In the intermediate phase, "sprouts" (outer bilayer being stripped off from the LPD) were formed and eventually broken down into smaller PEGylated lipid particles. The inner lipid bilayer was stabilized by charge-charge interaction and therefore, remained intact. Around 20% of the input DSPE-PEG was inserted into the outer leaflet of the supported bilayer. Approximately 10.6 mol% of the leaflet was modified with DSPE-PEG, which completely shielded the surface charge of

the LPD. At such a high degree of PEGylation, the PEG was shown to present on the surface in the brush mode [38], suggesting the surface was fully protected. On the other hand, the cationic liposomes without supported bilayer were not stable upon the challenge of DSPE-PEG micelle. The bilayer was stripped off from the liposomes and became smaller particles.

Depending on the surface density and molecular weight of the PEG grafted to the lipid bilayer, three PEG conformations can be identified [39]. Factors controlling the PEG conformation include the distance between the PEG chains in the lipid bilayer (D) and the Flory dimension, R_F, which is defined as $aN^{3/5}$ (a is the persistence length of the monomer, N is the number of monomer units in the PEG) [40]. Three regimes can be defined: (1) when $D>2\ R_F$ (interdigitated mushrooms); (2) when $D<2\ R_F$ (mushrooms); and (3) when $D<\ R_F$ (brushes) [40]. For a 100 nm-liposome grafted with DSPE-PEG_{2000}, PEG chains have been found to be arranged in the mushroom mode in the presence of <4 mol% DSPE-PEG; in the transition mode when 4-8 mol% modification; and in the brush mode when >8 mol% PEGylation [38]. The brush configuration ensures that the entire surface of NP is covered [41]. However, over-crowdedness of the PEG on the surface may decrease the mobility of the polymer chains and thus decreases the steric hindrance effect [41]. Therefore, we believe that surface modification of PEG_{2000} slightly greater than 8 mol% is desirable for a stealth NP. In our formulation, the nanoparticle was 10.6 mol% modified with PEG_{2000}, which falls in the optimal condition.

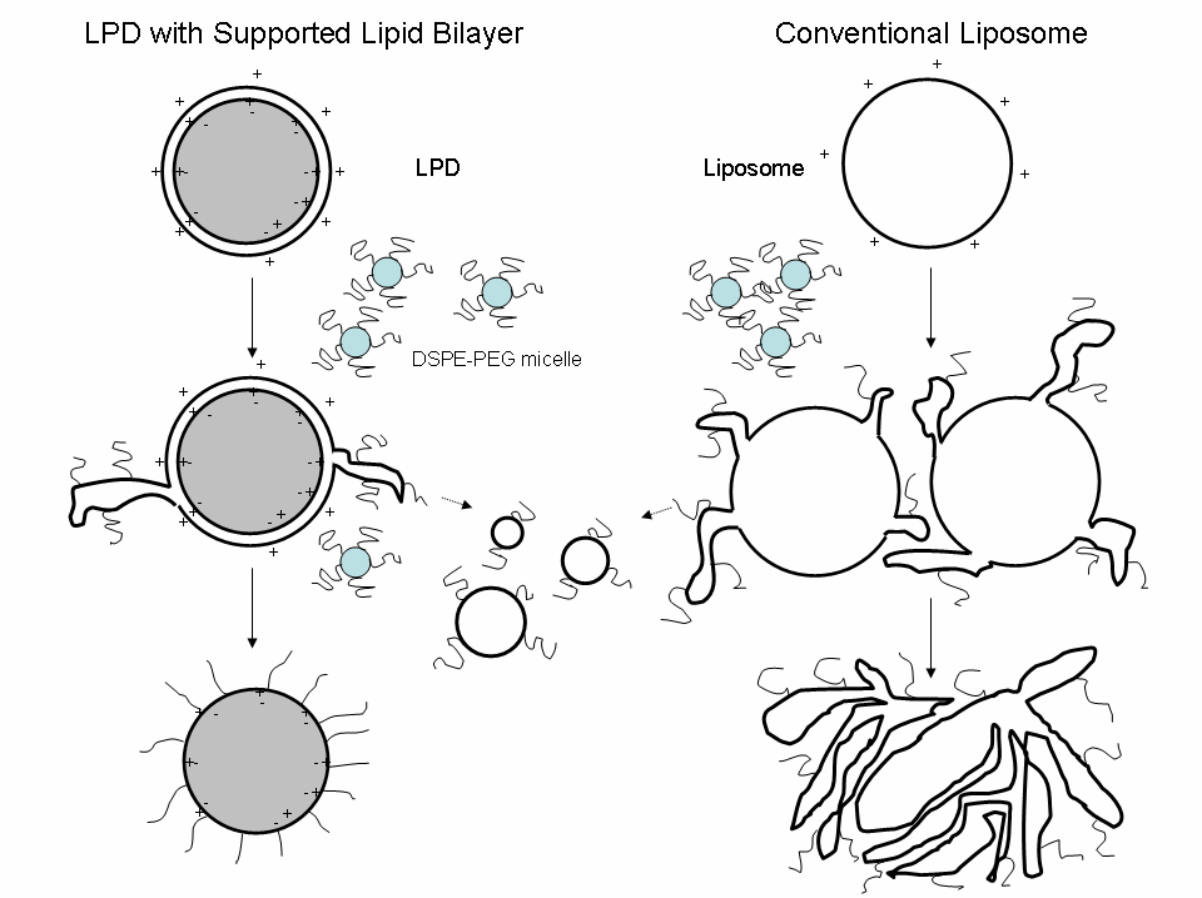

Figure 2.9 Proposed mechanism for the formation of PEGylated LPD.

In the following content, the LPD-PEG is referred to as the non-targeted nanoparticles (NP) and LPD-PEG-AA is referred to as the targeted nanoparticles.

3.0 TUMOR-TARGETED DELIVERY OF SIRNA BY SELF-ASSEMBLED NANOPARTICLES

We have developed a self-assembled nanoparticle (NP) that efficiently delivers small interfering RNA (siRNA) to the tumor by intravenous (i.v.) administration. The NP was obtained by mixing carrier DNA, siRNA, protamine, and lipids, followed by post-modification with polyethylene glycol and a ligand, anisamide. Four hours after i.v. injection of the formulation into a xenograft model, 70-80% of injected siRNA/g accumulated in the tumor, ~10% was detected in the liver and ~20% recovered in the lung. Confocal microscopy showed that fluorescent labeled siRNA was efficiently delivered into the cytoplasm of the sigma receptor expressing NCI-H460 xenograft tumor by the targeted NPs, whereas free siRNA and non-targeted NPs showed little uptake. Three daily injections (1.2 mg/kg) of siRNA formulated in the targeted NPs silenced the epidermal growth factor receptor (EGFR) in the tumor and induced ~15% tumor cell apoptosis. Forty percent tumor growth inhibition was achieved by treatment with targeted NPs, while complete inhibition lasted for 1 week when combined with cisplatin. The serum level of liver enzymes and body weight monitoring during the treatment indicated a low level of toxicity of the formulation. The carrier itself also showed little immunotoxicity.

3.1 INTRODUCTION

Selective oncogene silencing, mediated by small interfering RNA (siRNA), shows promise for cancer treatment. However, the obstacles in successfully delivering siRNA hinder the therapeutic viability of this treatment [1,4,42]. siRNA are susceptible to nuclease destruction and cannot penetrate the cell membrane when used in vivo due to the highly charged nucleic acid backbone. Although a variety of delivery systems have been developed for siRNA [2-4,12,19,24,43-51], the majority of the injected dose (ID) was taken up by the reticular endothelial system in the liver and spleen [52]. This typically left only 2-5% of the ID/g tissue for the tumor [49,52]; therefore, a more efficient delivery system still needs to be found.

Previously, we have shown that our nanoparticles (NPs) could efficiently deliver siRNA to the sigma receptor–expressing lung tumor cells (NCI-H1299), stimulate strong RNA interference effects and induce >80% apoptosis in vitro [33]. The targeting ligand, anisamide, used in the formulation had a moderate affinity (estimated at K_d ~30 nM) for sigma receptors and was shown to increase the intracellular delivery into prostate and lung cancer cells [33,34,53]. In this study, we used a more aggressive lung cancer cell line, NCI-H460, to grow highly vasculatured tumors in vivo. This is a pre-requisite for the enhanced permeability and retention (EPR) effect of any NP-based delivery systems [33,34,53]. In the **Chapter 2**, we have shown that the NP contained a supported lipid bilayer to tolerate a high degree of PEGylation (10.6 mol%) and thus, the reticuloendothelial uptake in the isolated liver perfusion model was completely inhibited. We hypothesized that the highly PEGylated NP would have much improved pharmacokinetics in vivo to achieve high tumor

accumulation. Additionally, anisamide ligand might further increase the cellular uptake and enhance the RNA interference effect.

The therapeutic target in this study was the epidermal growth factor receptor (EGFR). EGFR is over-expressed in a variety of tumors and has been shown to be associated with many adverse features of tumor, including increased proliferation, decreased apoptosis, enhanced metastasis, and resistance to chemo- and radiation therapy [54,55]. AntiEGFR therapy via tyrosine kinase inhibitors and monoclonal antibody has demonstrated great benefit for cancer patients [56-59]. Silencing EGFR by RNA interference is an alternative to antiEGFR therapy and has already shown some promising results [60-68]. EGFR silencing induces cell cycle arrest, apoptosis, tumor cell growth inhibition, and chemosensitization in vitro and in vivo [60-68].

3.2 MATERIALS AND METHODS

3.2.1 Materials

NCI-H460 (human lung cancer cells) were obtained from American Type Culture Collection. Cells were maintained in Roswell Park Memorial Institute medium 1640 supplemented with 10% fetal bovine serum (Invitrogen, Carlsbad, CA), 100 U/ml penicillin, and 100 µg/ml streptomycin (Invitrogen, Carlsbad, CA). NCI-H460 cells were shown to be sigma receptor positive by immunostaining and Western blot (data not shown). Primary antibodies against EGFR (epidermal growth factor receptor) (rabbit polyclonal), PAR-4 (prostate apoptotic response 4) (mouse monoclonal), AIF (apoptosis inducing factor) (rabbit polyclonal) and

actin/β-actin (mouse monoclonal) were purchased from Santa Cruz Biotechnologies (Santa Cruz, CA).

3.2.2 Experimental animals

Female athymic nude mice of age 6-8 weeks and female C57BL/6 mice of age 6-7 weeks (16-18 g) were purchased from Charles River Laboratories (Wilmington, MA). All work performed on animals was in accordance with and permitted by the University of North Carolina Institutional Animal Care and Use committee.

3.2.3 NP preparations

NPs were prepared by the method described in **Chapter 2**. Control siRNA that targets the sequence 5′-AATTCTCCGAACGTGTCACGT-3′ and EGFR siRNA that targets the sequence 5′-AACACAGTGGAGCGAATTCCT-3′ as described previously [67] were synthesized in Dharmacon (Lafayette, CO). The control sequence does not match any human genome sequence. FAM (fluorescein)-siRNA was also obtained from Dharmacon (Lafayette, CO).

3.2.4 In vitro cellular uptake study

NCI-H460 cells ($1X10^5$ cells/well) were seeded in 12-well plates (Corning Inc., Corning, NY) 20 h before experiments. Cells were treated with different formulations at a concentration of 320 nM of FAM-siRNA in serum containing medium at 37 ^oC for 4 h. Cells

were washed twice with PBS, fixed with 1% paraformaldehyde in PBS at room temperature for 15 min, mounted onto a glass slide, and imaged with a Nikon fluorescence phase contrast optical microscope.

3.2.5 In vitro gene silencing study

NCI-H460 cells ($1X10^5$ cells/well) were seeded in 12-well plates (Corning Inc., Corning, NY) 20 h before experiments. Cells were treated with different formulations at a concentration of 120 nM siRNA in serum containing medium at 37 ^oC for 48 h. Cells were washed, collected and analyzed for EGFR contents by Western Blotting. Western blot method is described in **3.2.10**,

3.2.6 In vitro cytotoxicity study.

$1X10^5$ NCI-H460 cells per well were seeded in 12-well plates (Corning Inc., Corning, NY) 20 h before experiments. Cells were treated with different formulations at a concentration of 320 nM siRNA in serum containing medium at 37 ^oC for 48 h. Cells were washed by PBS twice, trysinized, collected, incubated with propidium iodide (4 μl of 1 mg/ml stock for 1 ml sample), and analyzed by a BD FACScanto digital flow cytometer (San Diego, CA).

3.2.7 Immunocytochemistry

$1X10^5$ NCI-H460 cells per well were seeded in 12-well plates (Corning Inc., Corning, NY) 20 h before experiments. Cells were treated with different formulations at a concentration of

120 nM siRNA in serum containing medium at 37 ^{o}C for 48 h. Cells were washed twice with PBS and fixed with 1% paraformaldehyde in PBS at room temperature for 15 min. Immunostaining was then performed with rabbit anti-mouse AIF (apoptosis inducing factor) antibody (Santa Cruz Biotechnology, Santa Cruz, CA) and goat anti-rabbit IgG conjugated with FITC (Fluorescein isothiocyanate) (Santa Cruz Biotechnology, Santa Cruz, CA). Cells were mounted with DAPI (4',6-diamidino-2-phenylindole) containing medium (Vectorshield ®, Vector Lab, Inc. Burlingame, CA) and imaged by a Nikon fluorescence phase contrast optical microscope.

3.2.8 Pharmacokinetics (PK) study.

NCI-H460 cells (5×10^6) were subcutaneously injected into the right flank of nude mice. When tumors reached the size of ~1 cm^2, mice were i.v. injected with FAM-siRNA in different formulations at the dose of 1.2 mg/kg. At different time points, 50-100 μl of blood was collected from the tail artery and serum was isolated. Ten microliters of serum was mixed with 90 μl of lysis buffer (0.1% sodium dodecyl sulfate in PBS) and incubated at 65 °C for 10 min, followed by the addition of 200 μl methanol and incubation at 65 °C for 10 min. The sample was centrifuged at 14,000 rpm for 5 min and 200 μl supernatant was transferred to a black 96-well plate (Corning, Corning, NY). The fluorescence intensity of the sample was measured by a plate reader (Bioscan, Washington, DC) at λ_{ex}: 485 nm and λ_{em}: 535 nm. FAM-siRNA concentration in each sample was calculated from a standard curve. This extraction method provided 98% recovery of free FAM-siRNA and 48% recovery for

FAM-siRNA containing NP. The FAM-siRNA concentration was corrected for the degree of sample recovery.

3.2.9 Tissue distribution and tumor uptake study

Mice with tumor size of ~1 cm^2 were i.v. injected with FAM-siRNA in different formulations (1.2 mg/kg). Four h later, mice were killed and tissues were collected and imaged by the IVIS Imaging System (Xenogen Imaging Technologies, Alameda, CA). To quantify the accumulated doses, the excised tissues were homogenized in 300 or 1,000 μl lysis buffer (1,000 μl for livers and 300 μl for others) and incubated at 65 °C for 10 min. One hundred microliter of supernatant was collected after centrifugation at 14,000 rpm for 10 min. FAM-siRNA in the supernatant was extracted and quantified by the method described in the PK study. The accumulated dose in each tissue was calculated from a standard curve obtained by spiking known amounts of FAM-siRNA or FAM-siRNA containing NP in tissues obtained from uninjected animals. Alternatively, tumors were sectioned (7 μm thick) by a cryostat (H/I Hacker Instruments & Industries, Winnsboro, SC). Sections were counterstained with DAPI and imaged using a Leica SP2 confocal microscope.

3.2.10 Immunohistochemistry and Western blot

NCI-H460 xenograft tumor-bearing mice (tumor size ~1 cm^2) were i.v. injected with siRNA in different formulations (1.2 mg siRNA/kg, one injection per day for 3 days). One day after the third injection, mice were killed and tumor samples were collected. Tumors were frozen-sectioned and 7 μm thick section samples were immunostained with primary antibodies and

visualized with kits from Dakocytomation [DakoCytomation Envision + Dual Link System-HRP (DAB+), DakoCytomation, Carpinteria, CA]. Samples were imaged by using a Nikon Microphot SA microscope. The percentage of AIF nuclear localization was calculated based on 30 random images obtained from three individual tumors. Total protein (40 μg) isolated from the tumors was loaded on a polyacrylamide gel and electrophoresed. Protein bands in the gel were then transferred to a polyvinylidene difluoride and the EGFR was probed by antibodies. The level of the target proteins in each lysate was detected by enhanced chemiluminescence using ChemiGlow (Alpha Innotech, San Leandro, CA) followed by detection by the AlphaImager (Alpha Innotech, San Leandro, CA).

3.2.11 Tumor growth inhibition study.

NCI-H460 xenograft tumor-bearing mice (size 25-40 mm^2) were i.v. injected with siRNA containing formulations at the dose of 1.2 mg/kg (one injection per day for 3 days). For the chemocombination treatment, cisplatin (3 mg/kg) were intraperitoneally (i.p.) administered from the 3rd to 5th day after the first siRNA injection. Tumor growth in the treated mice was monitored thereafter. Mouse body weight was also monitored.

3.2.12 Cytokine induction studies.

Female athymic nude mice or C57BL/6 mice were injected with siRNA in different formulations at the dose of 1.2 mg siRNA/kg. Two h after the injection, blood samples were collected and serum was isolated. Tumor necrosis factor, interleukin-6, interleukin- 12 (BD Biosciences, San Diego, CA) and interferon-α levels (PBL Biomedical Laboratories,

Piscataway, NJ) were measured by enzyme-linked immunosorbent assay according to the manufacturer's protocol. MDM2 (mouse double minute 2) siRNA (target sequence: 5′-GCUUCGGAACAAGAGACUC-3′) without any known immunostimulatory sequences (5′-GUCCUUCAA-3′ and 5′-UGUGU-3′) [20,69] was used as a negative control. Calf thymus DNA alone was formulated into targeted NPs and injected into the mice at the dose of 2.4 mg DNA/kg. This formulation is also regarded as the empty NP (without siRNA). Targeted NPs containing EGFR siRNA and luciferase plasmid DNA were also prepared and injected.

3.2.13 Liver enzyme assay

Female athymic nude mice of age 6-7 week (Charles River Laboratories) were injected with siRNA in different formulations at the dose of 1.2 mg/kg. Two h after injections, serum samples were obtained and the liver enzyme [aspartate aminotransferase (AST) and alanine aminotransferase (ALT)] levels were analyzed by Antech Diagnostics.

3.2.14 Statistical analysis

All statistical analyses were performed by the one-way ANOVA or a two-tailed student t-test. Data were considered statistically significant when P value was less than 0.05.

3.3 RESULTS

3.3.1 PK studies, tissue distribution, and intracellular uptake of siRNA

Free FAM-siRNA was eliminated rapidly from the blood and the concentration was under the detection limit after a 40-minute time point (**figure 3.1**). In 40 min, only 1% ID of free siRNA was detected in the blood. No significant difference in the PK profiles was observed between the tumor free and the tumor-bearing mice treated with free siRNA. NP significantly prolonged the circulation of siRNA and there was no difference in PK between the targeted and nontargeted NPs. NPs showed a rapid distribution phase, in which serum concentrations dropped to 1/10 within 40 min. After that, concentrations remained steady for at least 24 h. Tumor-bearing mice cleared the NPs from the blood more quickly than the tumor-free mice. In 2 min, almost a 100% ID of the NPs remained in the blood of the tumor free mice, while only a 25% ID remained in that of the tumor-bearing mice. At the terminal phase (80 min-24 h), a 5-10% ID was detected in the blood of the tumor free mice, while only 1-2% ID was recovered in that of the tumor-bearing mice. The dose recoveries in the major organs of mice treated with free siRNA and siRNA in NP were ~30 and 60%, respectively.

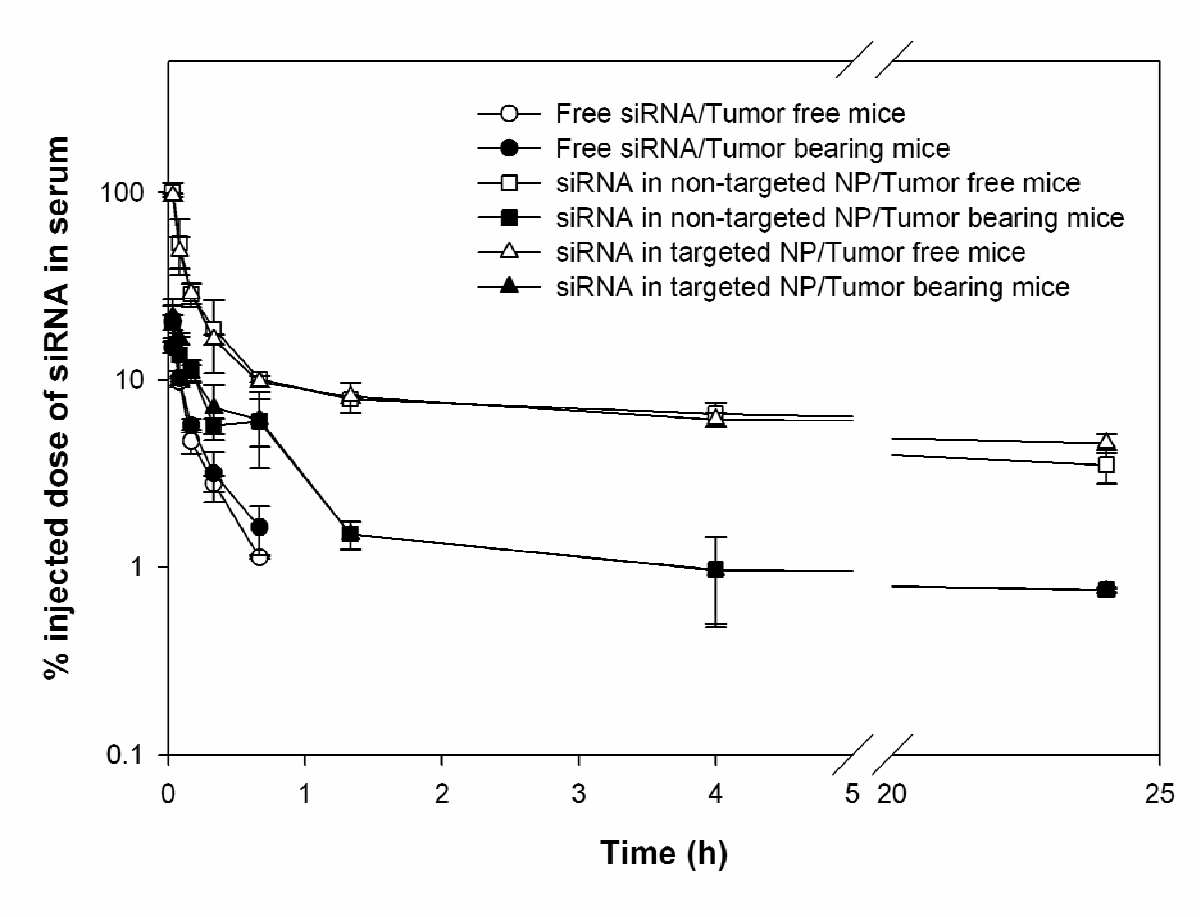

Figure 3.1 Serum concentration profiles of FAM-siRNA in different formulations.
Data = mean ± SD, n = 4-8

The PK profiles were fitted with a non-compartment model using the WinNonlin program and the key PK parameters were obtained (**Table 3.1**). For free siRNA, the parameters obtained from the tumor free and the tumor-bearing mice were similar to each other. NPs significantly increased the terminal phase halflife ($t_{1/2}$) 80-fold to 100-fold, and increased the area under the curve 15-fold to 100-fold and decreased the clearance 15-fold to 100-fold for siRNA. Again, there was no difference between the parameters of targeted and non-targeted NPs. However, the presence of tumor significantly changed some of the parameters of the NP. The area under the curve was reduced fourfold to sixfold, the clearance was increased fourfold to sixfold, and the steady state volume of distribution (V_{ss}) was

increased fivefold to sixfold in the tumor-bearing mice compared to the tumor free mice. The $t_{1/2}$ and mean residence time remained unchanged in the presence of tumor.

Table 3.1 Comparison of pharmacokinetic parameters of FAM-siRNA in different formulations in either NCI-H460 xenograft tumor-bearing mice or tumor free mice[a]

	T1/2 (λ_z) (h)	AUC (h·μg/ml)	CL (ml/h/kg)	MRT (h)	V_{ss} (ml/kg)
Free siRNA/tumor-bearing mice	0.29± 0.04	1.08± 0.03	1030.85± 66.5	0.36± 0.07	372.34± 63.21
Free siRNA/tumor free mice	0.25± 0	1.17± 0.08	1109.43± 28.65	0.25± 0.01	274.21± 17.89
siRNA in non-targeted NP/tumor-bearing mice	27.88± 11.3	16.71± 3.08	73.87± 15.08	37.43± 16.83	2609.91± 723.89
siRNA in non-targeted NP/tumor free mice	21.58± 5.98	72.6± 13.73	16.98± 3.56	28.42± 9.37	462.12± 89.25
siRNA in targeted NP/tumor-bearing mice	20.83± 5.86	15.25± 2.16	79.75± 11.86	27.11± 6.52	2127.43± 343.29
siRNA in targeted NP/tumor free mice	31.43± 8.26	98.68± 21.63	12.53± 2.54	43.63± 11.7	526.88± 25.25

[a] The serum concentration profiles (**figure 3.1**) were analyzed with the WinNonlin program and the key parameters were obtained.

We employed Xenogen IVIS imaging system to visualize the FAM-siRNA distribution in major tissues in the mice 4 h after i.v. injections. As shown in **figure 3.2a**, fluorescence signals were hardly detected in the tissues collected from the mice treated with free siRNA. While the liver showed the strongest signal, it was still minimal. Among the tissues excised from the mice treated with NP, the NCI-H460 xenograft tumors showed the strongest signal and all other tissues showed only background to moderate signals. In the quantitative results (**figure 3.2b**), the liver, lung, and tumor showed comparable uptake of free siRNA ranging from 10 to 20% ID/g. Other tissues showed minimal uptake of free siRNA (< 5% ID/g). Non-targeted and targeted NP had similar tissue distribution patterns, in which 70-80% ID/g accumulated in the tumor, whereas both the lung and liver took up <20% ID/g. The uptake of siRNA formulated in NP was under the detection limit in the heart,

spleen, and kidney. The bioavailability of siRNA in the tumor tissues was examined by confocal microscopy. As shown in **figure 3.3** (xyz images), the targeted NP showed strong cytosolic delivery of FAM-siRNA, while the non-targeted NP was less efficient in intracellular delivery and free siRNA showed no delivery. The percentages of fluorescence positive cells for free siRNA, non-targeted NP, and targeted NP were <1%, 5%, and 30%, respectively. The distribution of fluorescence in the tumor was heterogeneous. We used z-axis imaging to further address the intracellular delivery efficiency. Blue arrows indicate the extracellular space and pink arrows show the intracellular uptake of FAM-siRNA (**figure 3.3** xzy images). A majority of the siRNA formulated in non-targeted NPs remained in extracellular space while the siRNA in targeted NPs was mostly internalized into the cells.

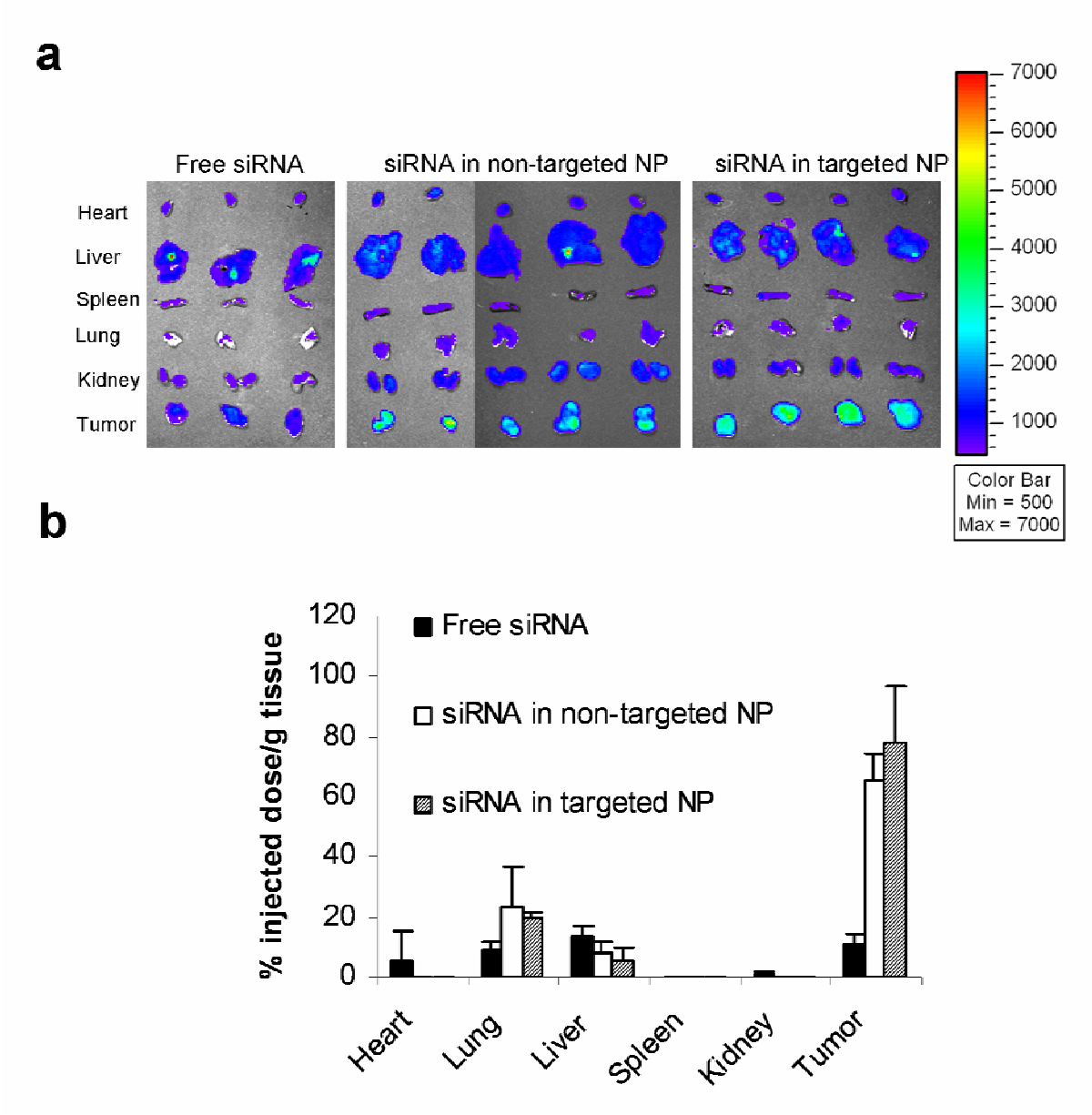

Figure 3.2 Tissue distribution study.
(a) Fluorescence signal of FAM-siRNA in different tissues detected by the Xenogen IVIS™ imaging system; (b) Tissue distribution of FAM-siRNA in different formulations. Data = mean ± SD, n = 3-4.

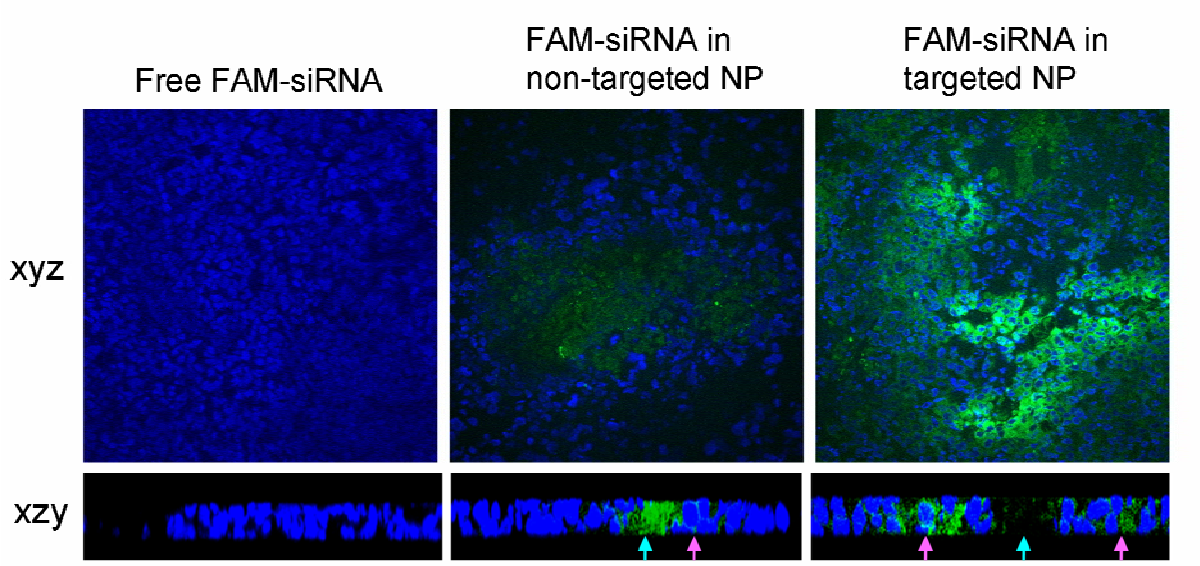

Figure 3.3 Tumoral uptake of FAM-siRNA in different formulations.
Blue arrows indicate the extracellular space and pink arrows indicate the intracellular uptake of FAM-siRNA. Magnification = 400X (xyz images), 630X (xzy images)

3.3.2 EGFR gene silencing, apoptosis induction, and tumor growth inhibition

To examine the biological activities of siRNA, EGFR levels in the tumor were detected by immunohistochemistry (**figure 3.4a** upper) and Western blot analysis (**figure 3.5**). The EGFR in NCI-H460 tumor was silenced by siRNA in targeted NPs. The non-targeted NPs showed only a partial effect, whereas free siRNA and the control siRNA in targeted NPs showed no effect. We also examined the apoptotic markers in the tumor (**figure 3.4a** middle and bottom). Prostate apoptotic response 4 levels were elevated after the treatment of siRNA in targeted NPs, while siRNA in non-targeted NPs showed only a moderate effect. Other control treatments had little effect. Immunostaining of the AIF showed similar results, in which siRNA in targeted NPs induced significant nuclear translocation of AIF (**figure 3.4a** bottom, $P < 0.01$). We calculated the percentage of AIF nuclear translocation to quantify the percentage of apoptosis. Tumor apoptosis in mice treated with PBS, free siRNA, siRNA in

non-targeted NPs, siRNA in targeted NPs, and control siRNA in targeted NPs were 2, 3, 7, 15, and 3%, respectively (**figure 3.4b**). Three injections of siRNA in targeted NPs showed a partial inhibition of tumor growth similar to that of i.p. cisplatin (**figure 3.6**). However, 2 weeks later, the tumor growth rate became comparable to the untreated control. Other control treatments had no effects. Combination of siRNA (formulated in targeted NP) and cisplatin completely inhibited tumor growth for an entire week. Tumor growth, however, resumed after 1 week.

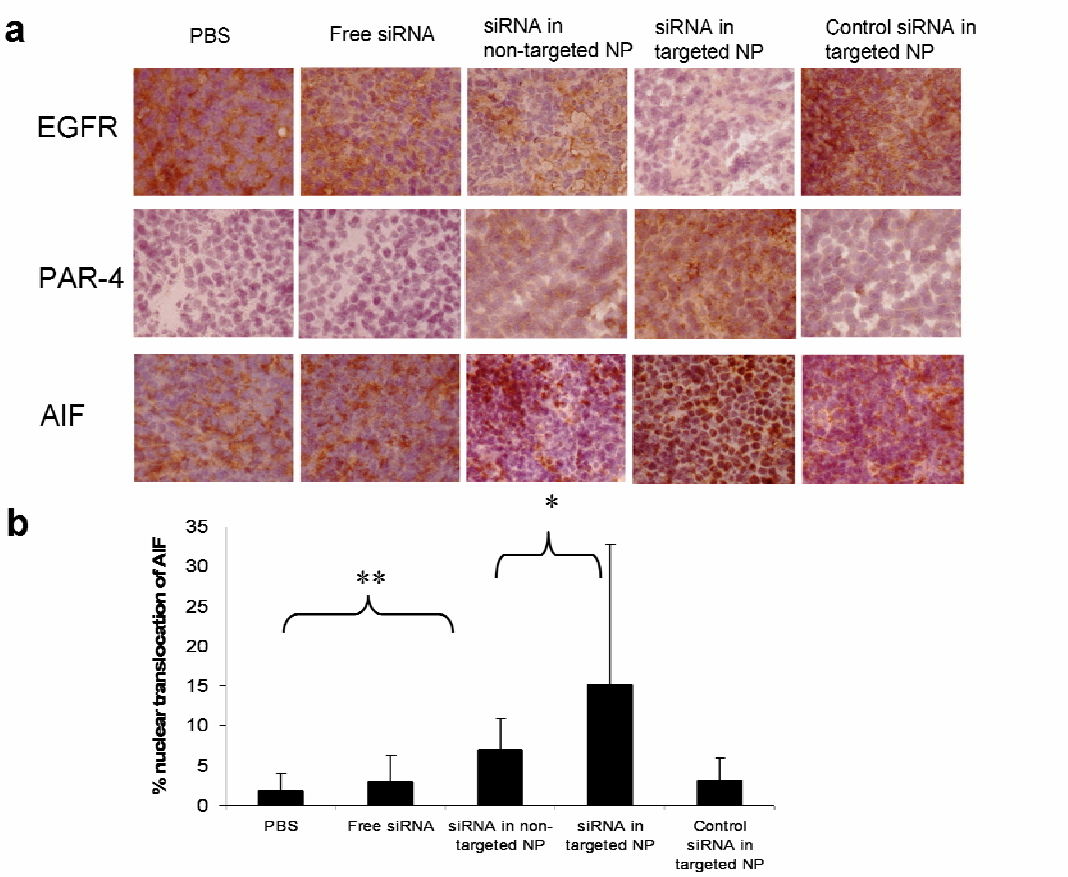

Figure 3.4 Immunohistochemical analysis of the tumor samples.
(a) Immunohistochemical staining on tumor sections: EGFR, PAR-4, and AIF. Magnification = 200X. (b) Quantitative analysis of nuclear translocation of AIF in the tumors treated with different formulations. ** indicates $p<0.01$, * indicates $p<0.05$

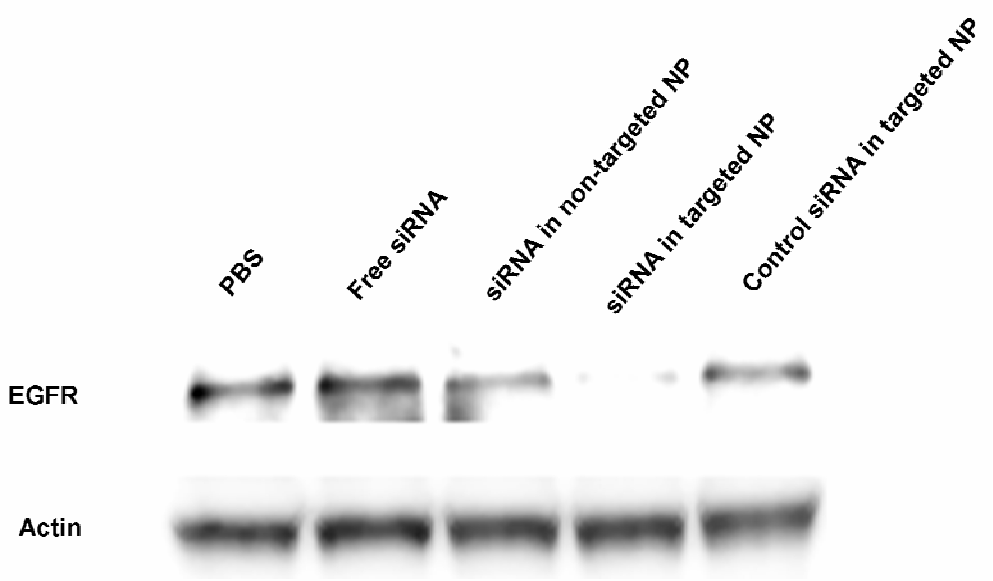

Figure 3.5 Western blot analysis of EGFR in the NCI-H460 xenograft tumor after treatment with different formulations.

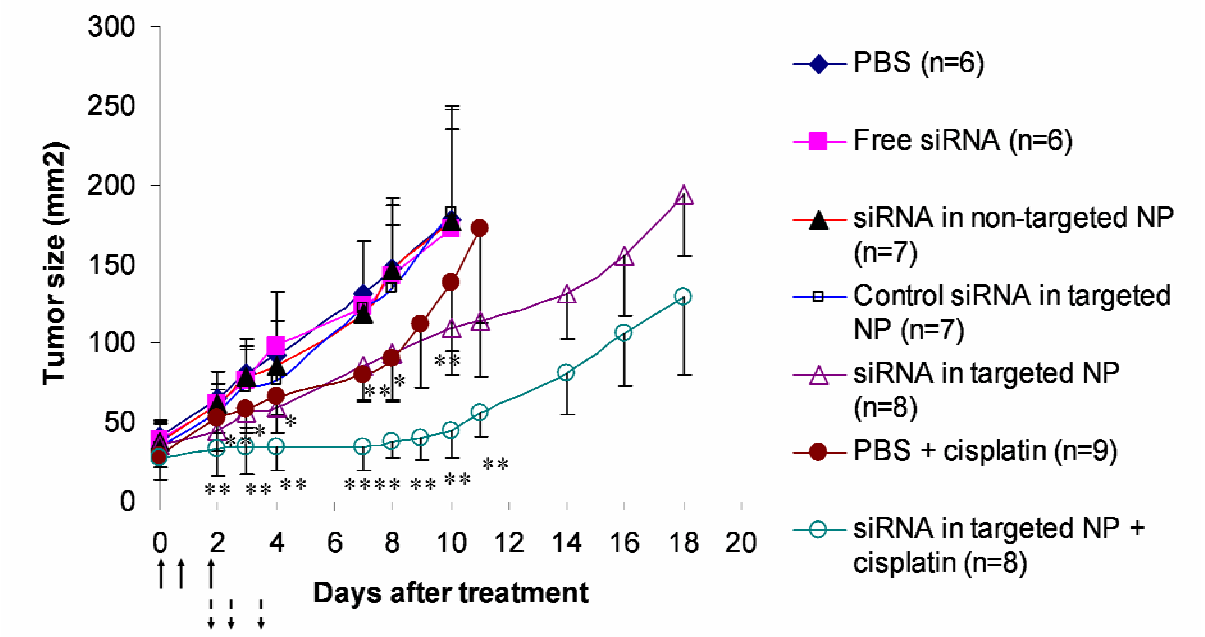

Figure 3.6 NCI-H460 xenograft tumor growth inhibition by siRNA in different formulations with or without the combination of cisplatin.
Solid arrows indicate the i.v. administrations of siRNA (1.2 mg/kg) and dash-line arrows indicate the i.p. injections of cisplatin (3 mg/kg). Data = mean ± SD, n = 6-9. * indicates $p<0.05$, ** indicates $p<0.01$

3.3.3 Toxicity and immune response studies in normal mice

As shown in **figure 3.7a**, siRNA alone (group B) or when formulated with calf thymus DNA into NPs induced a very mild production of inflammatory cytokines in the athymic nude mice (groups C-E). However, when plasmid DNA was co-formulated with siRNA (group G), the formulation became very immunogenic. In the C57BL/6 mice model (**figure 3.7b**), free siRNA (group B) did not induce cytokine production, while siRNA formulated in NPs (groups C and D) induced a significant production of all analyzed cytokines, except for the tumor necrosis factor. Targeted NPs (group D) induced higher levels of cytokines compared to the non-targeted formulation (group C). Unexpectedly, targeted NPs containing MDM2 siRNA (with no identifiable immunostimulatory motifs, group E) induced significantly higher levels of cytokines than the one containing EGFR siRNA (group D). Empty NP (group F) showed very mild immunotoxicity. When using plasmid as the carrier DNA in the targeted NP formulation (group G), all inflammatory cytokines were induced to high levels. Additionally, serum levels of AST and ALT in mice treated with siRNA in different formulations were all in the normal range (**figure 3.8**). Mouse body weight did not change significantly during the siRNA treatment (**figure 3.9**).

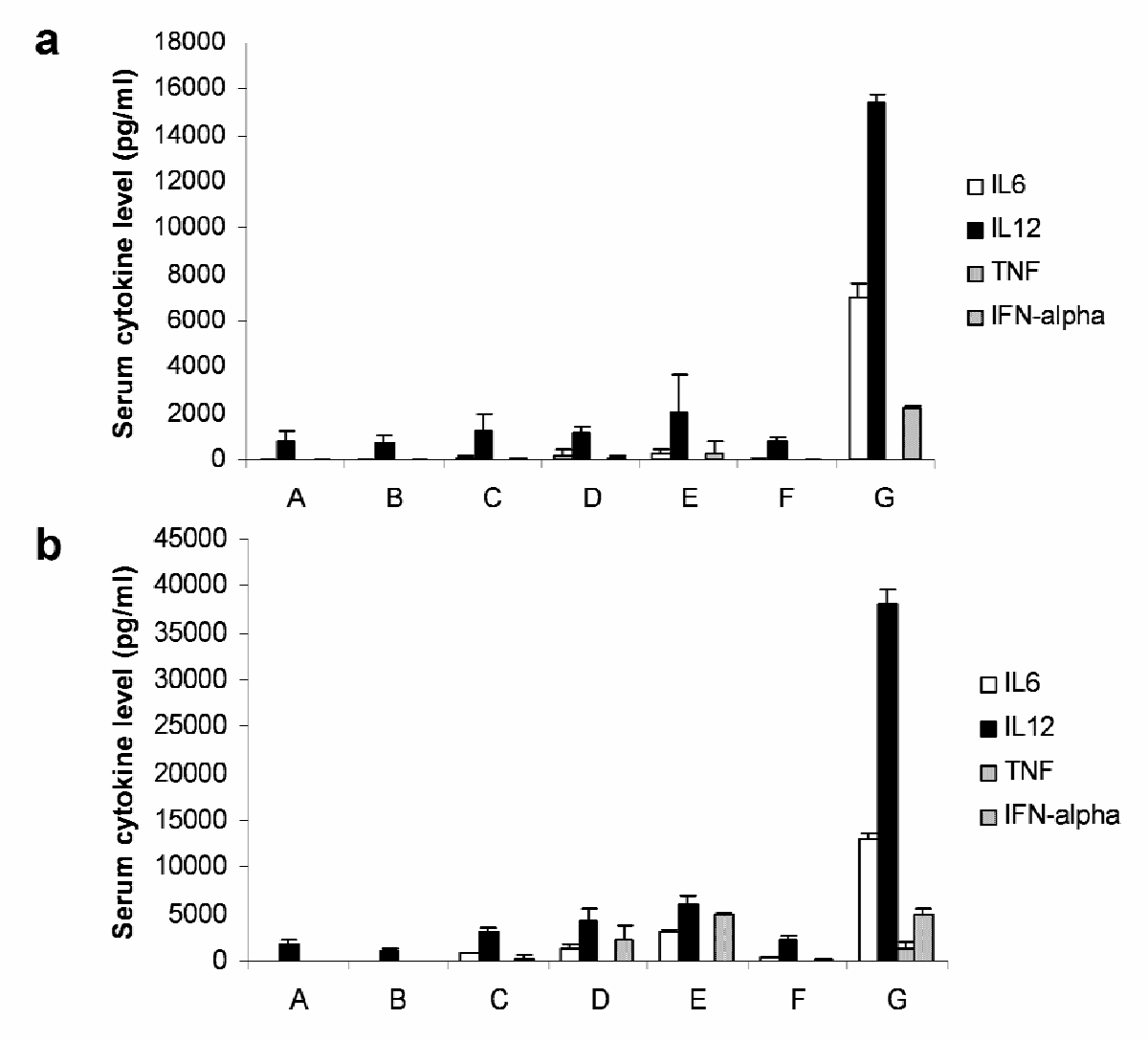

Figure 3.7 Serum cytokine analysis.
Serum cytokine levels in the athymic nude mice (a) and C57BL/6 mice (b) 2 h after the injection of different formulations at the dose of 1.2 mg siRNA/kg (2.4 mg DNA /kg for group F). A, PBS; B, EGFR siRNA in PBS; C, EGFR siRNA and calf thymus DNA in non-targeted NP; D, EGFR siRNA and calf thymus DNA in targeted NP; E, MDM2 siRNA and calf thymus DNA in targeted NP; F, calf thymus DNA in targeted NP (empty NP); G, EGFR siRNA and plasmid DNA in targeted NP. Data = mean ± SD, n = 3-8.

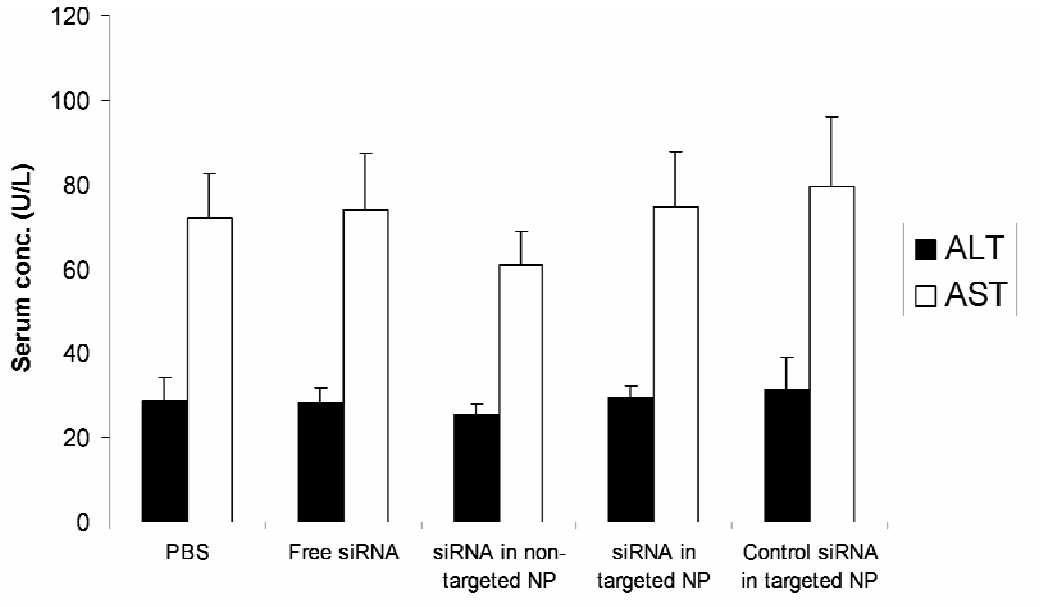

Figure 3.8 Serum ALT and AST analysis.
Serum ALT and AST levels in the mice 2 h after the treatment of PBS or siRNA in different formulations at the dose of 1.2 mg/kg. Data = mean ± SD, n = 4.

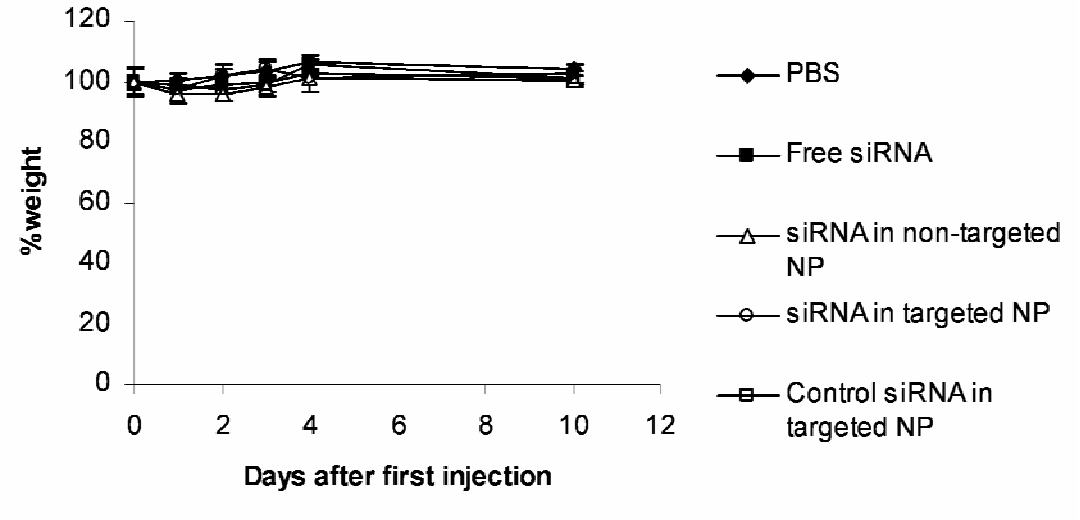

Figure 3.9 Mouse body weight during the treatment of different siRNA formulations.

3.4 DISCUSSION

In the in vitro preliminary studies, we showed that the targeted NP delivered a significantly higher amount of siRNA into NCI-H460 cells and showed a stronger gene silencing effect compared to non-targeted NP (**figure 3.10**). Targeted NP silenced the EGFR at the concentration of 120 nM (**figure 3.10b**). The cytotoxicity of the NP was siRNA sequence and formulation dependent (**figure 3.11**). The cell death mechanism was confirmed to be apoptosis by means of immunostaining of the apoptosis inducing factor (AIF) (**figure 3.11b**).

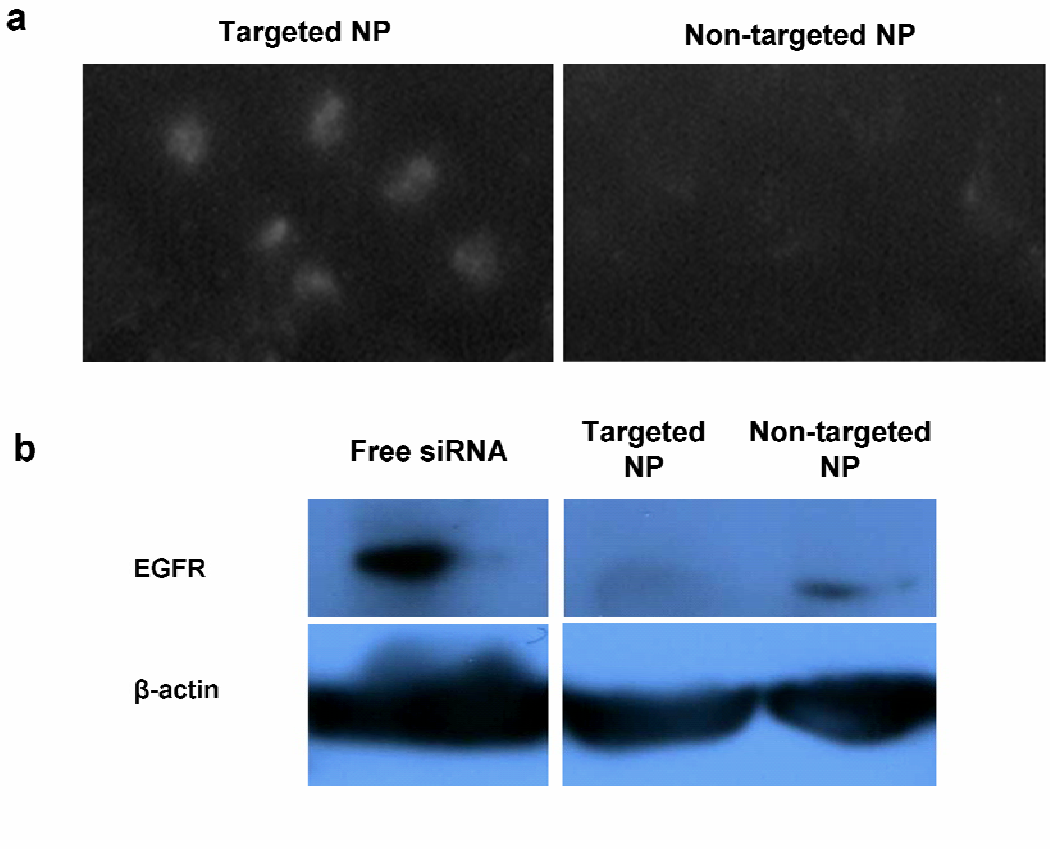

Figure 3.10 In vitro cellular uptake and gene silencing analysis
(a) Fluorescence photographs of NCI-H460 cells after treatment with FAM-siRNA in non-targeted NP or targeted NP at the conc. of 320 nM for 4 h. Magnification = 200X. (b) Western blot analysis of NCI-H460 cells after treatment with siRNA in different formulations at the conc. of 120 nM for 48 h

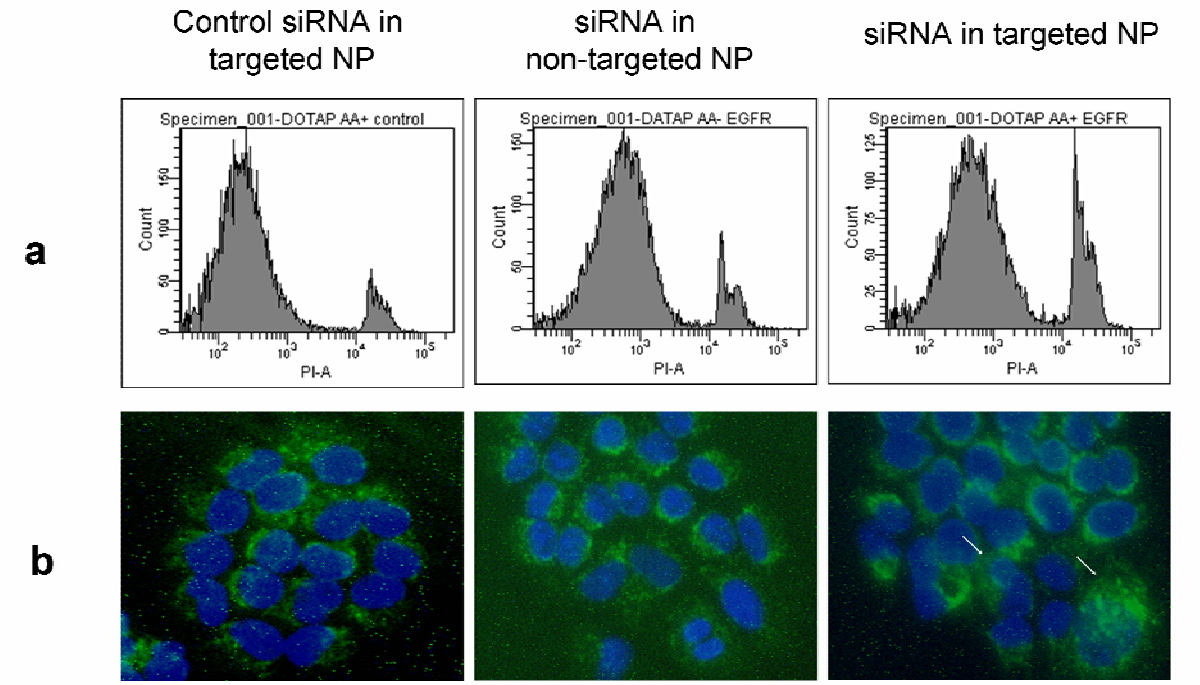

Figure 3.11 In vitro cytotoxicity assay
(a) Flow cytometry analysis of NCI-H460 cells after treatment with different formulations at the conc. of 320 nM siRNA for 48 h. Cells were stained with propidium iodide and analyzed for dead population. (b) Immunocytochemical analysis of AIF nuclear translocation of NCI-H460 cells after treatment with different formulations at the conc. of 120 nM siRNA for 48 h. Arrows indicate the nuclear translocation of AIF. Magnification = 200X.

The PK results suggest that the majority of the free siRNA was eliminated from the blood before it accumulated in the tissues. On the other hand, the tumor appeared to be the major uptake tissue for NPs and contributed a high uptake (70-80% ID/g) (**figure 3.2b**). Additionally, the liver and lung only took up 10-20% ID/g, which shows the high tumor selectivity of the NPs. The high tissue-selective delivery and tumor accumulation of the PEGylated NPs (with or without ligand) were probably due to the improved EPR effect, which was resulted from the high degree of PEG coating. As shown in the **Chapter 2**, approximately 10.6 mol% of the outer leaflet of the supported lipid bilayer was modified with DSPE-PEG. Normally, when DSPE-PEG is introduced to a regular lipid bilayer, the permeability of which is increased, resulting in the release of encapsulated drugs [40].

Therefore, 5 mol% of PEGylation is a common formulation for liposomes containing a regular bilayer in the compromise of surface protection and low membrane permeability. In the case of our NP formulation, the siRNA was complexed with protamine, and was further coated with a supported bilayer stabilized by the charge-charge interaction. Therefore, the bilayer could tolerate a high degree of PEGylation (10.6 mol%) with a full protection of the particle surface, leading to the much improved EPR effect.

The increase of V_{ss} for NPs in the tumor-bearing mice as compared to that of the tumor free mice suggests that the tumor served as a distribution sink for NPs. The decrease in the area under the curve and increase in clearance are also consistent with this observation. The presence of the targeting ligand facilitated the internalization of siRNA by the tumor cells (**figure 3.3**) but did not alter the PK (**figures 3.1** and **3.2**). The results indicate that extravasation of the vector, which was mainly dependent on the enhanced permeability and retention effect, was the rate limiting factor. Enhanced intracellular uptake of the vector did not cause further clearance. The internalization of siRNA formulation in the tumor was uneven (**figure 3.3**), suggesting that cells closer to the angiogenic capillaries are likely to take up more siRNA. However, the EGFR silencing in the entire tumor was nearly complete (**figures 3.4a** upper and **3.5**). This suggests only small amounts of siRNA, as long as properly delivered, are necessary for effective gene silencing. The in vivo RNA interference effect was highly dependent on the formulation and siRNA sequence. Only siRNA formulated in targeted NPs showed significant gene silencing activity (**figures 3.4a** upper and **3.5**). This targeted formulation also showed good efficiency in inducing apoptosis in the tumor (15%, $P < 0.05$) (**figure 3.4b**), inhibiting tumor growth (~40%, $P < 0.01$ on day 10) and sensitizing the tumor to chemotherapy (**figure 3.6**).

The cytokine induction effect was dependent on the model, formulation, and siRNA sequence. The results in **figure 3.7a** showed that the immune response of the nude mice were not sensitive to siRNA but to unmethylated CpG motifs. siRNA-mediated immune response is via toll-like receptor 7/8 (TLR7/8) [70,71], suggesting that the toll-like receptor 7/8 may be not be expressed or only at a low level in the nude mice. On the other hand, the toll-like receptor 9 was shown to be a good immunostimulatory target by CpG oligonucleotides in nude mice [72], and, therefore, a formulation containing plasmid showed strong immunotoxicity (**figure 3.7a**). In the C57BL/6 model, when siRNA was formulated into the NP, the immunostimulatory effect was strengthened (**figure 3.7b**). Additionally, the presence of the targeting ligand in the formulation increased the immunotoxicity of siRNA. This is probably due to the increased cellular uptake through endosomal pathway. Surprisingly, MDM2 siRNA containing no identifiable inflammatory sequences induced higher levels of cytokines than EGFR siRNA containing the immunostimulatory sequence (5′-UGUGU-3′) (**figure 3.7b**). MDM2 siRNA may contain some unknown, yet potent, sequences that induced the production of cytokines. Another possibility is that different toll-like receptor isoforms might be involved in the immunostimulatory effect of MDM2 siRNA, which is suggested by Wang and colleagues [73]. More importantly, empty NP (group F) showed very mild immunotoxicity (**figure 3.7a** and **b**), suggesting the carrier itself was safe. Although several siRNA delivery systems have exhibited high activity against tumors in vivo [2-4,12,19,24,43-51], our NP formulation provides the advantages of an almost complete encapsulation efficiency (>90%), the highest tumor delivery efficiency so far reported (70–80% ID/g at 4 h) (**figure 3.2b**) and relatively easy preparation. Our carrier also showed low toxicity (**figure 3.7, 3.8 and 3.9**).

4.0 EFFICIENT GENE SILENCING IN METASTATIC TUMOR BY SIRNA FORMULATED IN SURFACE-MODIFIED NANOPARTICLES

We have developed a nanoparticle (NP) formulation for systemically delivering siRNA into metastatic tumors. The NP, composed of nucleic acids, a polycationic peptide and cationic liposome, was prepared in a self-assembling process. The NP was then modified by PEG-lipid containing a targeting ligand, anisamide, and thus was decorated for targeting sigma receptor expressing B16F10 tumor. The activity of the targeted NP was compared with the naked NP (no PEGylation) and non-targeted NP (no ligand). The delivery efficiency of the targeted NP was 4-fold higher than the non-targeted NP and could be competed by excess free ligand. Luciferase siRNA was used to evaluate the gene silencing activity in the B16F10 cells, which were stably transduced with a luciferase gene. The in vitro gene silencing activity of the targeted NP was significantly higher than the other formulations and lasted for 4 days. While confocal microscopy showed the naked NP provided no tissue selectivity and nontargeted NP was ineffective for tumor uptake, the targeted NP effectively penetrated the lung metastasis, but not the liver. It resulted in 70-80% gene silencing in the metastasis model after a single i.v. injection (150 μg siRNA/kg). This effective formulation also showed very little immunotoxicity.

4.1 INTRODUCTION

siRNA has become a potential alternative for treating multi-drug resistant metastasis, which is the major cause of death in cancer patients [74]. Selective delivery of siRNA to metastatic tumors remains a major obstacle for siRNA based therapy. Although various delivery systems for siRNA have been developed, only a few successful cases have been reported on delivering siRNA into metastatic tumor [4,12,24,49,75]. Between viral and non-viral vectors, non-viral delivery offers several advantages, such as high tissue selectivity and low immunotoxicity [23]. In the **Chapter 2 and 3**, we have shown that the NP containing a supported lipid bilayer could be surface-modified with a high amount of PEG (10.6 mol%) by post-inserting DSPE-PEG. A complete shielding of the NP surface was found with a neutral zeta potential (-5.6 ± 4.5 mV) and abolishment of non-specific uptake in the liver. In the **Chapter 3**, this highly PEGylated NP delivered 70-80% injected dose/g into the tumor, inducing a significant gene silencing and antitumor activity. The data suggest that the NP having full surface protection showed improved EPR effect for solid tumor delivery. Here, we investigated the efficiency of the NP for delivering siRNA into an experimental metastatic tumor model, B16F10 lung metastasis in C57BL/6 mice. The cells were stably transduced with luciferase gene by using a retroviral vector before introduction to the animals. siRNA against luciferase was used in this study for the assessment of the gene silencing effect. We also compared the activities of different siRNA formulations, including free siRNA, naked NP (no PEGylation), non-targeted NP (PEGylated but without ligand) and targeted NP (PEGylated with ligand).

4.2 MATERIALS AND METHODS

4.2.1 Materials

DOTAP, cholesterol, and DSPE-PEG_{2000} were purchased from Avanti Polar Lipids, Inc. (Alabaster, AL). Protamine sulfate (fraction X from salmon) and calf thymus DNA (for hybridization, phenol-chloroform extracted and ethanol precipitated) were from Sigma-Aldrich (St. Louis, MO). DSPE-PEG2000-anisamide (DSPE-PEG-AA) was synthesized in our lab using the methods described previously [53].

Anti-luciferase siRNA (GL3) (target sequence 5'- CTT ACG CTG AGT ACT TCG A -3') was purchased from Dharmacon (Lafayette, CO) in deprotected, desalted, annealed form. For in vitro quantitative and tissue distribution studies, fluorescein (FAM) and cy3 labeled siRNA (3' end of the sense strand) provided by Dharmacon were used.

B16F10 cells, murine melanoma cells, were obtained from the American Type Cell Collection and were stably transduced with GL3 firefly luciferase gene using a retroviral vector in Dr. Pilar Blancafort's lab at the University of North Carolina at Chapel Hill (UNC). The cells were maintained in DMEM medium (Invitrogen, Carlsbad, CA) supplemented with 10% fetal bovine serum (FBS) (Invitrogen, Carlsbad, CA). B16F10 cells expressing sigma receptors [76] were used as model cells in our study.

4.2.2 Experimental animals

Female C57BL/6 mice of age 6-8 week (16-18 g) were purchased from Charles River Laboratories (Wilmington, MA). All work performed on animals was in accordance with and approved by the IACUC committee at UNC.

4.2.3 Preparation of siRNA containing nanoparticles

Nanoparticles (NP) were prepared as previously described in the **Chapter 2**. The formulations were used without further purification.

4.2.4 In vitro cellular uptake study

B16F10 cells (1×10^5 cells/0.5 ml/well) were seeded in 24-well plates (Corning Inc., Corning, NY) 20 h before experiments. Cells were treated with different formulations containing 500 nM FAM-siRNA in the culture medium at 37°C for 4 h. Cells were washed three times with PBS followed by incubation with 300 μl lysis buffer (0.3% Triton X-100 in PBS) at 37°C for 0.5 h. Fluorescence intensity of 100 μl cell lysate was determined by a plate reader (λ_{ex}: 485 nm, λ_{em}: 535 nm) (PLATE CHAMELEON Multilabel Detection Platform, Bioscan Inc., Washington, DC). For free ligand competition study, cells were co-incubated with 50 μM haloperidol with different formulations.

4.2.5 In vitro luciferase gene silencing study

B16F10 cells (5 x 10^5 cells/5 ml/flask) were seeded in 25T culture flasks (Becton Dickinson Co., Franklin Lakes, NJ) 20 h before experiments. Cells were treated with different formulations at a concentration of 250 nM siRNA in DMEM containing 10% FBS at 37°C for 24 h. Cells were trypsinized and 2 x 10^5 cells were collected for luciferase activity assay and the rest of cells were re-cultured in a 25T culture flask for the assay of the next time point. Collected cell pellets were incubated with 100 µl lysis buffer (0.05% Triton X-100 and 2 mM EDTA in 0.1 M Tris-HCl) at room temperature for 10 min. Ten microliter lysate was mixed with 100 µl substrate (Luciferase Assay System, Promega Co., Madison, WI) and the luminescence was measured by a plate reader. The protein concentrations of the samples were determined by using a protein assay kit (Micro BCA™ protein assay kit, Pierce). Luciferase activity of a sample was normalized with the protein content and expressed as percent luminescence intensity compared to the untreated control. Percent luciferase activity of cells treated with different formulations was plotted against the time. The AAC (area above the curve) of different formulations was calculated and compared with each other. AAC = AUC (area under the curve)$_{untreated}$ – AUC$_{treated}$.

4.2.6 Tissue distribution study

C57BL/6 mice were injected with 2 x 10^5 B16F10 cells via the tail vein. Seventeen days later, mice were i.v. injected with cy3-siRNA formulated in PBS, naked NP, non-targeted NP or targeted NP at the dose of 1.2 mg/kg. After 4 h, mice were euthanized and major tissues were collected. Paraffin embedded tissue sections of 5 µm in thickness were prepared. Sections

were re-hydrated, mounted with the DAPI containing medium (Vectashield®, Vector Laboratories Inc., Burlingame, CA) and imaged using a Leica SP2 confocal microscopy.

4.2.7 Immunohistochemistry

B16F10 metastasis loaded lungs and normal lungs from C57BL/6 mice were collected for the preparation of paraffin embedded sections (5 μm thick). Sigma receptor expression in the sections was stained by using the rabbit anti-mouse sigma receptor antibody (Santa Cruz Biotechnologies) and a kit (mouse-to-mouse detection system, Chemicon International, Temecula, CA). Tissue sections were counter stained with hematoxylin for nuclei, mounted and imaged using a Nikon phase contrast light microscopy.

4.2.8 In vivo gene silencing study

C57BL/6 mice were i.v. injected with 2 x 10^5 B16F10 cells via the tail vein. Seventeen days later, mice were given i.v. injections of anti-luciferase siRNA at the dose of 150 μg/kg formulated in PBS, naked NP, non-targeted NP or targeted NP. Control siRNA (target sequence: 5'-AATTCTCCGAACGTGTCACGT-3') [67] formulated in targeted NP was also prepared to verify if the silencing effect was sequence dependent. For the dose-response study, tumor bearing mice were i.v. injected with siRNA in targeted NP at doses of 18.75, 37.5, 75, 150, 300, 600 and 1,200 μg/kg. After 48 h, mice were euthanized and the tumor loaded lungs were collected. The lung was homogenized in 1 ml lysis buffer (0.05% Triton X-100 and 2 mM EDTA in 0.1 M Tris-HCl) followed by centrifugation at 5,000 rpm for 5

min. Ten µl supernatant was mixed with 100 µl luciferase substrate and the luciferase activity was measured by a plate reader.

4.2.9 Cytokine induction assay

C57BL/6 mice were i.v. injected with anti-luciferase siRNA formulated in PBS, naked NP, non-targeted NP and targeted NP at the dose of 150 µg/kg. Targeted NP formulated with plasmid DNA (pNGVL-Luc prepared by Bayou Biolabs) [77] instead of calf thymus DNA was prepared and used as a positive control for the evaluation of immunotoxicity of calf thymus DNA. Two h after the injections, blood samples were collected from the tail artery and allowed to stand at room temperature for 0.5 h for coagulation. Serum was obtained by centrifuging the clotted blood at 16,000 rpm for 20-40 min. Cytokine levels were determined by using ELISA kits for TNF, IL6, IL12 (BD Biosciences, San Diego, CA) and IFN-α (PBL Biomedical Laboratories, Piscataway, NJ).

4.2.10 Statistical analysis

Data are presented as the mean ± SD. The statistical significance was determined by using the analysis of variance (ANOVA). P values of <0.05 were considered significant.

4.3 RESULTS

4.3.1 Characterization of NP

The characteristics of the NP are summarized in **table 4.1**. The particle sizes of the three NP formulations were similar to each other. DSPE-PEG modification significantly reduced the zeta potential of the NP. Targeted NP showed a slight increase in the zeta potential compared to the non-targeted NP. It is noted that the formulations were not further purified.

Table 4.1 Characterization of nanoparticle formulations

	Naked NP	Non-targeted NP	Targeted NP
Particle size (nm)	117.6 ± 13.2	115.1 ± 14.8	110.6 ± 13.8
Zeta potential (mV)	43.2 ± 3.62	20.4 ± 2.08	25.51 ± 1.22

Data are representative data from repeated measures of 4-5 samples.

4.3.2 In vitro cellular uptake

To investigate the delivery efficiency of our NP formulations, we performed the cellular uptake study using FAM labeled siRNA. The fluorescence intensity of the cell lysate represents the intracellular delivery efficiency for siRNA by a given formulation. As shown in **figure 4.1**, cell lysate from cells treated with free FAM-siRNA showed background fluorescence, while those from cells treated with NP formulations had significantly higher fluorescence intensities. After PEGylation, the delivery efficiency of non-targeted NP was

significantly reduced to 1/10 compared to the naked NP. However, targeted NP showed 4-fold increased delivery efficiency compared to non-targeted NP. The addition of free haloperidol, a known agonist for sigma receptors, significantly reduced the delivery efficiency of targeted NP but not other formulations.

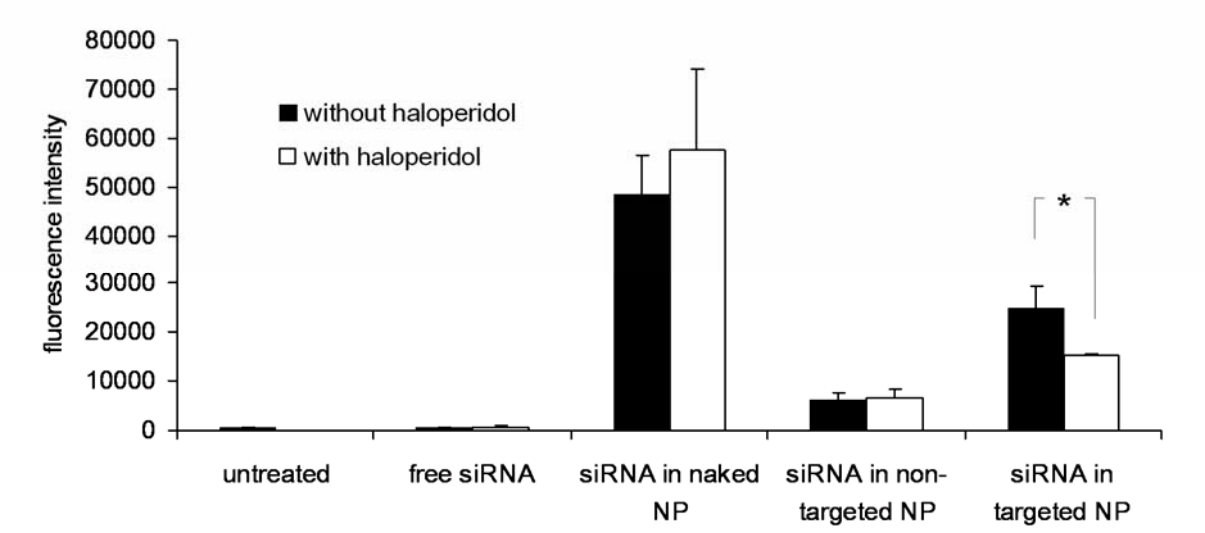

Figure 4.1 Fluorescence intensities of cell lysate from cells treated with FAM-siRNA containing formulations.
B16F10 cells were incubated with different formulations at 37°C for 4 h in the absence or presence of 50 μM haloperidol. Cells were washed and lysed. Cell lysate was analyzed for fluorescence intensity by a plate reader. Data = mean ± SD (n=3), * indicates $p<0.05$.

4.3.3 In vitro luciferase gene silencing

We examined both the extent and the duration of the gene silencing effect by siRNA in different formulations. As shown in **figure 4.2**, free siRNA showed minimal effect, while the NP formulations had moderate to strong gene silencing effect ($p<0.05$ compared to free siRNA). siRNA formulated in the naked NP and the targeted NP had 2-2.5 fold higher activity than in the non-targeted NP ($p<0.05$). The gene silencing effect decreased right after the dosing stopped for the naked NP, while the targeted NP showed a prolonged activity for 4 days. Therefore, the overall activity (AAC) of the targeted NP was significantly higher than

the naked NP ($p<0.05$). Control siRNA formulated in the targeted NP showed moderate but very transient effect and the overall effect (AAC) was not significantly higher than that of the free siRNA ($p>0.05$).

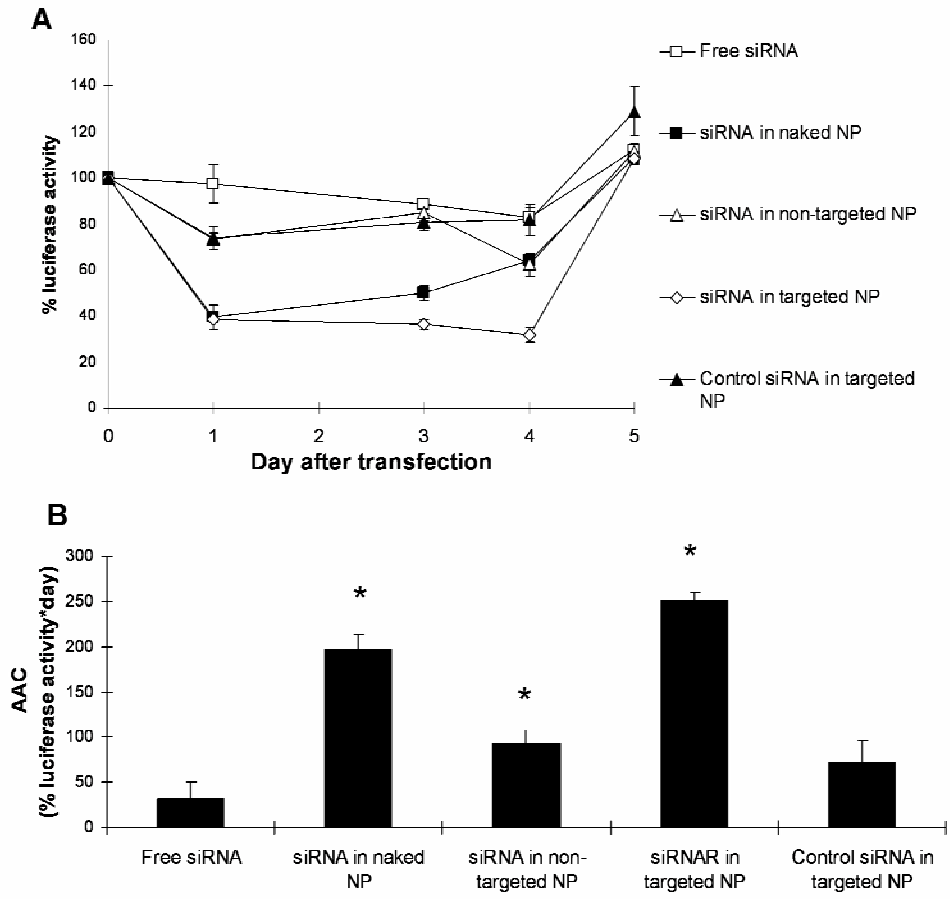

Figure 4.2 In vitro luciferase gene silencing effect of different siRNA formulations (A) and the AAC (area above the curve) of different formulations in figure 4.2A (B).
B16F10 cells were incubated with different siRNA formulations at 37°C for 24 h. At the end of incubation, formulations containing medium was removed and cells were washed. Luciferase activities of the cells (2 x 10^5) were analyzed at different time points after the treatment. Data = mean ± SD (n=3), * indicates $p<0.05$ compared to the free siRNA.

4.3.4 Tissue distribution of cy3-siRNA

Tissue distribution study was performed to evaluate the in vivo tumor delivery by different NP formulations. Free cy3-siRNA showed poor tissue accumulation in both tumor free and

tumor loaded lungs, as very little cy3 signal was detected in the sections (**figure 4.3A**). Naked NP effectively delivered cy3-siRNA to the lung alveolar cells, but showed relatively poor penetration into the tumor nodules. Non-targeted NP showed poor tissue uptake in both tumor free and tumor loaded lungs. On the other hand, targeted NP provided the highest tumor penetration and uptake among the four formulations. Other normal organs (heart, spleen and kidney) only showed minimal fluorescence signal except liver. As shown in **figure 4.3B**, naked NP showed significant liver accumulation at 4 h in both tumor free and tumor bearing mice. However, PEGylated NP (with or without ligand) only accumulated in the liver of tumor free mice but not tumor bearing mice at 4 h. Liver uptake of free cy3-siRNA was very little in both tumor free and tumor bearing mice.

4.3.5 Immunohistochemistry of sigma receptor

Tissue distribution results indicated that the tissue surrounding the tumor significantly contributed to uptake of the targeted NP in the tumor loaded lung. To address if the uptake of targeted NP was associated with the presence of small B16F10 metastasis, we performed immunostaining of the sigma receptor on the lung tissues. Brown staining in the tissue section indicated the expression of sigma receptor, while nuclei were counter stained blue by hematoxylin. As shown in **figure 4.3C**, sigma receptor was expressed in a significantly higher level in the B16F10 tumor cells and the surrounding tissue than that in the normal lung, which only showed a basal level (**figure 4.3C**).

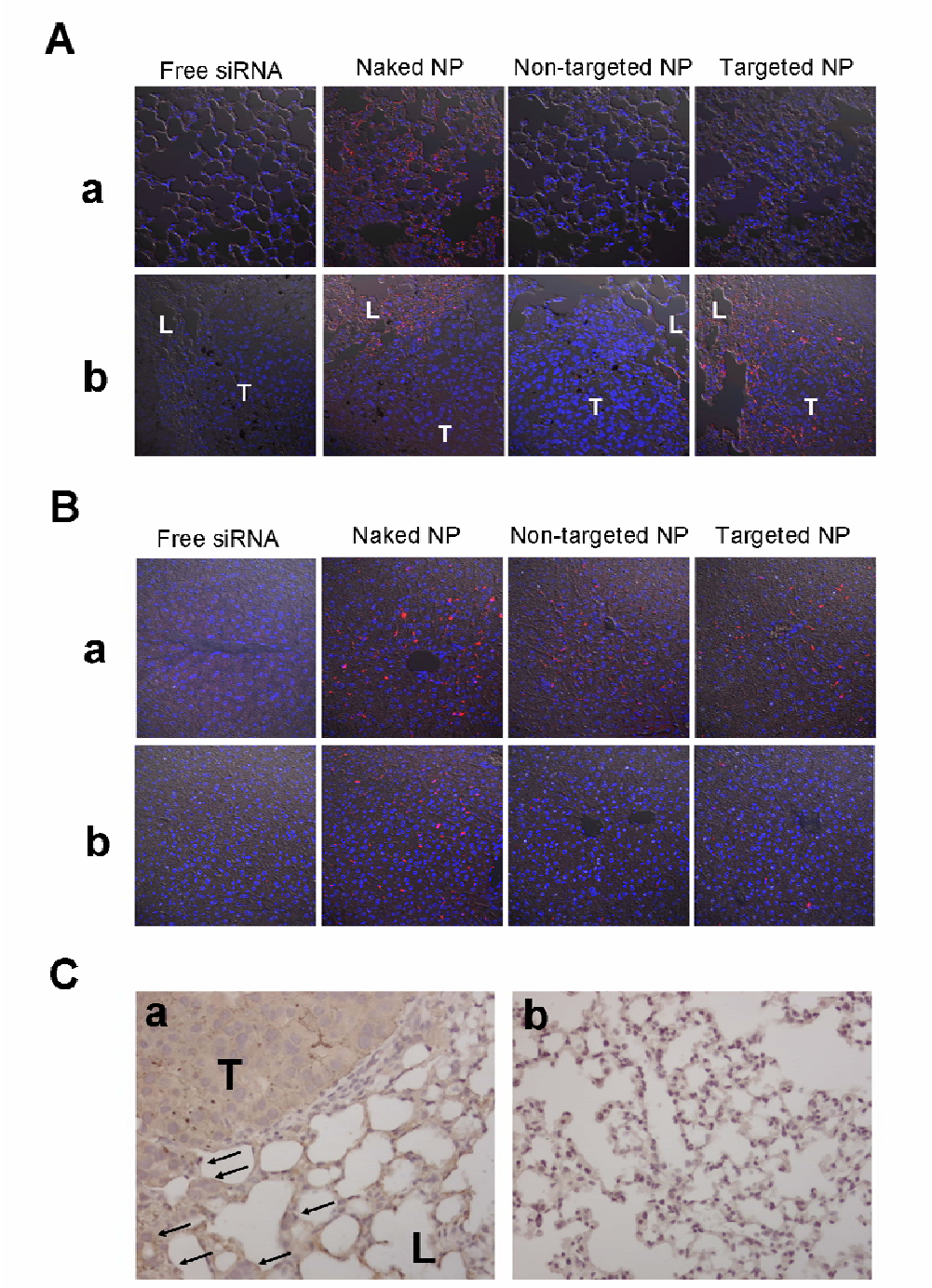

Figure 4.3 Confocal microscopy photographs of the lungs (A) and livers (B) collected from the tumor free (a) and B16F10 tumor bearing mice (b).
Mice were i.v. injected with cy3-siRNA in different formulations. After 4 h, mice were sacrificed and major tissues were collected and processed for paraffin embedded sections. Tissue sections were re-hydrated, mounted with the DAPI containing medium and imaged by confocal microscopy. Pictures are the overlay of phase contrast, DAPI fluorescence signal (blue, nuclei) and cy3 signal (red, siRNA). T and L indicate the presence of tumor and lung tissue, respectively. Magnification = 400x. C, immunohistochemistry of sigma receptor in tumor loaded lung (a) and tumor free lung (b). T and L indicate the presence of tumor and lung tissue, respectively. Arrows indicate the presence of B16F10 cells. Magnification = 200 x

4.3.6 In vivo luciferase gene silencing

The in vivo activity of the NP formulations was assessed by the luciferase gene silencing in the whole B16F10 tumor loaded lungs. **Figure 4.4A** shows the activity of siRNA in different formulations. The luciferase activity was compared with the untreated control. siRNA in PBS, naked NP, non-targeted NP and targeted NP silenced 0%, 50%, 10% and 75% luciferase activity, respectively (**figure 4.4A**). Only the naked NP and the targeted NP showed a significant effect (**figure 4.4A**, $p<0.05$). Control siRNA formulated in the targeted NP had no effect. **Figure 4.4B** indicates that ED50 of the targeted NP formulation was 75 μg/kg. The optimal dose for the maximum gene silencing effect (70-80%) was 150 μg/kg, and further increase of the dose did not result in a higher activity (**figure 4.4B**).

4.3.7 Cytokine induction study

The immunotoxicity of the NP formulations was monitored by measuring the serum concentrations of proinflammatory cytokines 2 h after injections (**figure 4.5**). None of the NP formulations composed of calf thymus DNA induced significant production of the proinflammatory cytokines (IL6, IL12, TNF and IFN-α). The targeted NP formulated with plasmid DNA, however, was very immunotoxic

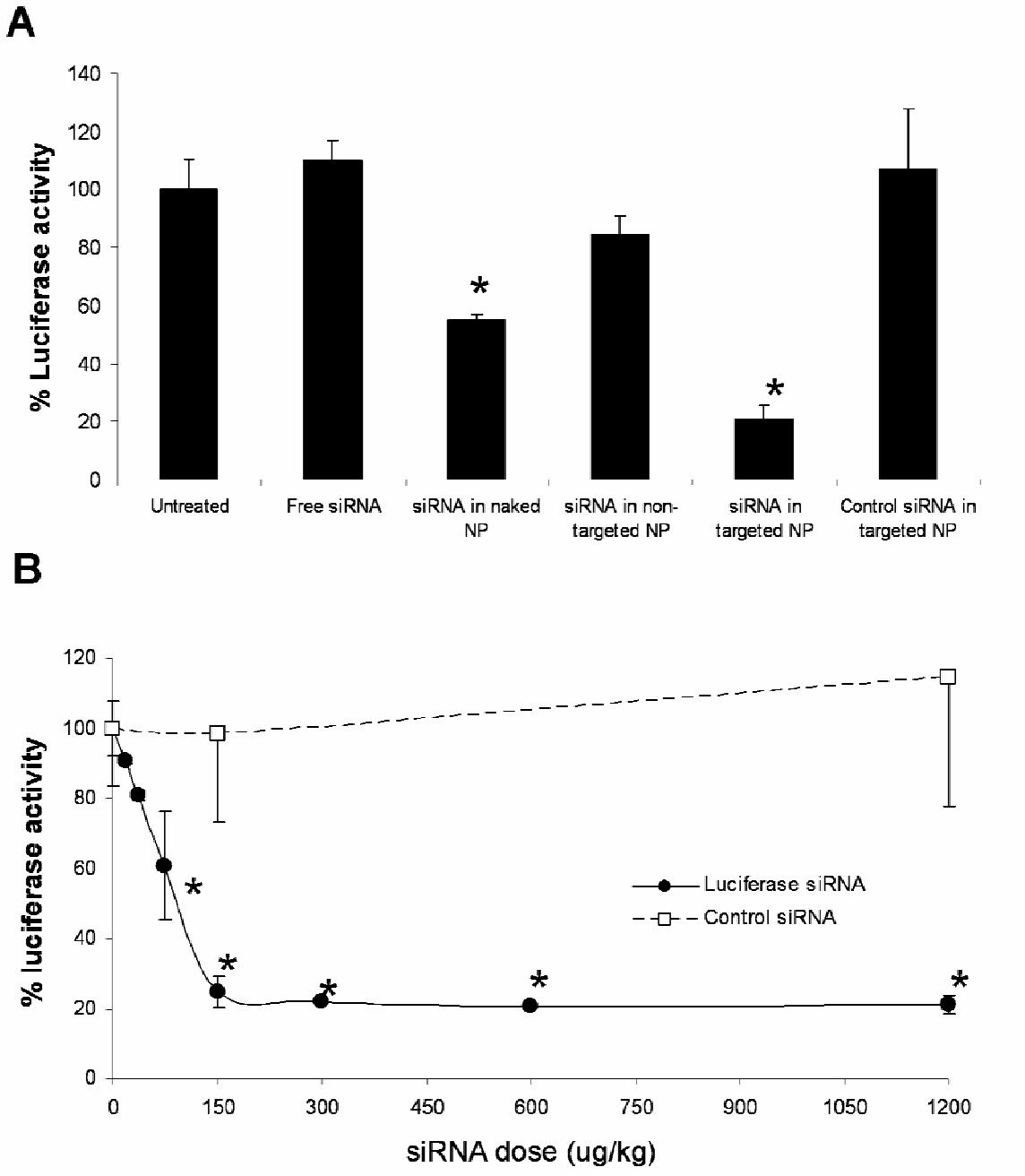

Figure 4.4 In vivo luciferase gene silencing effect of different siRNA formulations at the dose of 150 µg/kg (A) and that of the targeted NP at various doses (B).
B16F10 tumor bearing mice were i.v. injected with different siRNA formulations. After 48 h, mice were sacrifice and the tumor loaded lungs were excised for the luciferase activity assay. Luciferase activity was compared to the untreated control and expressed as % luciferase activity. Data = mean ± SD (n=3-8), * indicates $p<0.05$ compared to the untreated control.

.

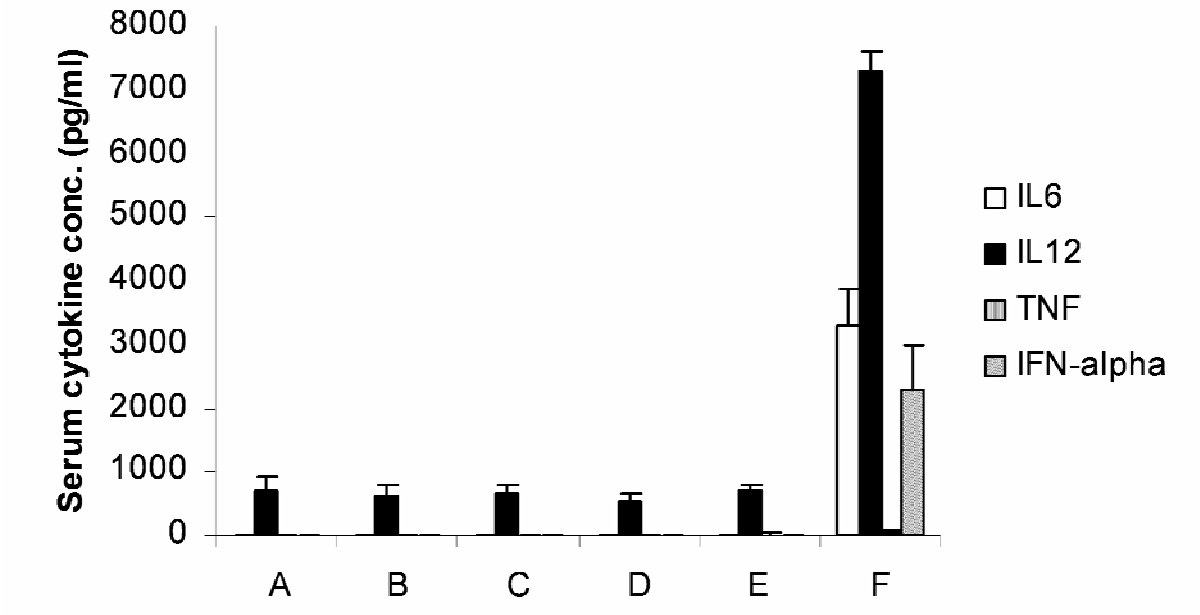

Figure 4.5 The serum cytokine concentrations of the mice 2 h after the i.v. injections of siRNA in different formulations.
C57BL/6 mice were i.v. injected with different siRNA formulations (A, untreated; B, siRNA in PBS; C, siRNA and calf thymus DNA in naked NP; D, siRNA and calf thymus DNA in non-targeted NP; E, siRNA and calf thymus DNA in targeted NP; F, siRNA and plasmid DNA in targeted NP. After 2 h, blood was collected from the tail artery and serum concentrations of the cytokines were analyzed by the ELISA method. Data = mean ± SD (n=4), * indicates $p<0.05$ compared to the untreated control.

4.4 DISCUSSION

This highly positively charged NP formulation (naked NP, zeta potential ~40 mV) tends to aggregate when incubated with high salt buffer or serum [33] and had strong charge-charge interaction with the cells. Surface PEGylation offered steric hindrance for the NP, which stabilized the formulation in the serum containing medium [33] but also reduced the association with the cells (**figure 4.1**). A targeting ligand (anisamide) tethered to the end of PEG retargeted the NP to the sigma receptor expressing cells (**figure 4.1** and [33]), which was partially inhibited by the presence of free haloperidol, a known agonist for the receptor.

Although the zeta potential of the targeted NP was slightly higher than that of the non-targeted NP due to the positively charged anisamide ligand, the targeted NP did not show increased delivery efficiency for sigma receptor negative cells (CHO and CT26 cells, data not shown). Additionally, neither the non-targeted nor the targeted NP formed aggregates with the FBS [33]. The data suggest that the PEGylated NPs (with or without ligand) were sterically stabilized by the PEG coating and the entry mechanism for the targeted NP was via a sigma receptor dependent pathway.

The in vitro gene silencing effect of different formulations showed high correlation with the siRNA sequence and the intracellular delivery efficiency (**figure 4.2**). When anti-luciferase siRNA was formulated into NP formulations, the gene silencing activity was significantly improved ($p<0.05$, **figure 4.2B**) due to the enhanced intracellular delivery (**figure 4.1**). Interestingly, targeted NP providing lower delivery efficiency (**figure 4.1**) showed higher gene silencing activity than the naked NP (**figure 4.2B**). It is also noted that the silencing activity of targeted NP was significantly prolonged for 4 days, while that of naked NP was relatively transient (**figure 4.2A**). First, the delivery efficiency was determined at 4 h, which favors the naked NP that entered into the cells via a strong charge-charge interaction. Targeted NP, on the other hand, delivered siRNA through a receptor mediated pathway, which is dependent on the receptor recycling/trafficking that usually takes longer time but is a continuous process. For a short half-life drug such as siRNA, continuous input of drugs often results in enhanced therapeutic effect. Second, naked NP formed aggregates before internalization and siRNA release from aggregates could be slow, which would result in a reduced bioavailability. Targeted NP did not form aggregates with serum and the intracellular release of siRNA should be faster and more complete, leading to a

prolonged gene silencing effect. Although the control sequence showed only very transient activity, which was probably due to an off-target effect, the overall activity was not significantly higher than that of the free siRNA (**figure 4.2B**). The result indicated that the gene silencing activity was highly sequence dependent.

The in vivo activity results are consistent with the in vitro observation, in which the targeted NP showed significantly higher activity (70-80% gene silencing) than other formulations (**figure 4.4A**). The enhanced activity of the targeted NP was mainly due to the significantly improved tumor uptake as shown in **figure 4.3A** (panel b). Naked NP having poor tumor tissue penetration (panel b of **figure 4.3A**) provided only 50% gene silencing (**figure 4.4A**), which was probably resulted from the formation of large aggregate when i.v. injected. Other formulations, including free siRNA, non-targeted NP and control siRNA in targeted NP, had little effect (**figure 4.4A**, $p>0.05$). Again, the results suggested that significant gene silencing activity was highly dependent on the correct siRNA sequence and sufficient tumor delivery.

Naked NP delivered siRNA via a non-specific charge-charge interaction mechanism. As shown in **figure 4.3**, siRNA formulated in the naked NP accumulated in the lung, tumor and liver with little selectivity. The tissue uptake was particularly significant in the lung, the first pass organ for i.v. injection. Non-targeted NP, however, showed little lung uptake due to the steric hindrance provided by PEG (**figure 4.3A**). In the tumor free mice, the liver appeared to be the major organ for eliminating the PEGylated NP (with or without ligand) (**figure 4.3**). Nevertheless, the liver uptake of the PEGylated NP was significantly reduced in the tumor bearing mice (panel b of **figure 4.3B**), which was probably due to the kinetic competition of the uptake by the tumor (panel b of **figure 4.3A**). In other words, in the tumor

bearing mice, PEGylated NP effectively accumulated in the tumor by the EPR effect (enhanced permeability and retention) [78], resulting in a reduced liver uptake. It is noted that confocal microscopy only showed the intracellularly delivered and released cy3-siRNA signal. Signal of cy3-siRNA that were compactly formulated in NP and accumulated extracellularly was quenched and therefore, could not be shown in **figure 4.3A** (panel b). Our previous results suggest that PEGylated NP delivered comparable amount of siRNA to the tumor tissue but only targeted NP showed significant intracellular delivery [8]. Again, the improved metastatic tumor delivery via the PEGylated NP may be due to the improved stability mediated through the highly PEGylated supported lipid bilayer on the NP surface. It is anticipated that the tumor nodules in the lung (17 days after tumor inoculation) were big enough to allow the PEGylated NP to accumulate via the EPR effect in this study. As shown in **figure 4.3C**, normal lung expressed a basal level of sigma receptor and therefore, the targeted NP showed enhanced uptake in the lung compared to the non-targeted NP (**figure 4.3A**). Additionally, the surrounding tissue around the tumor contained small amounts of B16F10 cells (**figure 4.3C**, as indicated by the arrows), which also contributed to the significant uptake of the targeted NP. The enhanced uptake of the targeted NP in the surrounding tissue may be via these metastatic cells, which were closer to the blood supply and more accessible compared to the cells in the large tumor nodules.

The toxicity of the NP formulations was evaluated by their induction of the proinflammatory cytokines (IL6, IL12, TNF, IFN-α) (**figure 4.5**). At such a low dose (150 μg/kg), none of the NP formulations were immunotoxic. Additionally, no body weight decrease was observed for any of the mice treated with the formulations (data not shown).

To summarize, free siRNA could hardly penetrate through the cell membrane (**figure 4.1**) due to its highly hydrophilic nucleic acid backbone. Therefore, siRNA itself with low bioavailability showed no gene silencing activity (**figures 4.2 and 4.4**). Encapsulation of siRNA into the naked NP dramatically increased the intracellular delivery and the gene silencing activity (**figures 4.1, 4.2 and 4.4**) through the charge-charge interaction of the formulation with cells. However, the non-specific nature of the charge charge interaction resulted in the formation of large aggregates when injected into the blood [30] and low tissue selectivity (**figure 4.3**). PEGylation of the naked NP abolished the non-specific interaction with negatively charged cells or proteins [33] but also reduced the cellular and tissue uptake (**figures 4.1 and 4.3**), resulting in low silencing activity (**figures 4.2 and 4.4**). Introduction of a targeting ligand at the distal end of PEG chain restored the intracellular delivery to the sigma receptor positive cells (**figures 4.1 and 4.3**), while the tissue selectivity was maintained (**figure 4.3**). This targeted NP formulation with improved tissue specificity and delivery efficiency silenced the luciferase gene in the lung metastasis effectively (**figure 4.4**) without any significant immunotoxicity (**figure 4.5**).

4.5 CONCLUSIONS

We have developed a surface-modified NP formulation that selectively delivered siRNA to the sigma receptor expressing B16F10 lung metastasis. With high delivery efficiency, a low dose (150 μg/kg) was required to achieve 70-80% gene silencing in the whole lung metastasis. This targeted NP formulation also showed little immunotoxicity, which promises its potential use for metastasis treatment.

5.0 EFFICIENT ONCOGENE SILENCING AND METASTASIS INHIBITION VIA SYSTEMIC DELIVERY OF SIRNA

Selective delivery of siRNA to metastatic tumor remains challenging. We have developed a nanoparticle (NP) formulation composed of siRNA, a carrier DNA, a polycationic peptide and cationic liposomes. The NP was obtained by a self assembling process, followed by surface modification with a PEG conjugated ligand, anisamide. Thus, the NP was PEGylated and a ligand was presented to target sigma receptor expressing murine melanoma cells, B16F10. The lung metastasis model was established by i.v. injecting the B16F10 cells into the C57BL/6 mice. A mixture of siRNA against MDM2, c-myc and VEGF co-formulated in the targeted NP caused simultaneous silencing of each oncogene in the metastatic nodules. Two consecutive i.v. injections of siRNA in the targeted NP significantly reduced approximately 70-80% of the lung metastasis at a relatively low dose (0.45 mg/kg), while free siRNA and the non-targeted NP showed little effect. This targeted NP formulation significantly prolonged the mean animal survival time by 30% compared to the untreated control. At the therapeutic dose, the targeted NP showed little local and systemic immunotoxicity and did not decrease the body weight or damage the major organs.

5.1 INTRODUCTION

The lung is a common location of secondary tumor that metastasizes from the primary source tumor [79-82]. To date, when pulmonary metastasis are diagnosed, aggressive surgical resection is usually performed for the best chance of long-term cure [79]. Unfortunately, a high relapse rate (~70%) results in a low survival rate (30%) even after complete resection [79]. Lung metastasis relapse usually occurs during chemotherapy [79], indicating that conventional anticancer drugs are no longer effective against the metastasis. Such a life-threatening condition urgently needs a new and systemic treatment.

Among anticancer agents, siRNA draws much attention due to its high specificity, high efficiency and low toxicity. By targeting oncogenes, siRNA can be applied as a therapeutic agent in cancer therapy [1]; however, delivery of siRNA remains challenging. Despite various delivery carriers for siRNA that have been developed, few successful cases have been reported on treating metastatic tumor by systemically delivered siRNA [12,24,49,75].

Previously, we have shown that our targeted nanoparticle (NP) could deliver significant amounts of siRNA (70-80% injected dose/g) into the cytoplasm of a xenograft tumor in a nude mouse model, which led to the silencing of EGFR, tumor growth inhibition and chemosensitization [8]. To address if the targeted NP can also deliver siRNA to a metastatic tumor, we used an established experimental lung metastasis model by i.v. injecting the murine melanoma cells (B16F10 cells stably transduced with the luciferase gene) into the C57BL/6 mice. We have performed several feasibility studies, which showed that the targeted NP improved the delivery and efficacy of the siRNA [32]. First, the targeted NP showed an enhanced delivery of cy3-siRNA into the metastatic nodules. The luciferase gene

in the metastatic nodules could be effectively silenced by anti-luciferase siRNA formulated in the targeted NP; approximately 70-80% luciferase activity was silenced by a single i.v. injection (0.15 mg/kg) [32]. ED50 was only 0.075 mg/kg. The significantly improved primary and metastatic tumor delivery was likely due to the high PEGylation (10.6 mol%) on the NP surface, which contained a supported lipid bilayer stabilized by a charge-charge interaction. The 10.6 mol% coating of PEG on the NP surface provided full protection and improved the pharmacokinetics of which, leading to enhanced RNAi activity. The data reported in the **Chaper 2, 3 and 4** suggest that the targeted NP formulation may be used for the treatment of lung metastasis.

Combination treatment with three different siRNA sequences (MDM2, c-myc and VEGF) has been shown to have a synergistic antiproliferation effect on the B16 cells [48]. Therefore, we used the combined sequences (MDM2: c-myc: VEGF = 1:1:1, weight ratio) for the therapeutic studies.

5.2 MATERIALS AND METHODS

5.2.1 Materials

DOTAP, cholesterol, and DSPE-PEG_{2000} were obtained from Avanti Polar Lipids, Inc. (Alabaster, AL). Protamine sulfate (fraction X from salmon) and calf thymus DNA (for hybridization, phenol-chloroform extracted and ethanol precipitated) were purchased from Sigma-Aldrich (St. Louis, MO). DSPE-PEG_{2000}-anisamide (DSPE-PEG-AA) was synthesized in our lab using the methods described previously [53].

B16F10 cells, sigma receptor positive [76] and commonly used for establishing an experimental lung metastasis model [32], were used in the study. The cells were obtained from American Type Culture Collection and stably transduced with GL3 firefly luciferase gene using a retroviral vector in Dr. Pilar Blancafort's lab at the University of North Carolina at Chapel Hill (UNC). The cells were maintained in DMEM medium (Invitrogen, Carlsbad, CA) supplemented with 10% fetal bovine serum (FBS) (Invitrogen, Carlsbad, CA).

Primary antibodies (mouse monoclonal antibodies against mouse MDM2, c-myc, luciferase, β-actin and rabbit polyclonal antibodies against VEGF) and secondary antibodies conjugated with horse reddish peroxidase (HRP) (goat anti-mouse IgG-HRP and goat anti-rabbit IgG-HRP) were purchased from Santa Cruz Biotechnologies (Santa Cruz, CA).

5.2.2 siRNA

MDM2 siRNA (target sequence 5' GCUUCGGAACAAGAGACUC 3'), c-myc siRNA (target sequence 5' GAACAUCAUCAUCCAGGAC 3'), VEGF siRNA (target sequence 5' CGAUGAAGCCCUGGAGUGC 3'), and control siRNA (target sequence: 5'-AATTCTCCGAACGTGTCACGT-3') were purchased from Dharmacon (Lafayette, CO) in deprotected, desalted, annealed form. The sequences were adopted from the literature [48,67].

5.2.3 Experimental animals

Female C57BL/6 mice of age 6-7 week (16-18 g) were purchased from Charles River Laboratories (Wilmington, MA). All work performed on animals was in accordance with

and approved by the IACUC committee at UNC. Murine model of lung metastasis was established by i.v. injection of 2×10^5 B16F10 cells into the C57BL6 mice.

5.2.4 Preparation of siRNA containing NP

NP were prepared as previously described in the **Chapter 2**. Each component (siRNA, calf thymus DNA, protamine, cationic liposome) of the formulation was dissolved or prepared in the cloning grade water with non-detectable endotoxin (Sigma-Aldrich, St. Louis, MO). The solution or suspension was then sterile filtered, and the formulations were prepared in the laminar flow hood using autoclaved tubes and pipette tips. The characteristics of the formulations were similar to the one reported earlier [32].

5.2.5 In vitro gene silencing study

B16F10 cells (5×10^4 cells/2 ml/well) were seeded into the 6-well plates 20 h before experiments. Cells were treated with different formulations at a concentration of 100 nM for total siRNA (MDM2: c-myc: VEFG = 1:1:1, weight ratio) in 10% FBS containing medium at 37 °C for 48 h. Cells were washed three times with PBS and fixed with cold acetone for 10 min. Immunostaining was then performed according to the method described in **5.2.6**. Nuclei were counterstained with methylgreen.

5.2.6 In vivo gene silencing study

Tumor bearing mice were given i.v. injections of total siRNA (MDM2: c-myc: VEFG = 1:1:1, weight ratio) at the dose of 0.45 mg/kg formulated in PBS, the non-targeted NP or the targeted NP on day 10 and 11. One day after the second injection, mice were euthanized and the tumor loaded lungs were collected for the preparation of paraffin embedded sections (5 μm thick). MDM2, c-myc and VEGF expression in the sections were examined by immunohistochemistry using the antibodies with the kit (DakoCytomation Envision + Dual Link System-HRP (DAB+), DakoCytomation, Carpinteria, CA) by following the product protocol. Nuclei were counterstained by hematoxylin and samples were imaged with a Nikon phase contrast light microscope. Total protein (10 μg) isolated from the tumor loaded lung was resolved on a polyacrylamide/SDS gel and then transferred to a polyvinylidene difluoride membrane. The membranes were blocked with 5% non-fat milk in PBS for 1 h and then incubated overnight with primary antibody at 4 ◦C. After washing the membrane with TBS (1% Tween 20 in PBS) five times, the membrane was incubated with the HRP conjugated secondary antibody for 1 h. The peroxidase activity associated with the protein bands was detected by enhanced chemiluminescence using ECL plus (GE Health Care, Buckinghamshire, UK) followed by autoradiography.

5.2.7 In vivo metastasis inhibition study and survival analysis

Tumor bearing mice were given i.v. injections of total siRNA (MDM2: c-myc: VEFG = 1:1:1, weight ratio) at the dose of 0.45 mg/kg formulated in PBS, the non-targeted NP or the targeted NP on day 10 and 11. Control siRNA formulated in the targeted NP was also

prepared as a negative control. Mice were euthanized and the tumor loaded lungs were collected on day 17. One lobe of the lung was analyzed for the luciferase activity to quantify the lung metastasis nodules. The lobe was homogenized in 1 ml of the lysis buffer (0.05% Triton X-100 and 2 mM EDTA in 0.1 M Tris-HCl) followed by centrifugation at 5,000 rpm for 5 min. Ten µl of the supernatant was mixed with 100 µl luciferase substrate (Luciferase Assay System, Promega Co., Madison, WI) and the luciferase activity was measured by a plate reader (PLATE CHAMELEON Multilabel Detection Platform, Bioscan Inc., Washington, DC). The rest of the lung was fixed in 3.6% formalin solution overnight and imaged. The fixed lung was processed for paraffin sections followed by H&E staining. For survival analysis study, tumor bearing mice were treated on day 10, 11, 17 and 18. Mice were euthanized when suffered from weight loss greater than 10% or showed ruffled fur.

5.2.8 Cytokine induction assay

The C57BL/6 mice were i.v. injected with siRNA (MDM2: c-myc: VEGF = 1:1:1) formulated in the targeted NP at various doses and the serum cytokine level was determined by the method described previously [8].

5.2.9 Local cytokine production analysis.

Tumor bearing mice were given i.v. injections of siRNA (MDM2: c-myc: VEFG = 1:1:1, weight ratio) in different formulations on day 10 at the dose of 0.45 mg/kg. Two h later, mice were sacrificed and the lungs were collected. The lung was homogenized in 300 µl lysis buffer (0.05% Triton X-100 and 2 mM EDTA in 0.1 M Tris-HCl), followed by

centrifugation at 10,000 rpm for 20 min. The supernatant was collected for the assay of the cytokines by the ELISA method as described previously [8].

5.2.10 Quantitative RT-PCR

$2X10^5$ B16F10 cells per well were seeded in 6-well plates (Corning Inc., Corning, NY) 20 h before the experiment. Cells were treated with different formulations at a concentration of 33.3 nM for single siRNA or 100 nM for combined siRNA (c-myc: MDM2: VEGF = 1:1:1, weight ratio) formulated in the targeted NP at 37^{o}C for 12 h. Total RNA were extracted with the RNeasy® Mini Kit (Qiagen, Valencia, CA) by following the manufacturer protocol. cDNA was then prepared in the presence of reverse transcriptase (Promega, Madison, WI). The mRNA levels were determined by an ABI PRISM HT7900 sequence detection system (Applied Biosystems, Foster City, CA) as described previously [48]. The primer pairs for detecting the mRNA are listed as **Table 5.1**.

Table 5.1 Primer sequences for qRT-PCR

Gene	Primer sequences	References
Mouse MDM2	Forward 5’ CTC TGG ACT CGG AAG ATT ACA GCC 3’ Reverse 5’ CCT GTC TGA TAG ACT GTG ACC CG 3’	[83]
Mouse VEGF	Forward 5’ GGA GAT CCT TCG AGG AGC ACT T 3’ Reverse 5’ GGC GAT TTA GCA GCA GAT ATA AGA A 3’	[84]
Mouse c-myc	Forward 5’ CCC CTG GTG CTC CAT GAG 3’ Reverse 5’ TCC TCC TCA GAG TCG C 3’	[48]
Mouse GAPDH	Forward 5’ TTC ACC ACC ATG GAG AAG GC 3’ Reverse 5’ GGC ATG GAC TGT GGT CAT GA 3’	[48]

5.2.11 Toxicity assay.

Tumor bearing mice were given i.v. injections of siRNA (MDM2: c-myc: VEFG = 1:1:1, weight ratio) in different formulations on day 10 and 11 at the dose of 0.45 mg/kg. The body weight of the mice was monitored during the treatment. One day after the second injection, the mice were killed and the major organs (heart, lung, liver, spleen and kidney) were collected, sectioned, H&E stained and imaged.

5.2.12 Statistical analysis

Data are presented as the mean ± SD. The statistical significance was determined by using one-way ANOVA. The animal survival data were analyzed by the Kaplan-Meier survival analysis. P values of <0.05 were considered significant.

5.3 RESULTS

5.3.1 In vivo gene silencing study

We encapsulated the combined siRNA sequences into different formulations, treated the lung metastasis bearing mice on day 10 and 11 with two consecutive i.v. injections (dose = 0.45 mg/kg) and examined the gene silencing activities by immunohistochemistry (**figure 5.1**) and Western blotting (**figure 5.2**). As shown in **figure 5.1**, only siRNA formulated in the targeted NP simultaneously silenced MDM2, c-myc and VEGF in the B16F10 lung

metastasis (**figure 5.1**). The Western blotting data (**figure 5.2**) confirmed the observation in the immunohistochemical analysis.

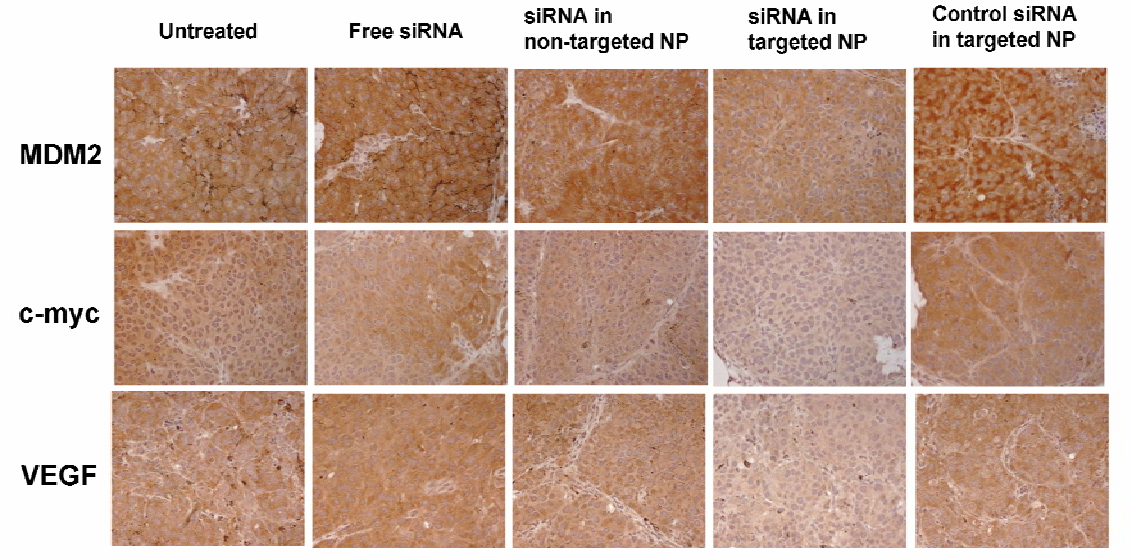

Figure 5.1 Immunohistochemical analysis on the lung metastasis.
Immunohistochemical staining of MDM2, c-myc and VEGF in the B16F10 lung metastatic nodules after treatment with siRNA in different formulations. Magnification = 100x.

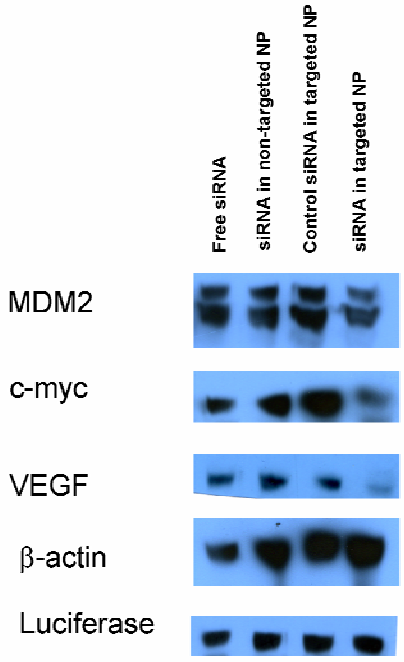

Figure 5.2 Western blot analysis on the tumor loaded lung.
Western blot analysis of MDM2, c-myc and VEGF in the B16F10 tumor loaded lung after treatment with siRNA in different formulations.

5.3.2 In vivo antitumor/antimetastasis study

To evaluate the therapeutic outcomes, we initiated two consecutive injections of siRNA (0.45 mg/kg, MDM2: c-myc: VEGF = 1:1:1, weight ratio) in different formulations 10 days after i.v. injection of B16F10 cells, which were stably transduced with a luciferase gene. As shown in **figure 5.3a**, metastasis nodules were significantly reduced in the lung collected from the mice treated with siRNA formulated in the targeted NP. Other control treatments, including free siRNA, siRNA in the non-targeted NP and control siRNA in the targeted NP, had very little therapeutic effect (**figure 5.3a**). The H&E stained tissue sections also showed that the lung treated by siRNA in the targeted NP only had a few small nodules, and most of the lung was free of tumor (**figure 5.3b**). However, metastasis nodules occupied most of the lung when mice were given with other control treatments (**figure 5.3b**). To quantify the B16F10 nodules in the lung, we collected one lobe of the excised lung and assayed for the luciferase activity. As indicated in **figure 5.3c**, siRNA in the targeted NP significantly reduced the tumor load to 20-30% compared to the untreated control ($p<0.01$), while other control treatments showed no significant effect. The therapeutic outcome was also analyzed by animal survival (**figure 5.3d**). On day 23, the survival rates for untreated control or mice treated with free siRNA, siRNA in the non-targeted NP, siRNA in the targeted NP and control siRNA in the targeted NP were 0%, 0% 50%, 90%, and 40%, respectively (**figure 5.3d**), and the mean survival time for which were 22, 22, 23.5, 28 and 22.5 d, respectively. Only siRNA in non-targeted NP or targeted NP significantly improved the animal survival compared to the free siRNA formulation ($p<0.05$). Control siRNA in the targeted NP did not improve the animal survival compared to the free siRNA ($p>0.05$). Although 2 injections of

siRNA in the non-targeted NP did not reduce the tumor metastasis (**figure 5.3a, b, c**), 4 injections of the same significantly improved the animal survival (**figure 5.3d**).

5.3.3 Toxicity study

At the therapeutic dose (0.45 mg/kg), the targeted NP did not induce significant production of all analyzed cytokines, including IL6, IL12, TNF and IFN-α (**figure 5.4**). Even after two consecutive injections, the IL6 and IL12 levels were not significantly elevated (data not shown). However, when the dose was increased, the inflammatory toxicity was significantly enhanced (**figure 5.4**), although moderate. At the therapeutic dose, no formulations elevated the cytokine production in the lung (**figure 5.5a**). Additionally, the body weight did not significantly decrease during the treatment at the therapeutic dose (**figure 5.5b**). The targeted NP formulation did not damage the major organs (heart, liver, spleen, lung and kidney) examined by the tissue section and H&E staining (**figure 5.6**).

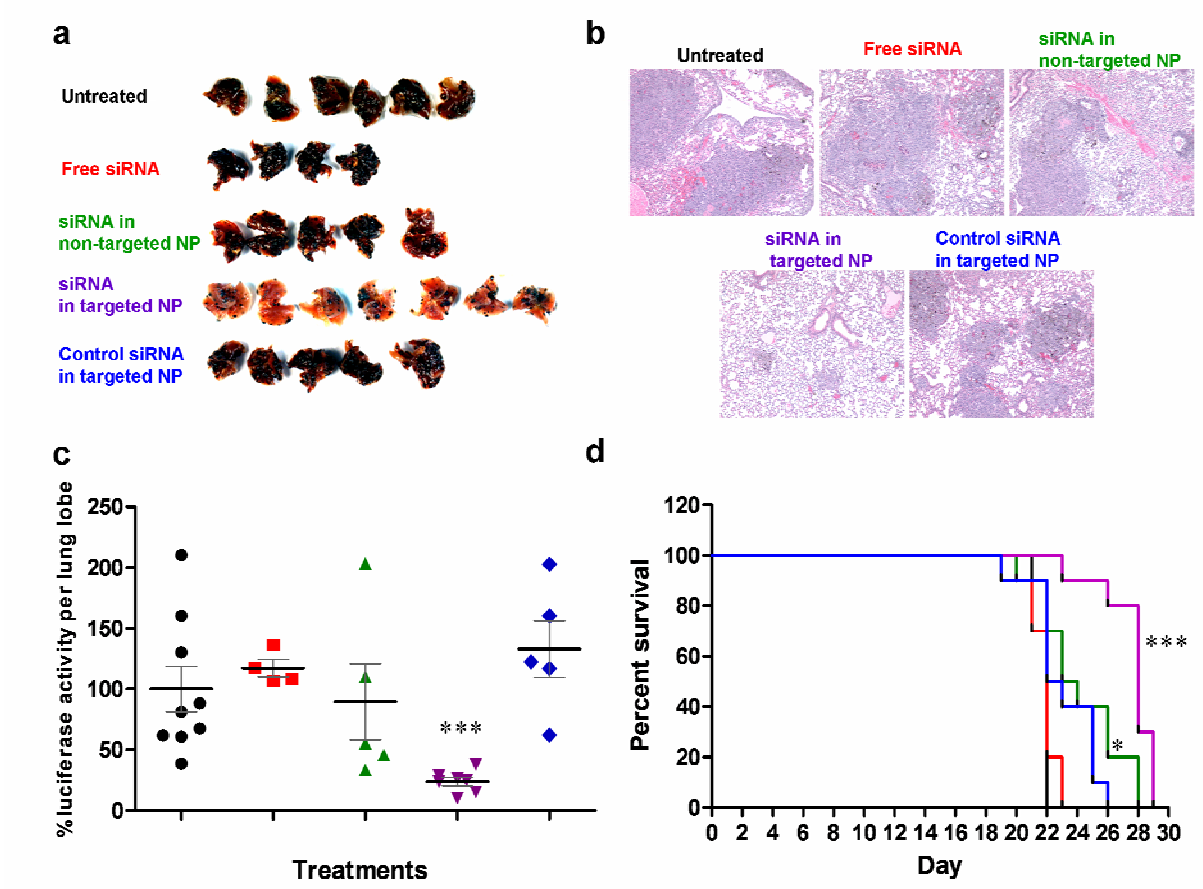

Figure 5.3 Anti-metastasis efficacy of different siRNA formulations.
(a) Images of lungs excised from the tumor bearing mice on day 17 after two consecutive treatments. (b) Photographs of the H&E stained tissue sections processed from the excised lungs. Magnification = 40x. (c) Luciferase activity in the tumor loaded lungs on day 17 after two consecutive i.v. injections of siRNA in different formulations on day 10 and 11. n = 4 – 9. *** indicates $p<0.0001$ compared to the siRNA in PBS formulation. Formulations from left to right: untreated control (black), siRNA in PBS (red), siRNA in non-targeted NP (green), siRNA in targeted NP (purple), control siRNA in targeted NP (blue). (d) Survival analysis of B16F10 lung metastasis bearing mice. Tumor bearing mice were i.v. injected with different siRNA formulations on day 10, 11, 17 and 18. n = 10. * indicates $p< 0.05$, *** indicates $p<0.0001$ compared to the siRNA in PBS formulation. Formulations: untreated control (black), siRNA in PBS (red), siRNA in non-targeted NP (green), siRNA in targeted NP (purple), control siRNA in targeted NP (blue).

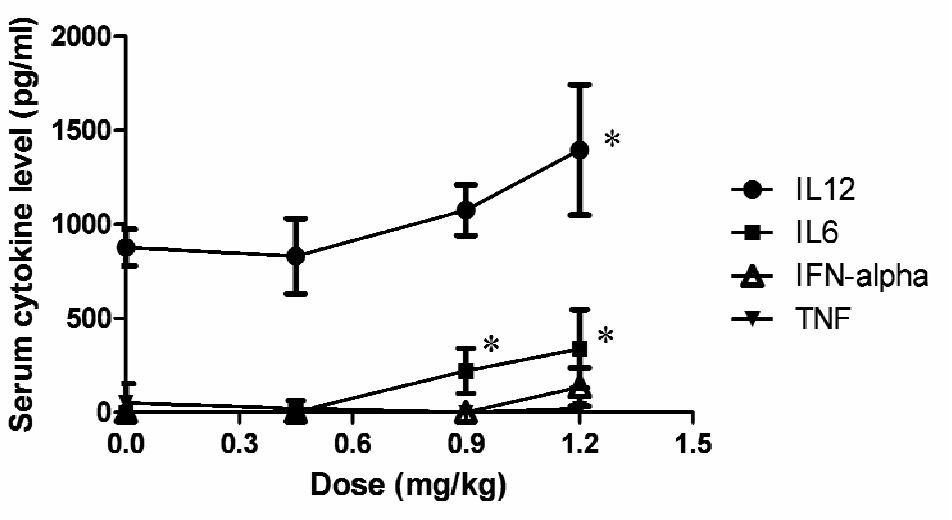

Figure 5.4 Serum cytokine analysis.
Serum cytokine levels of C57BL/6 mice 2 h after receiving i.v. injections of siRNA in targeted NP at different doses. Data = mean ± SD, n = 4. * indicates $p<0.05$; ** indicates $p<0.01$ compared to the untreated control.

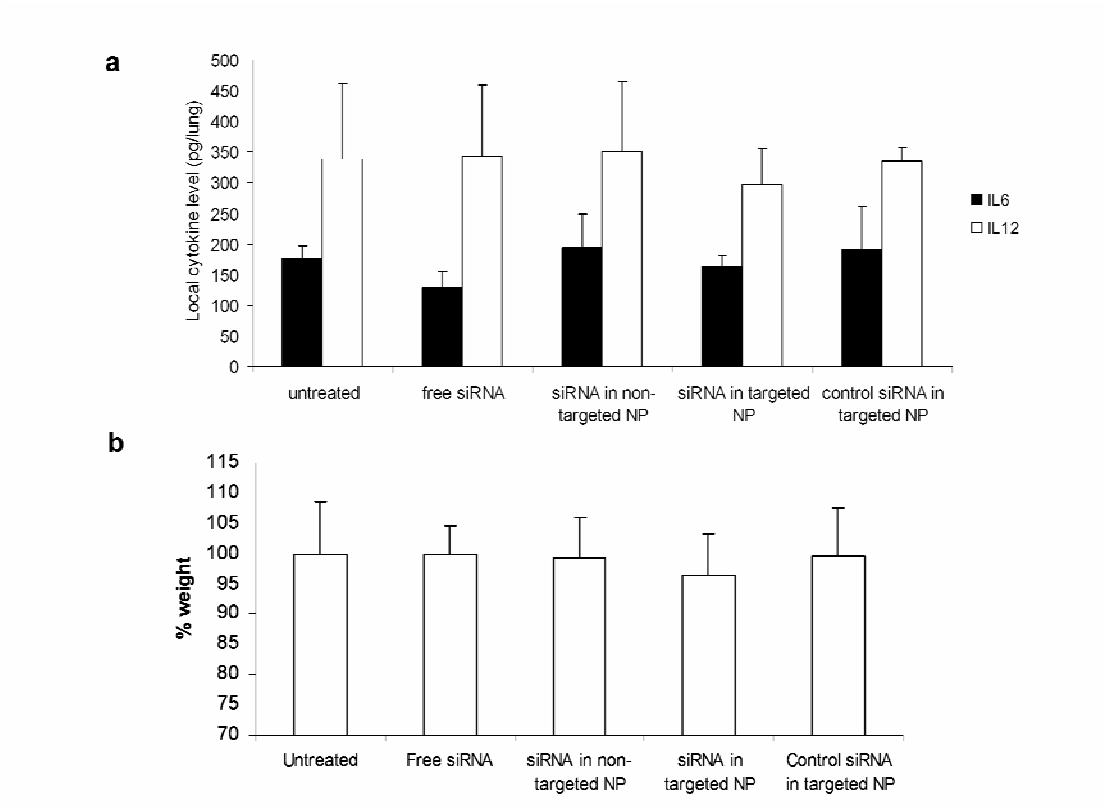

Figure 5.5 Toxicity assay.
(a) Cytokine production in the tumor loaded lung of the tumor bearing mice 2 h after the i.v. injection of siRNA in different formulations (dose = 0.45 mg/kg). Data = mean + SD, n = 3-4. (b) Mouse body weight one day after the second treatment of siRNA in different formulations. Data = mean + SD, n = 3-4.

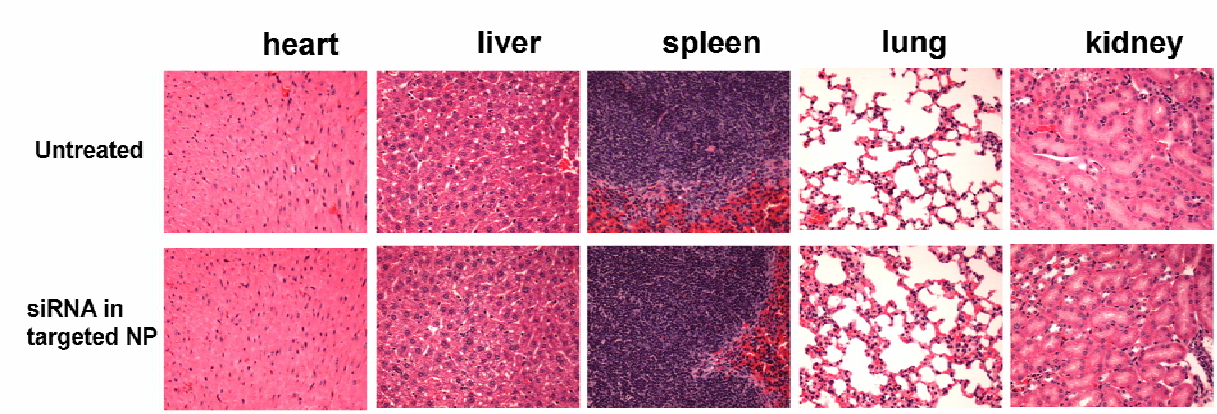

Figure 5.6 Tissue section examination.
Microscopic examination of the H&E stained tissue sections collected from the untreated control mouse or the targeted NP treated mouse. Magnification = 200x

5.4 DISCUSSION

To improve the antitumor/antimetastasis effect, we used combined siRNA sequences (MDM2: c-myc: VEGF = 1:1:1, weight ratio) to attack multiple oncogene pathways. MDM2 is an inactivator for p53 [85] and c-myc serves as an activated transcription factor, which promotes cell proliferation [86]. VEGF is a growth factor secreted by the tumor and mediates angiogenesis and metastasis [87]. According to the literature, simultaneous silence of these oncogenes by siRNA resulted in enhanced antiproliferation on the B16 cells [48]. Recently, it was demonstrated that combined delivery of different siRNA sequences resulted in siRNA competition for incorporation into RISC (RNA-induced silencning complex) and reduced RNAi efficacy [26,88]. To determine if combination of the three siRNA sequences interferes with the gene silencing activity of each sequence, we employed qRT-PCR method to quantify the RNAi activity of single sequence and pooled sequences delivered by the targeted NP. Indeed, we found the sequence competition effect, as the pooled siRNA formulation showed significantly reduced gene silencing activity on the c-myc and MDM2

genes but not on the VEGF gene compared to the single siRNA formulations (**figure 5.7**). However, the competition effect was moderate and significant gene knock-down (45-85%) was observed in all genes when 100 nM pooled siRNA was used. The data suggest that combined delivery of these three sequences may be acceptable. We have also checked the RNAi activity in protein level by immunocytochemistry. As shown in **figure 5.8**, siRNA in the targeted NP silenced MDM2, c-myc and VEGF in the B16F10 cells at the concentration of 100 nM (total siRNA), while other control treatments, including free siRNA, siRNA in non-targeted NP and control siRNA in targeted NP showed little effect. This resulted in an enhanced antiproliferation effect on the B16f10 cells by the targeted NP (data not shown). Both the in vitro and in vivo gene silencing results (**figure 5.1, 5.2 and 5.8**) showed that the gene silencing activity was highly formulation and siRNA sequence dependent, suggesting that only sufficient delivery of the correct sequences of siRNA resulted in significant activity. The antitumor activities of different formulations were highly correlated to their RNAi activities, in which only the targeted NP significantly reduced the tumor load (**figure 5.3a, b, c**).

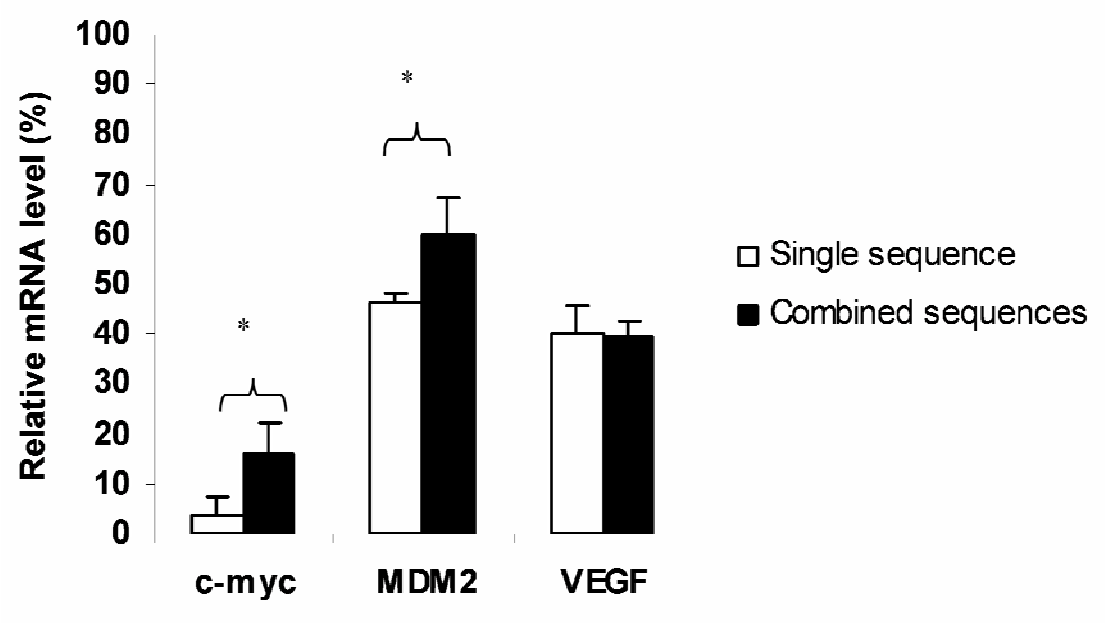

Figure 5.7 Relative mRNA level in the B16F10 cells 12 h after treatment with single or combined sequences formulated in the targeted NP.
Data = mean ± SD, n = 4. * indicates $p<0.05$

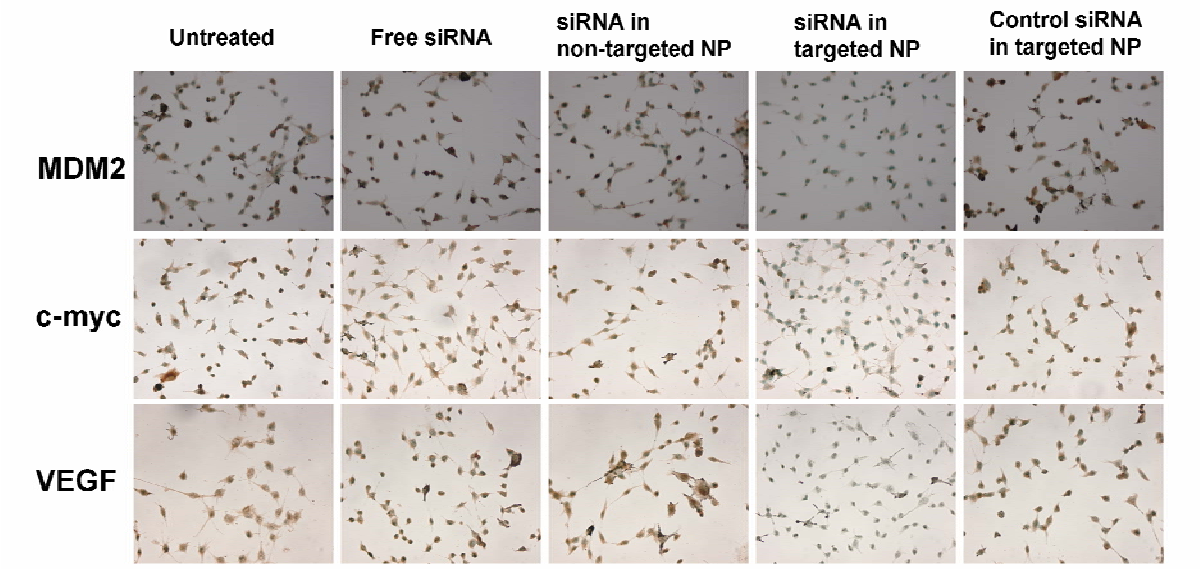

Figure 5.8 Immunocytochemical analysis on the B16F10 cells.
Immunocytochemical staining of MDM2, c-myc and VEGF in the B16F10 cells after treatment with siRNA in different formulations (from left to right: untreated control, siRNA in PBS, siRNA in non-targeted NP, siRNA in targeted NP, control siRNA in targeted NP). Total siRNA concentration = 100 nM. Magnification = 100x.

Although 2 injections of siRNA in the non-targeted NP did not reduce the tumor load in the lung (**figure 5.3a, b, c**), 4 injections of the same significantly improved the animal survival (**figure 5.3d,** $p<0.05$). The results suggest that multiple dosing may compensate the poor delivery of the non-targeted formulation. However, the survival prolongation of the non-targeted NP was moderate, although statistically significant. Targeted NP, on the other hand, with superior delivery efficiency for metastasis [32] not only significantly reduced the tumor load in the lung (**figure 5.3a, b, c**), but also prolonged the survival by approximately 30% (**figure 5.3d**). Targeted NP showed significantly improved therapeutic effects compared to any other siRNA formulations (**figure 5.3**). While unlikely, it is possible that the off-target effects of the combinatorial siRNA contributed to the in vivo reduction of tumor load. The off-target effect of siRNA causing non-specific gene down-regulation was first reported by Scacheri et al. [89]. It is speculated that partial complementary sequence of the siRNA matches to the off-target genes, and the genes are silenced via the micro-RNA mechanism. This is particular a concern when multiple siRNA sequences are used. Whether the off-target effects of the siRNA contributed to the antitumor effect of our formulation is not clear at the present time. However, the primary goal of this research is to develop a delivery system, the off-target effects contributing the antitumor activity will be studied and reported later. Additionally, the toxicity study showed that the targeted NP was safe at the therapeutic dose (**figure 5.4, 5.5, 5.6**).

To summarize, with the improved delivery of siRNA by the targeted NP [32], the corresponding oncogenes were simultaneously silenced, mass of lung metastasis was greatly reduced and animal survival was significantly prolonged with a relatively low and non-toxic

dose (0.45 mg/kg). Thus, we conclude that siRNA formulated in the targeted NP has the potential to become a useful method for cancer therapy.

6.0 DISCUSSION

6.1 SUMMARY OF RESEARCH RESULTS AND FUTURE PLANS

It is known that sufficient modification on the nanoparticle (NP) surface with an inert hydrophilic polymer is prerequisite for prolonged in vivo circulation time and the enhanced permeability and retention (EPR) effect for tumor delivery. With a supported lipid bilayer structure, the LPD NP could accomodate an increased degree of PEGylation compared to the conventional liposomes with a regular lipid bilayer. We have shown that approximately 10.6 mol% of the outer leaflet of the supported lipid bilayer was modified with DSPE-PEG, resulting in complete surface charge shielding and reduction in the reticuloendothelial uptake in the isolated liver model (**Chapter 2**). This highly PEGylated NP formulation delivered a high dose of siRNA (70-80% injected dose/g) to the s.c. tumor and induced significant RNAi and antitumor effects. The high tumor accumulation effect was primarily due to an improved EPR effect, since the targeting ligand (anisamide) containing formulation did not show further enhancement of tumor delivery. However, the targeted NP had increased intracellular delivery compared to the non-targeted NP (**Chapter 3**). The targeted NP also showed improved delivery to the lung metastasis, resulting in significant gene silencing, tumor load reduction and survival prolongation (**Chapter 4 and 5**).

Our future plan is to further optimize the formulation to enhance the antitumor effect and make the formulation suitable for human use. **First**, in the LPD formulation, we use a foreign DNA, calf thymus DNA, to improve the complex formation. However, the concerns of hypersensitivity, unexpected immune responses and the expression of foreign proteins in the patients receiving the formulation may prevent clinical use of the formulation. We plan to employ a biocompatible and negatively charged polymer, such as heparin and hyaluronic acid, to replace the calf thymus DNA to develop a new formulation. Since the LPD is formed by the charge-charge interaction, we predict that this new approach has a good chance of success. In addition, both heparin and hyaluronic acid have been approved by the US FDA for human use. However, intensive toxicity studies need to be done. **Second**, in the preliminary study (Chen and Huang, unpublished data), our lab has found that the DOTAP used in the formulation transiently activated some survival signals in the tumor cells, including p-ERK and survivin, which may compromise the antitumor effect of the formulation. We plan to synthesize a new class of cationic lipids that show higher delivery efficiency but no activation on survival pathways in the tumor cells. This may greatly enhance the antitumor activity of the new formulation. **Third**, the anisamide ligand is employed in the LPD for increasing the intracellular delivery into the sigma receptor expressing cells. However, sigma receptor is only expressed in certain type of human tumors. To further increase the spectrum of our formulation, we will have to develop other types of tumor targeting ligands. A small molecule ligand with high specificity is preferred due to the cost-effectiveness concern and low immunogenecity. A possible direction is to develop a ligand that targets angiogenic endothelial cells to improve the anti-angiogenesis and antitumor effect. **Fourth**, to facilitate the endosomal escape of the formulation, we plan

to synthesize and incorporate a diblock polypeptide [poly(histidine)-poly(arginine)] in the formulation. The protamine will be totally or partially replaced with the polypeptide in the new formulation. The poly-arginine segment will condense the nucleic acid into a nano-complex, while the poly-histidine can induce the proton sponge effect in the endosome to improve the release and bioavailability of siRNA.

6.2 SUPPLEMENTARY INFORMATION

6.2.1 Formulation

The LPD formulation was prepared in a self-assembling process upon charge-charge interaction. The process must be done in a diluted and salt-free condition to prevent aggregation. In this dissertation research, we prepared the formulation in the cloning water. Several concerns may be raised. **First**, low osmolarity of the nanoparticle suspension may cause transient hemolysis once i.v. administered. This potential problem can be solved by preparing the formulation in a salt-free and isotonic solution, such as 5% dextrose. **Second**, a mouse was given approximately 250-350 μl of the nanoparticle formulations (dose = 1.2 mg/kg), contributing to 18-20% of the blood volume of a mouse. Ideally, 10% of the blood volume is the maximum for i.v. administration. High volume injection may alter the physiology of the mouse. However, the nanoparticle must be prepared in a diluted condition to avoid aggregation and thus, a large volume is required to achieve the therapeutic dose. In future clinical practice, the LPD formulation can be given by slow i.v. infusion, which was used in the clinical trials for the SNALP formulation developed by the Protiva

Pharmaceuticals. For an 80 kg-patient, 0.4-1.2 L of the LPD formulation will be needed (0.45-1.2 mg/kg). **Third**, the pH of the LPD formulations was 5, which is tolerable for i.v. injection. **Fourth**, endotoxin has been known to trigger immunological responses in the host and free of endotoxin is a basic requirement for parenteral drugs used in human and animals. The upper limit for endotoxin in parenteral drugs generally acceptable to the U.S. Food and Drug Administration (FDA) is 5 EU/kg. For a 20 g-mouse, the tolerated endotoxin dose is 0.1 EU. The endotoxin level in the LPD formulation was 0.46 EU/ml and approximately 0.15 EU was injected into a 20 g-mouse at the dose of 1.2 mg siRNA/kg, which is slightly higher than the upper limit. Although the formulation was prepared with the cloning water (endotoxin free), the tips and eppendorff tubes were not properly treated to remove pyrogens, leaving the final suspension potentially contaminated with a low amount of endotoxin. To address this issue, the formulation must be prepared in an endotoxin free condition and the final product must be checked for its endotoxin level. The interference from the excepients on measurement of endotoxin should also be studied.

Another issue for the formulation is stability. We found precipitates in the formulation after storage at 4^{o}C for 1 week. The naked LPD has been shown to be stable in the same condition for 4 weeks. The DSPE-PEG micelle, on the other hand, precipitated during the storage at 4^{o}C. Therefore, it is likely that the instability of the PEGylated LPD formulation was due to the addition of DSPE-PEG micelle. It is anticipated that the purified formulation (by gel filtration) will have an improved stability. However, the high degree of dilution after purification is a critical disadvantage. Fortunately, the nanoparticles were prepared by a quick self-assembling procedure. With these, we decided to prepare the formulations freshly and used them without purification. Alternatively, LPD can be

lyophilized for long term storage [35]. We expect that the PEGylated LPD can also be stabilized the same way.

6.2.2 Pharmacokinetic study

6.2.2.1 Extraction recovery and the dose recovery from the major organs

The extraction recoveries of the free FAM-siRNA and FAM-siRNA in nanoparticles from the mouse serum were 98% and 48%, respectively. The serum concentration of the FAM-siRNA was determined by dividing the measured value by the extraction recovery. To determine the tissue accumulation of FAM-siRNA, a dose calibration curve for each organ was obtained by spiking known amounts of free FAM-siRNA or FAM-siRNA in nanoparticles in the tissue lysates. The extraction recoveries for the nanoparticle formulation in the organs is assumed to be 48% (not determined), which limited the detection range and led to the failure of detecting low amounts of the dose distributed in organs, such as the kidney, spleen and heart. This may contribute to the relatively low total dose recovery from the major organs (~60%). The loss of the dose in the tail, urine, bile or by the degradation in the liver may also contribute to the low recovery.

6.2.2.2 Can the high tumor uptake of the FAM-siRNA in nanoparticles be model dependent?

Four h after the i.v. administration of the FAM-siRNA in the nanoparticles, the dose remaining in the blood decreased to 10% injected dose (ID) in the tumor free mice. Majority of the siRNA distributed to the liver in the tumor free nude mice (**figure 6.1**, upper panel). Relatively speaking, the nanoparticle formulation was not very stealth. However, the

formulation delivered 70-80% ID into the NCI-H460 xenograft tumor. One possible explanation is that the nanoparticle had a high tendency to extravasate to the highly vascularized tissues, such as the liver and tumor. In the tumor free mice, the liver contributed majority of the uptake. In the tumor-bearing mice, the tumor competed the uptake of the formulation with the liver, resulting in reduced liver uptake. To address if the high tumor uptake of the formulation was model dependent, we performed the tissue distribution study in two other tumor models, including TC-1 tumor in C57BL/6 mice and CT-26 tumor in Balb/c mice. As shown in **figure 6.1** (lower panel), both the liver and tumor contributed significant uptake of the nanoparticle formulation in both models, indicating that some unique features of the NCI-H460 model may contribute to the high tumor uptake. Nevertheless, the nanoparticle formulation delivered a significant amount of siRNA to the tumor in both models. Quantitative tissue distribution studies will be performed to confirm the observation.

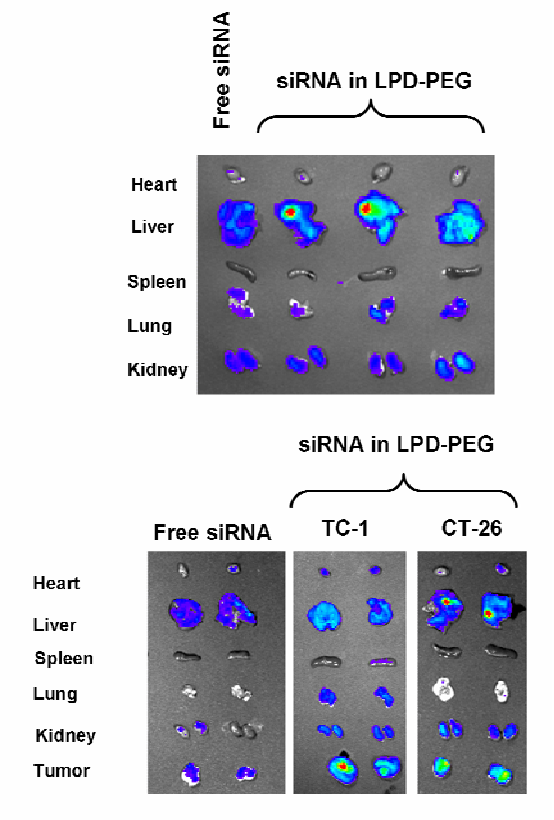

Figure 6.1 Tissue distribution of fluorescently labeled siRNA in different animal models.

Upper panel: tissue distribution in tumor free nude mice. Lower panel: tissue distribution in tumor-bearing mice. Tissues were analyzed 4 h after i.v. injection by the Xenogen IVIS™ imaging system.

6.3 FURTHER DIRECTIONS

The key success of the research is based on the existence of the supported lipid bilayer on surface of the NP. With the supported bilayer, a high degree of PEGylation can be achieved to provide full protection for the NP, leading to improved pharmacokinetics and tumor targeting. NP containing a supported bilayer can be designed by a variety of methods. The key point is to employ an extra force to stabilize one or both leaflet of the bilayer, such as electrostatic force or covalent bonding. Here, two strategies are proposed to prepare a

nanoparticle formulation with a supported bilayer for a hydrophilic drug. In both cases, the supported bilayer is stabilized with covalent bonds. We propose to utilize the amphipathic polymer to prepare the nanoparticles (**figure 6.2**). Amphipathic polymer contains a backbone polymer structure with an alternative arrangement of hydrophilic and hydrophobic side chains. The polymer can be used to prepare water in oil nano-emulsion with a water soluble drug in the aqueous phase. Organic solvent that is immiscible with water and volatile will be used for the oil phase, such as chloroform and dichloromethane. Then, the reverse-phase evaporation method will be performed to remove the solvent and coat the W/O nano-emulsion with another layer of the polymer [90]; and thus, the nanoparticle with a supported bilayer is obtained.

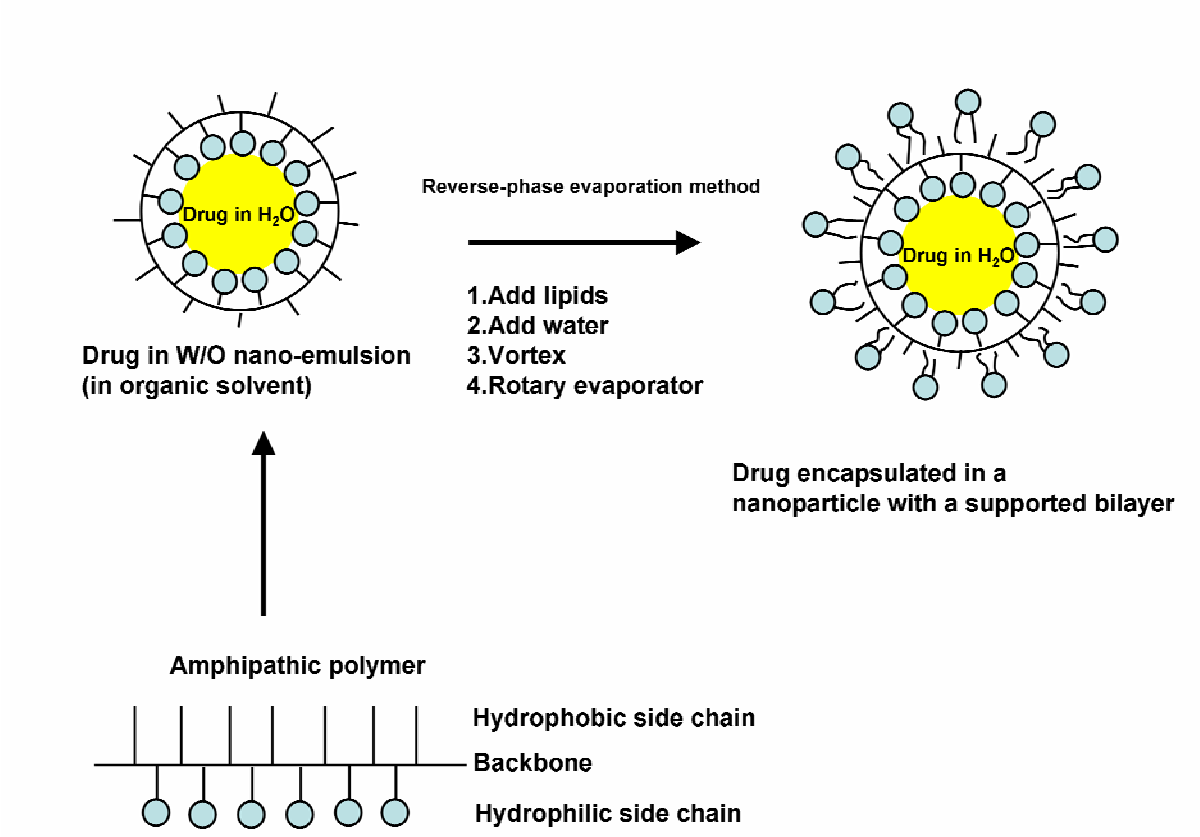

Figure 6.2 Proposed method for preparing a nanoparticle with a supported bilayer by amphipathic polymer

Another approach involves using a lipid-like surfactant with a polymerizable head group to prepare the nano-emulsion encapsulating a water soluble drug in the aqueous phase (**figure 6.3**). Then, the surfactants surrounding the aqueous phase are polymerized by the addition of an initiator. Finally, the reverse-phase evaporation method is used to coat another lipid leaflet on the particle and the nanoparticle with a supported bilayer is formed. It is noted that only the inner leaflet of the bilayer is cross-linked and the outer leaflet is of high fluidity for post-insertion of DSPE-PEG.

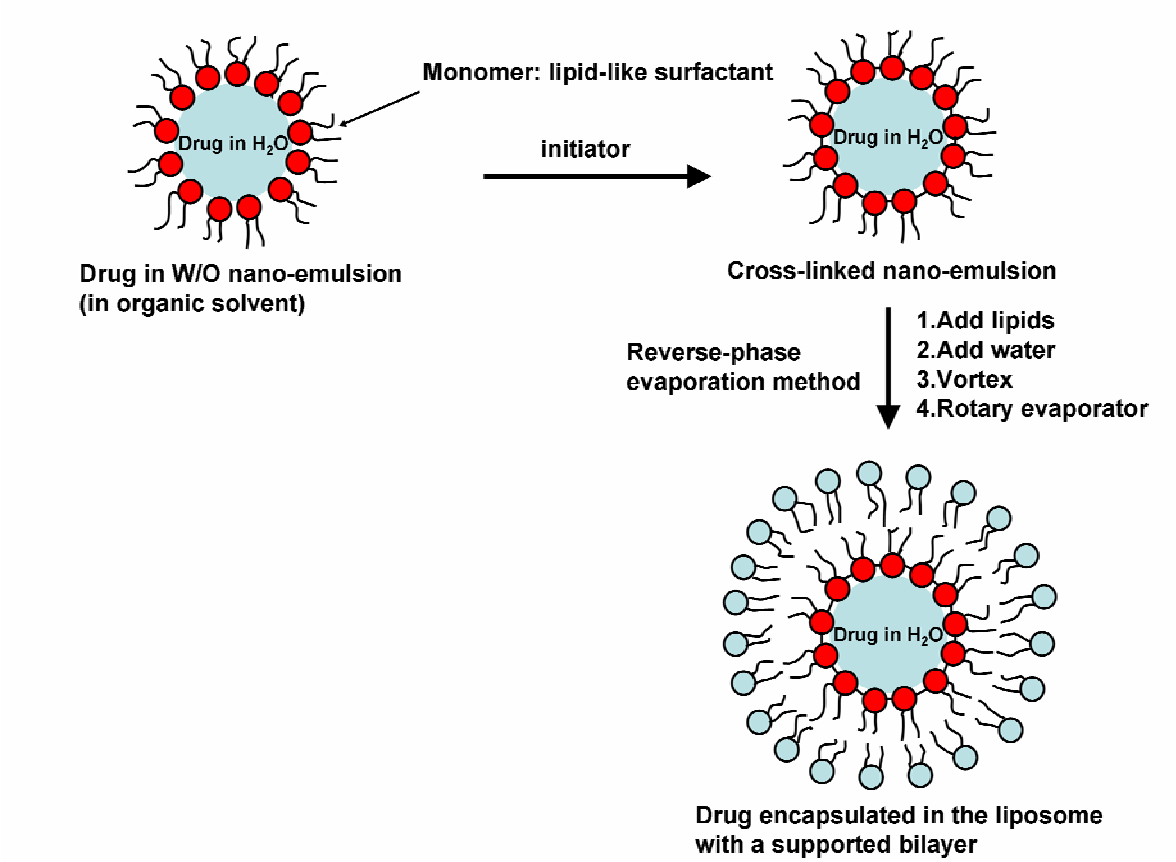

Figure 6.3 Preparation of a nanoparticle with a supported bilayer by the polymerization method

In both case, the hydrophilic group of the lipid or polymer in the outer leaflet is preferred to be positively charged for facilitating drug release from the endosome. As discussed in the **Chapter 1**, formation of charge complex between the cationic lipid and the anionic endosomal lipid may lead to local dehydration and destabilization of the endosomal membrane [18], resulting in the release of encapsulated drugs into the cytoplasm.

Another possible approach is to use a lipid with cross-linkable acyl chains to prepare the liposomes and then trigger the cross-linking reaction for the preparation of a supported bilayer. However, the cross-linking reaction in the interface is usually not complete and hard to control, leaving the lipid membrane a mixture of cross-linked lipid grafts of low fluidity

and single lipids with high fluidity. This results in increased membrane permeability and drug release.

6.4 ENDING REMARKS

siRNA based gene therapy has enjoyed a great success over the past few years. The success of siRNA is mainly due to three reasons. First, siRNA can be chemically synthesized in the pharmaceutical grade and can be chemically modified to have improved pharmacokinetics. Second, the fast advance of siRNA delivery technology is based on the foundation of experiences from plasmid DNA delivery accumulating since 1980s. Third, efficient nuclear delivery that has prevented the success of gene therapy is not required for siRNA.

The first clinical trial for siRNA has been successfully completed in 2005. The product, sirna-027, was developed by the Sirna Therapeutics, which was acquired by Merck for approximately $1.1 billion in 2006. This chemically modified siRNA is designed for treating macular degeneration by silencing VEGFR in the eyes. The results in the trial have encouraged Merck to move sirna-027 forward into phase II clinical trials. In addition to many small biotech companies devoting their research on siRNA based therapy, big pharmaceutical companies, such as Merck, Novartis, Roche, Pfizer, AstraZeneca and GlaxoSmithKline, have also put significant investments on this technology. Therefore, an increased number of clinical trials for siRNA products are to come and the bright future of siRNA is expected.

APPENDIX A

THEORY OF DYNAMIC LIGHT SCATTERING FOR PARTICLE SIZE ANALYSIS

The Nicomp Particle Size Analyzer uses Dynamic Light Scattering (DLS) to obtain the particle size distribution for samples with particles ranging from 1 nm to 5 microns. Through the use of the proprietary Nicomp analysis algortihm, the instrument can analyze multi-modal distributions with high resolution and reproducibility.

DLS, also known as Photon Correlation Spectroscopy (PCS), works by first measuring the scattered light intensity at one angle, which tends to decay with time periodically. These fluctuations in the intensity are caused by the constant moving of the particle brought on by Brownian motion. Larger particles tend to move more slowly. The time-dependent fluctuations in the scattered light are measured by a fast photon counter. The fluctuations are directly related to the rate of diffusion of the particle. Therefore, the fluctuations can be analyzed to determine a hydrodynamic radius of the particles.

The fluctuations are quantified via a second order correlation function measured by the instrument. The second order correlation function is given by

$$g^{(2)}(\tau) = \frac{\langle I(t)I(t+\tau)\rangle}{\langle I(t)\rangle^2} \qquad \textbf{(1)}$$

where I(t) is the intensity of the scattered light at time t, and the brackets indicate averaging over all t. The correlation function depends on the delay τ, the amount that a duplicate intensity trace is shifted from the original before the averaging is performed.

The correlation function for a monodisperse sample can be analyzed by the equation:

$$g^{(2)}(\tau) = B + \beta \times \exp(-2\Gamma\tau) \quad \textbf{(2)}$$

where B is the baseline of the correlation function at infinite delay, β is the correlation function amplitude at zero delay, and Γ is the decay rate. The software uses a nonlinear least squares fitting algorithm to fit the measured correlation function to equation 2 to obtain the decay rate Γ. Then, Γ can be converted to the diffusion constant (D) of the particle via the equation:

$$D = \frac{\Gamma}{q^2} \quad \textbf{(3)}$$

here, q is the magnitude of the scattering vector, and is given by:

$$q = \frac{4\pi n}{\lambda}\sin(\theta/2) \quad \textbf{(4)}$$

where n is the solvent index of refraction, λ is the vacuum wavelength of the incident light, and θ is the scattering angle.

Finally, the hydrodynamic radius (r_k) of a diffusing spherical particle can be obtained via the Stokes-Einstein equation:

$$r_k = \frac{kT}{6\pi\eta D} \quad \textbf{(5)}$$

where k is Boltzmann's constant, T is the temperature in K, and η is the solvent viscosity.

APPENDIX B

THEORY OF ZETA POTENTIAL MEASUREMENT

The ZetaPlus zeta potential analyzer (Brookhaven) calculates the zeta potential by determining the electrophoretic mobility and then applying the Henry equation. The electrophoretic mobility is measured by performing an electrophoresis experiment on the sample and determining the velocity of the particles.

What is zeta potential

The net charge at the particle surface attracts counter ions close to the surface (as shown in **figure 6.1**), resulting in formation of an electrical double layer around each particle.

The electrical double layer contains two layers, stern layer and diffuse layer. In the stern layer, the ions are strongly bound to the particle surface; while in the diffuse region, the ions are less firmly attached. Within the diffuse layer there is a boundary which the ions and particles form a stable entity. When a particle moves, ions within the boundary move with it, but not the ions beyond the boundary. The boundary is called the shear plane or slipping plane. The potential that exists at this boundary is known as the zeta potential.

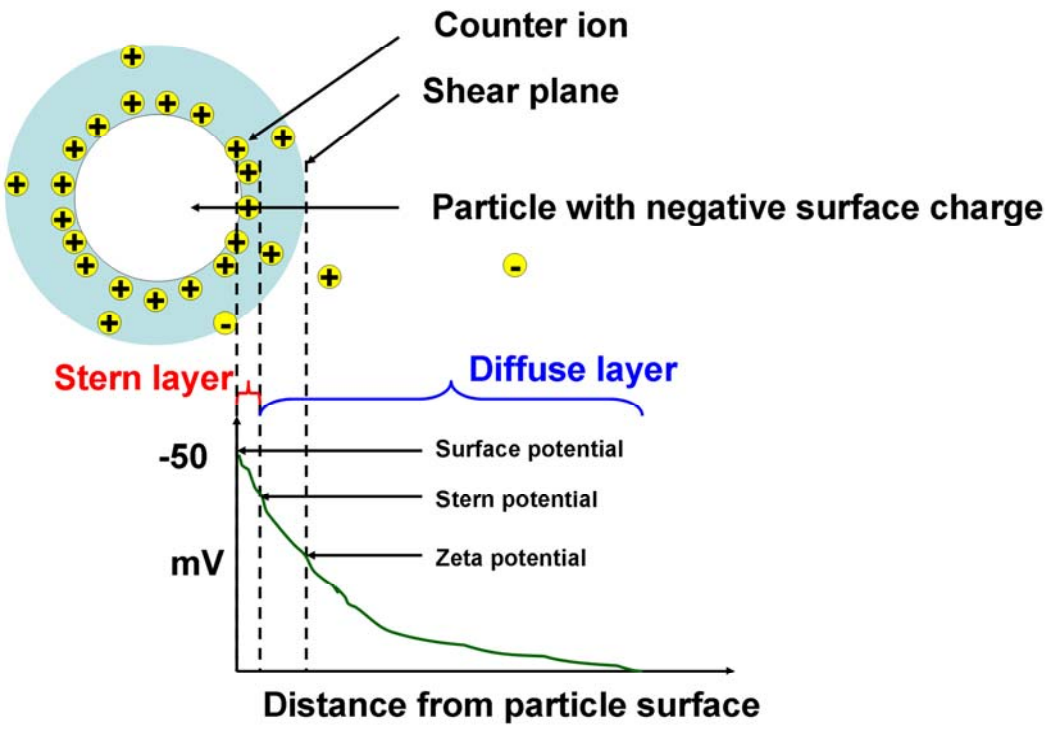

Figure 6.4 Illustration of the electrical double layer and zeta potential of a negatively charged particle

Measurement of zeta potential

When an electric field is applied, charged particles are attracted moving toward the electrode of opposite charge. When equilibrium is reached, the particles move in a constant velocity. The velocity of a particle in a given electric filed is referred to as its electrophoretic mobility. The zeta potential can be calculated by application of the Henry equation:

$$UE = \frac{2\varepsilon z f(ka)}{3\eta} \qquad \textbf{(6)}$$

z: zeta potential

U_E: electrophoretic mobility

ε: dielectric constant

η: viscosity

f(ka): Henry's function. Two values are generally used as approximations for the *f(ka)* determination, either 1.5 or 1.0. When electrophoretic determinations of zeta potential are made in aqueous media and moderate electrolyte concentration, *f(ka)* is 1.5 (referred to as the Smoluchowski approximation, for particles larger than 200 nm). For small particles in low dielectric constant media, *f(ka)* becomes 1.0 (referred to as the Huckel approximation).

APPENDIX C

SHYH-DAR LI'S PUBLICATION

Peer-reviewed Papers

- **Shyh-Dar Li** and Leaf Huang. Nanoparticles Stabilized with a Supported Bilayer. (submitted)
- **Shyh-Dar Li**, Sumio Chono, and Leaf Huang. Efficient Oncogene Silencing and Metastasis Inhibition via Systemic Delivery of siRNA. Mol Ther (accepted)
- **Shyh-Dar Li**, Sumio Chono, and Leaf Huang. Efficient Gene Silencing in Metastatic Tumor by siRNA Formulated in Surface-modified Nanoparticles. J Controlled Release 126 (1): 77-84, 2008
- **Shyh-Dar Li**, Yung-Ching Chen, Michael J. Hackett and Leaf Huang. Targeted Delivery of siRNA by Self-assembled Nanoparticles. Mol Ther 16 (1): 163-169, 2008
- Feng Liu, Demet Sag, Jue Wang, Lisa M Shollenberger, Feilong Niu, Xing Yuan, **Shyh-Dar Li**, Mike Thompson and Paul Monahan. Sine-wave Current for Efficient and Safe *In Vivo* Gene Transfer. Molecular Therapy 15 (10): 1842–1847, 2007
- **Shyh-Dar Li** and Leaf Huang. Surface-modified LPD Nanoparticles for Tumor Targeting. Ann N Y Acad Sci. 1082:1-8, 2006
- **Shyh-Dar Li** and Leaf Huang. Targeted Delivery of Antisense Oligodeoxynucleotide and Small Interference RNA into Lung Cancer Cells. Mol Pharm. 3 (5):579-88, 2006

Review Papers and Perspectives

- **Shyh-Dar Li** and Leaf Huang. Non-viral is Superior to Viral Gene Delivery (perspective). J Controlled Release 123 (3): 181-183, 2007
- **Shyh-Dar Li** and Leaf Huang. Gene Therapy Progress and Prospects: Non-viral Gene Therapy by Systemic Delivery (review). Gene Ther. 13(18):1313-9, 2006
- **Shyh-Dar Li** and Leaf Huang. Targeted Delivery of siRNA: Lessons from the Recent Advances. Current Opinion in Molecular Therapy (under review)
- **Shyh-Dar Li** and Leaf Huang. Pharmacokinetics and Biodistribution of Nanoparticles. Molecular Pharmaceutics (in preparation)

Book Chapter

- **Shyh-Dar Li**, Song Li and Leaf Huang. Lipoplex and LPD Nanoparticles for In Vivo Gene Delivery. In "Gene Transfer. Delivery and Expression of DNA and RNA", Eds, Friedman, T and Rossi J. Cold Spring Harbor Laboratory Press. Chapter 39, pp 433 – 438, 2006.

Conference Abstracts

- **Shyh-Dar Li**, Sumio Chono and Leaf Huang. Efficient Gene Silencing in Metastatic Tumors by Systemically Delivered siRNA. NCI Alliance Meeting. Chapel Hill, NC, USA, 2007
- **Shyh-Dar Li** and Leaf Huang. Targeted Delivery of siRNA for Lung Cancer and Lung Metastases Therapy. AAPS Annual Meeting. San Diego, USA, 2007 (**Selected for oral and poster presentation in AAPS graduate student symposium in drug delivery and pharmaceutical technologies**)
- **Shyh-Dar Li** and Leaf Huang. Targeted Delivery of Antisense Oligonucleotide and siRNA into Lung Cancer Cells. 9th Annual Meeting of American Society of Gene Therapy. Baltimore, Maryland, USA. 2006
- **Shyh-Dar Li** and Leaf Huang. Tumor Targeted Delivery of siRNA by i.v. injection. 10th Liposome Research Days Conference, Chapel Hill, NC, USA, 2006 (**Selected Oral Presentation. Genzyme Pharmaceutics Outstanding Poster Award**)
- **Shyh-Dar Li** and Leaf Huang. Targeted delivery of antisense oligodeoxynucleotide and small interference RNA into lung cancer cells. Ann N Y Acad Sci. Fist Oligonucleotide Meeting. NYC, NY 2005 (**Invited Speaker**)

BIBLIOGRAPHY

1. Jana S, Chakraborty C, Nandi S, Deb JK: **RNA interference: potential therapeutic targets**. *Appl Microbiol Biotechnol* 2004, **65**:649-657.

2. Kim DH, Rossi JJ: **Strategies for silencing human disease using RNA interference**. *Nat Rev Genet* 2007, **8**:173-184.

3. Kim WJ, Chang CW, Lee M, Kim SW: **Efficient siRNA delivery using water soluble lipopolymer for anti-angiogenic gene therapy**. *J Control Release* 2007, **118**:357-363.

4. Li SD, Huang L: **Gene therapy progress and prospects: non-viral gene therapy by systemic delivery**. *Gene Ther* 2006, **13**:1313-1319.

5. Wolfrum C, Shi S, Jayaprakash KN, Jayaraman M, Wang G, Pandey RK, Rajeev KG, Nakayama T, Charrise K, Ndungo EM, et al.: **Mechanisms and optimization of in vivo delivery of lipophilic siRNAs**. *Nat Biotechnol* 2007, **25**:1149-1157.

6. DiFiglia M, Sena-Esteves M, Chase K, Sapp E, Pfister E, Sass M, Yoder J, Reeves P, Pandey RK, Rajeev KG, et al.: **Therapeutic silencing of mutant huntingtin with siRNA attenuates striatal and cortical neuropathology and behavioral deficits**. *Proc Natl Acad Sci U S A* 2007, **104**:17204-17209.

7. Rozema DB, Lewis DL, Wakefield DH, Wong SC, Klein JJ, Roesch PL, Bertin SL, Reppen TW, Chu Q, Blokhin AV, et al.: **Dynamic PolyConjugates for targeted in vivo delivery of siRNA to hepatocytes**. *Proc Natl Acad Sci U S A* 2007, **104**:12982-12987.

8. Li SD, Chen YC, Hackett MJ, Huang L: **Tumor-targeted Delivery of siRNA by Self-assembled Nanoparticles**. *Mol Ther* 2008, **16**:163-169.

9. Bolcato-Bellemin AL, Bonnet ME, Creusat G, Erbacher P, Behr JP: **Sticky overhangs enhance siRNA-mediated gene silencing**. *Proc Natl Acad Sci U S A* 2007, **104**:16050-16055.

10. Bartlett DW, Su H, Hildebrandt IJ, Weber WA, Davis ME: **Impact of tumor-specific targeting on the biodistribution and efficacy of siRNA nanoparticles measured by multimodality in vivo imaging**. *Proc Natl Acad Sci U S A* 2007, **104**:15549-15554.

11. Heidel JD, Yu Z, Liu JY, Rele SM, Liang Y, Zeidan RK, Kornbrust DJ, Davis ME: **Administration in non-human primates of escalating intravenous doses of**

targeted nanoparticles containing ribonucleotide reductase subunit M2 siRNA. *Proc Natl Acad Sci U S A* 2007, **104**:5715-5721.

12. Pirollo KF, Rait A, Zhou Q, Hwang SH, Dagata JA, Zon G, Hogrefe RI, Palchik G, Chang EH: **Materializing the potential of small interfering RNA via a tumor-targeting nanodelivery system**. *Cancer Res* 2007, **67**:2938-2943.

13. Kumar P, Wu H, McBride JL, Jung KE, Kim MH, Davidson BL, Lee SK, Shankar P, Manjunath N: **Transvascular delivery of small interfering RNA to the central nervous system**. *Nature* 2007, **448**:39-43.

14. Harding JA, Engbers CM, Newman MS, Goldstein NI, Zalipsky S: **Immunogenicity and pharmacokinetic attributes of poly(ethylene glycol)-grafted immunoliposomes**. *Biochim Biophys Acta* 1997, **1327**:181-192.

15. Andresen TL, Jensen SS, Jorgensen K: **Advanced strategies in liposomal cancer therapy: problems and prospects of active and tumor specific drug release**. *Prog Lipid Res* 2005, **44**:68-97.

16. Boussif O, Zanta MA, Behr JP: **Optimized galenics improve in vitro gene transfer with cationic molecules up to 1000-fold**. *Gene Ther* 1996, **3**:1074-1080.

17. Sonawane ND, Szoka FC, Jr., Verkman AS: **Chloride accumulation and swelling in endosomes enhances DNA transfer by polyamine-DNA polyplexes**. *J Biol Chem* 2003, **278**:44826-44831.

18. Wattiaux R, Jadot M, Warnier-Pirotte MT, Wattiaux-De Coninck S: **Cationic lipids destabilize lysosomal membrane in vitro**. *FEBS Lett* 1997, **417**:199-202.

19. Medarova Z, Pham W, Farrar C, Petkova V, Moore A: **In vivo imaging of siRNA delivery and silencing in tumors**. *Nat Med* 2007, **13**:372-377.

20. Judge AD, Sood V, Shaw JR, Fang D, McClintock K, MacLachlan I: **Sequence-dependent stimulation of the mammalian innate immune response by synthetic siRNA**. *Nat Biotechnol* 2005, **23**:457-462.

21. Judge AD, Bola G, Lee AC, MacLachlan I: **Design of noninflammatory synthetic siRNA mediating potent gene silencing in vivo**. *Mol Ther* 2006, **13**:494-505.

22. Robbins M, Judge A, Liang L, McClintock K, Yaworski E, MacLachlan I: **2'-O-methyl-modified RNAs act as TLR7 antagonists**. *Mol Ther* 2007, **15**:1663-1669.

23. Li SD, Huang L: **Non-viral is superior to viral gene delivery**. *J Control Release* 2007, **123**:181-183.

24. Hu-Lieskovan S, Heidel JD, Bartlett DW, Davis ME, Triche TJ: **Sequence-specific knockdown of EWS-FLI1 by targeted, nonviral delivery of small interfering RNA inhibits tumor growth in a murine model of metastatic Ewing's sarcoma**. *Cancer Res* 2005, **65**:8984-8992.

25. Bartlett DW, Davis ME: **Physicochemical and biological characterization of targeted, nucleic acid-containing nanoparticles**. *Bioconjug Chem* 2007, **18**:456-468.

26. Castanotto D, Sakurai K, Lingeman R, Li H, Shively L, Aagaard L, Soifer H, Gatignol A, Riggs A, Rossi JJ: **Combinatorial delivery of small interfering RNAs reduces RNAi efficacy by selective incorporation into RISC**. *Nucleic Acids Res* 2007, **35**:5154-5164.

27. Oh P, Borgstrom P, Witkiewicz H, Li Y, Borgstrom BJ, Chrastina A, Iwata K, Zinn KR, Baldwin R, Testa JE, et al.: **Live dynamic imaging of caveolae pumping targeted antibody rapidly and specifically across endothelium in the lung**. *Nat Biotechnol* 2007, **25**:327-337.

28. Li B, Li S, Tan Y, Stolz DB, Watkins SC, Block LH, Huang L: **Lyophilization of cationic lipid-protamine-DNA (LPD) complexes**. *J Pharm Sci* 2000, **89**:355-364.

29. Klibanov AL, Maruyama K, Torchilin VP, Huang L: **Amphipathic polyethyleneglycols effectively prolong the circulation time of liposomes**. *FEBS Lett* 1990, **268**:235-237.

30. Li S, Huang L: **In vivo gene transfer via intravenous administration of cationic lipid-protamine-DNA (LPD) complexes**. *Gene Ther* 1997, **4**:891-900.

31. Vangasseri DP, Han SJ, Huang L: **Lipid-protamine-DNA-mediated antigen delivery**. *Curr Drug Deliv* 2005, **2**:401-406.

32. Li SD, Chono S, Huang L: **Efficient gene silencing in metastatic tumor by siRNA formulated in surface-modified nanoparticles**. *J Control Release* 2007.

33. Li SD, Huang L: **Targeted delivery of antisense oligodeoxynucleotide and small interference RNA into lung cancer cells**. *Mol Pharm* 2006, **3**:579-588.

34. Li SD, Huang L: **Surface-modified LPD nanoparticles for tumor targeting**. *Ann N Y Acad Sci* 2006, **1082**:1-8.

35. Tan Y, Whitmore M, Li S, Frederik P, Huang L: **LPD nanoparticles--novel nonviral vector for efficient gene delivery**. *Methods Mol Med* 2002, **69**:73-81.

36. Yan X, Scherphof GL, Kamps JA: **Liposome opsonization**. *J Liposome Res* 2005, **15**:109-139.

37. Dos Santos N, Allen C, Doppen AM, Anantha M, Cox KA, Gallagher RC, Karlsson G, Edwards K, Kenner G, Samuels L, et al.: **Influence of poly(ethylene glycol) grafting density and polymer length on liposomes: relating plasma circulation lifetimes to protein binding**. *Biochim Biophys Acta* 2007, **1768**:1367-1377.

38. Garbuzenko O, Barenholz Y, Priev A: **Effect of grafted PEG on liposome size and on compressibility and packing of lipid bilayer**. *Chem Phys Lipids* 2005, **135**:117-129.

39. Kenworthy AK, Hristova K, Needham D, McIntosh TJ: **Range and magnitude of the steric pressure between bilayers containing phospholipids with covalently attached poly(ethylene glycol)**. *Biophys J* 1995, **68**:1921-1936.

40. Nicholas AR, Scott MJ, Kennedy NI, Jones MN: **Effect of grafted polyethylene glycol (PEG) on the size, encapsulation efficiency and permeability of vesicles**. *Biochim Biophys Acta* 2000, **1463**:167-178.

41. Owens DE, 3rd, Peppas NA: **Opsonization, biodistribution, and pharmacokinetics of polymeric nanoparticles**. *Int J Pharm* 2006, **307**:93-102.

42. Li W, Szoka FC, Jr.: **Lipid-based nanoparticles for nucleic acid delivery**. *Pharm Res* 2007, **24**:438-449.

43. Grzelinski M, Urban-Klein B, Martens T, Lamszus K, Bakowsky U, Hobel S, Czubayko F, Aigner A: **RNA interference-mediated gene silencing of pleiotrophin through polyethylenimine-complexed small interfering RNAs in vivo exerts antitumoral effects in glioblastoma xenografts**. *Hum Gene Ther* 2006, **17**:751-766.

44. Halder J, Kamat AA, Landen CN, Jr., Han LY, Lutgendorf SK, Lin YG, Merritt WM, Jennings NB, Chavez-Reyes A, Coleman RL, et al.: **Focal adhesion kinase targeting using in vivo short interfering RNA delivery in neutral liposomes for ovarian carcinoma therapy**. *Clin Cancer Res* 2006, **12**:4916-4924.

45. McNamara JO, 2nd, Andrechek ER, Wang Y, Viles KD, Rempel RE, Gilboa E, Sullenger BA, Giangrande PH: **Cell type-specific delivery of siRNAs with aptamer-siRNA chimeras**. *Nat Biotechnol* 2006, **24**:1005-1015.

46. Santel A, Aleku M, Keil O, Endruschat J, Esche V, Fisch G, Dames S, Loffler K, Fechtner M, Arnold W, et al.: **A novel siRNA-lipoplex technology for RNA interference in the mouse vascular endothelium**. *Gene Ther* 2006, **13**:1222-1234.

47. Schiffelers RM, Ansari A, Xu J, Zhou Q, Tang Q, Storm G, Molema G, Lu PY, Scaria PV, Woodle MC: **Cancer siRNA therapy by tumor selective delivery with ligand-targeted sterically stabilized nanoparticle**. *Nucleic Acids Res* 2004, **32**:e149.

48. Song E, Zhu P, Lee SK, Chowdhury D, Kussman S, Dykxhoorn DM, Feng Y, Palliser D, Weiner DB, Shankar P, et al.: **Antibody mediated in vivo delivery of small interfering RNAs via cell-surface receptors**. *Nat Biotechnol* 2005, **23**:709-717.

49. Takeshita F, Minakuchi Y, Nagahara S, Honma K, Sasaki H, Hirai K, Teratani T, Namatame N, Yamamoto Y, Hanai K, et al.: **Efficient delivery of small interfering RNA to bone-metastatic tumors by using atelocollagen in vivo**. *Proc Natl Acad Sci U S A* 2005, **102**:12177-12182.

50. Wang Y, Gao S, Ye WH, Yoon HS, Yang YY: **Co-delivery of drugs and DNA from cationic core-shell nanoparticles self-assembled from a biodegradable copolymer**. *Nat Mater* 2006, **5**:791-796.

51. Yang R, Yang X, Zhang Z, Zhang Y, Wang S, Cai Z, Jia Y, Ma Y, Zheng C, Lu Y, et al.: **Retraction. Single-walled carbon nanotubes-mediated in vivo and in vitro delivery of siRNA into antigen-presenting cells**. *Gene Ther* 2007, **14**:920.

52. de Wolf HK, Snel CJ, Verbaan FJ, Schiffelers RM, Hennink WE, Storm G: **Effect of cationic carriers on the pharmacokinetics and tumor localization of nucleic acids after intravenous administration**. *Int J Pharm* 2007, **331**:167-175.

53. Banerjee R, Tyagi P, Li S, Huang L: **Anisamide-targeted stealth liposomes: a potent carrier for targeting doxorubicin to human prostate cancer cells**. *Int J Cancer* 2004, **112**:693-700.

54. Jones HE, Gee JM, Hutcheson IR, Knowlden JM, Barrow D, Nicholson RI: **Growth factor receptor interplay and resistance in cancer**. *Endocr Relat Cancer* 2006, **13 Suppl 1**:S45-51.

55. Nicholson RI, Gee JM, Harper ME: **EGFR and cancer prognosis**. *Eur J Cancer* 2001, **37 Suppl 4**:S9-15.

56. Byers LA, Heymach JV: **Dual targeting of the vascular endothelial growth factor and epidermal growth factor receptor pathways: rationale and clinical applications for non-small-cell lung cancer**. *Clin Lung Cancer* 2007, **8 Suppl 2**:S79-85.

57. Dassonville O, Bozec A, Fischel JL, Milano G: **EGFR targeting therapies: monoclonal antibodies versus tyrosine kinase inhibitors. Similarities and differences**. *Crit Rev Oncol Hematol* 2007, **62**:53-61.

58. Sathornsumetee S, Rich JN: **New approaches to primary brain tumor treatment**. *Anticancer Drugs* 2006, **17**:1003-1016.

59. Wong SF: **Cetuximab: an epidermal growth factor receptor monoclonal antibody for the treatment of colorectal cancer**. *Clin Ther* 2005, **27**:684-694.

60. Fan QW, Weiss WA: **RNA interference against a glioma-derived allele of EGFR induces blockade at G2M**. *Oncogene* 2005, **24**:829-837.

61. Kang CS, Pu PY, Li YH, Zhang ZY, Qiu MZ, Huang Q, Wang GX: **An in vitro study on the suppressive effect of glioma cell growth induced by plasmid-based small interference RNA (siRNA) targeting human epidermal growth factor receptor**. *J Neurooncol* 2005, **74**:267-273.

62. Kang CS, Zhang ZY, Jia ZF, Wang GX, Qiu MZ, Zhou HX, Yu SZ, Chang J, Jiang H, Pu PY: **Suppression of EGFR expression by antisense or small interference RNA inhibits U251 glioma cell growth in vitro and in vivo**. *Cancer Gene Ther* 2006, **13**:530-538.

63. Nozawa H, Tadakuma T, Ono T, Sato M, Hiroi S, Masumoto K, Sato Y: **Small interfering RNA targeting epidermal growth factor receptor enhances chemosensitivity to cisplatin, 5-fluorouracil and docetaxel in head and neck squamous cell carcinoma**. *Cancer Sci* 2006, **97**:1115-1124.

64. Vollmann A, Vornlocher HP, Stempfl T, Brockhoff G, Apfel R, Bogdahn U: **Effective silencing of EGFR with RNAi demonstrates non-EGFR dependent proliferation of glioma cells**. *Int J Oncol* 2006, **28**:1531-1542.

65. Wu X, Deng Y, Wang G, Tao K: **Combining siRNAs at two different sites in the EGFR to suppress its expression, induce apoptosis, and enhance 5-fluorouracil sensitivity of colon cancer cells**. *J Surg Res* 2007, **138**:56-63.

66. Zhang M, Zhang X, Bai CX, Chen J, Wei MQ: **Inhibition of epidermal growth factor receptor expression by RNA interference in A549 cells**. *Acta Pharmacol Sin* 2004, **25**:61-67.

67. Zhang X, Chen ZG, Choe MS, Lin Y, Sun SY, Wieand HS, Shin HJ, Chen A, Khuri FR, Shin DM: **Tumor growth inhibition by simultaneously blocking epidermal growth factor receptor and cyclooxygenase-2 in a xenograft model**. *Clin Cancer Res* 2005, **11**:6261-6269.

68. Zhang Y, Zhang YF, Bryant J, Charles A, Boado RJ, Pardridge WM: **Intravenous RNA interference gene therapy targeting the human epidermal growth factor receptor prolongs survival in intracranial brain cancer**. *Clin Cancer Res* 2004, **10**:3667-3677.

69. Hornung V, Guenthner-Biller M, Bourquin C, Ablasser A, Schlee M, Uematsu S, Noronha A, Manoharan M, Akira S, de Fougerolles A, et al.: **Sequence-specific potent induction of IFN-alpha by short interfering RNA in plasmacytoid dendritic cells through TLR7**. *Nat Med* 2005, **11**:263-270.

70. Agrawal S, Kandimalla ER: **Role of Toll-like receptors in antisense and siRNA [corrected]**. *Nat Biotechnol* 2004, **22**:1533-1537.

71. Robbins MA, Rossi JJ: **Sensing the danger in RNA**. *Nat Med* 2005, **11**:250-251.

72. Gekeler V, Gimmnich P, Hofmann HP, Grebe C, Rommele M, Leja A, Baudler M, Benimetskaya L, Gonser B, Pieles U, et al.: **G3139 and other CpG-containing immunostimulatory phosphorothioate oligodeoxynucleotides are potent suppressors of the growth of human tumor xenografts in nude mice**. *Oligonucleotides* 2006, **16**:83-93.

73. Wang L, Smith D, Bot S, Dellamary L, Bloom A, Bot A: **Noncoding RNA danger motifs bridge innate and adaptive immunity and are potent adjuvants for vaccination**. *J Clin Invest* 2002, **110**:1175-1184.

74. Dong Z, Radinsky R, Fan D, Tsan R, Bucana CD, Wilmanns C, Fidler IJ: **Organ-specific modulation of steady-state mdr gene expression and drug resistance in murine colon cancer cells**. *J Natl Cancer Inst* 1994, **86**:913-920.

75. Takahashi Y, Nishikawa M, Kobayashi N, Takakura Y: **Gene silencing in primary and metastatic tumors by small interfering RNA delivery in mice: quantitative analysis using melanoma cells expressing firefly and sea pansy luciferases**. *J Control Release* 2005, **105**:332-343.

76. Pham TQ, Berghofer P, Liu X, Greguric I, Dikic B, Ballantyne P, Mattner F, Nguyen V, Loc'h C, Katsifis A: **Preparation and biologic evaluation of a novel radioiodinated benzylpiperazine, 123I-MEL037, for malignant melanoma**. *J Nucl Med* 2007, **48**:1348-1356.

77. Zhang JS, Liu F, Conwell CC, Tan Y, Huang L: **Mechanistic studies of sequential injection of cationic liposome and plasmid DNA**. *Mol Ther* 2006, **13**:429-437.

78. Brannon-Peppas L, Blanchette JO: **Nanoparticle and targeted systems for cancer therapy**. *Adv Drug Deliv Rev* 2004, **56**:1649-1659.

79. Ashley AC, Deschamps C, Alberts SR: **Impact of prognostic factors on clinical outcome after resection of colorectal pulmonary metastases**. *Clin Colorectal Cancer* 2006, **6**:32-37.

80. Bacci G, Avella M, Picci P, Briccoli A, Dallari D, Campanacci M: **Metastatic patterns in osteosarcoma**. *Tumori* 1988, **74**:421-427.

81. Geschwind JF, Dagli MS, Vogel-Claussen J, Seifter E, Huncharek MS: **Metastatic breast carcinoma presenting as a large pulmonary embolus: case report and review of the literature**. *Am J Clin Oncol* 2003, **26**:89-91.

82. Murakami T, Cardones AR, Hwang ST: **Chemokine receptors and melanoma metastasis**. *J Dermatol Sci* 2004, **36**:71-78.

83. Iwakuma T, Parant JM, Fasulo M, Zwart E, Jacks T, de Vries A, Lozano G: **Mutation at p53 serine 389 does not rescue the embryonic lethality in mdm2 or mdm4 null mice**. *Oncogene* 2004, **23**:7644-7650.

84. Shih SC, Robinson GS, Perruzzi CA, Calvo A, Desai K, Green JE, Ali IU, Smith LE, Senger DR: **Molecular profiling of angiogenesis markers**. *Am J Pathol* 2002, **161**:35-41.

85. Halaby MJ, Yang DQ: **p53 translational control: a new facet of p53 regulation and its implication for tumorigenesis and cancer therapeutics**. *Gene* 2007, **395**:1-7.

86. de Nigris F, Balestrieri ML, Napoli C: **Targeting c-Myc, Ras and IGF cascade to treat cancer and vascular disorders**. *Cell Cycle* 2006, **5**:1621-1628.

87. Grothey A: **Future directions in vascular endothelial growth factor-targeted therapy for metastatic colorectal cancer**. *Semin Oncol* 2006, **33**:S41-49.

88. Vickers TA, Lima WF, Nichols JG, Crooke ST: **Reduced levels of Ago2 expression result in increased siRNA competition in mammalian cells**. *Nucleic Acids Res* 2007, **35**:6598-6610.

89. Scacheri PC, Rozenblatt-Rosen O, Caplen NJ, Wolfsberg TG, Umayam L, Lee JC, Hughes CM, Shanmugam KS, Bhattacharjee A, Meyerson M, et al.: **Short interfering RNAs can induce unexpected and divergent changes in the levels of untargeted proteins in mammalian cells**. *Proc Natl Acad Sci U S A* 2004, **101**:1892-1897.

90. Kirby CJ, Gregoriadis G: **Preparation of liposomes containing factor VIII for oral treatment of haemophilia**. *J Microencapsul* 1984, **1**:33-45.